

**Swelling of Carbon Nano-Filler Modified Polydimethylsiloxane**

by

Bo Yang

A thesis submitted in partial fulfillment of the requirements for the degree of

Master of Science  
Department of Mechanical Engineering  
University of Alberta

© Bo Yang, 2018

## ABSTRACT

Polymers may absorb fluids from their surroundings via the natural phenomenon of swelling. Dimensional changes due to swelling can affect the function of polymer components, such as in the case of O-ring seals and microfluidic components. An understanding of the swelling behaviour and means for controlling it can improve the design of polymer components, for example, for the previously mentioned applications. Carbon-based fillers have risen in popularity to be used for the property enhancement of resulting polymer composites. The present investigation focused on the effects of three carbon-based nano-fillers (graphene nano-platelets, carbon black, and graphene nano-scrolls) on the dimensional changes of polydimethylsiloxane composites due to swelling when immersed in certain organic solvents. The study also assessed the mechanical and physical properties of the respective polymer composites. The primary experimental technique for this study is comprised of optical measurements in conjunction with digital image analysis to assess swelling dimensional changes of the prepared composites. Other experimental characterization techniques included polymer cross-linking density and electrical resistance measurements, electron and helium ion microscopy, X-ray diffraction and mechanical testing. The study showed that the extent and rate of swelling depended on the organic solvent in which the composites were immersed in. The investigation also revealed that the type of nano-fillers had no correlation to the degree of swelling; however, the addition of any carbon-based nano-filler increased the overall swelling. The experimental results led to the postulate that the increase of swelling was primarily caused by filler agglomeration.

## ACKNOWLEDGMENTS

I would like to express my appreciation to a number of people who have supported me along this journey. First, I would like to thank my supervisor, Dr. Pierre Mertiny, who provide guidance and mentorship towards more than research. The opportunities that he provided throughout my graduate degree opened doors to my future career. Whether it is travelling for aboard experience or educational, there were very little times he said no. However, the greatest thanks are given towards his character. Thank you for all the understanding, compassion, and care that you have shown through all these years.

Specifically, towards my research, I would like to thank Dr. M. Arjmand, Ivonne Otero, and Professor U. Sundararaj from the Polymer Processing Group in the Department of Chemical Engineering at the University of Calgary; Priscilla Gao and Dr. X. Sun from the Cross-Cancer Institution at the University of Alberta; Peng Li, Shihong Xu, Anqiang He, and Nancy Zhang in NanoFab at the University of Alberta; Diane Card in the Department of Earth and Science at the University of Alberta; and Professor J. Doucette, Professor D. Sameoto, Professor K. Duke, Dr. G. Melenka, Bernie Faulkner, Tuula Hilvo, Andrew Campbell, Roger Marchand, Richard Groulx, Gail Dowler, Alex Hunt, Dan Aldrich, Balakrishnan Nagarajan, Razim Refei, and Ben Cheung from the Department of Mechanical Engineering at University of Alberta

For my overall graduate experience, I would like to Professor J. Carey, Professor A. McDonald, Professor M. Lipsett, eHub at the University of Alberta, and the Center for Teaching and Learning.

# TABLE OF CONTENTS

ABSTRACT.....	ii
ACKNOWLEDGMENTS .....	iii
TABLE OF CONTENTS.....	iv
LIST OF FIGURES .....	vii
LIST OF TABLES.....	xi
NOMENCLATURE .....	xiii
1 INTRODUCTION .....	1
1.1 Multifunctional Polymer Composites .....	1
1.2 Polymer Matrix and Nano-filler.....	2
1.2.1 Carbon Based Nano-fillers.....	3
1.3 Manufacturing of Nanocomposites .....	5
1.3.1 Shear Mixing.....	6
1.3.2 In-Situ Polymerization/Solution Mixing.....	6
1.4 Swelling Theory.....	9
1.5 Swelling Experiment and Characterizations of Nanocomposite.....	12
1.5.1 Swelling Equilibrium.....	12
1.5.2 Existing Experimental Studies of Nanocomposite Swelling .....	12
1.5.3 Swelling Experiment: Gravimetric vs Optical.....	14
1.5.4 Characterization of Dispersion and Distribution .....	15
1.6 Thesis Objectives .....	18
1.7 Thesis Organization.....	18
2 EXPERIMENTAL METHODOLOGY .....	20

2.1	Materials.....	20
2.2	Manufacture .....	20
2.2.1	Safety .....	20
2.2.2	Manufacture of Bulk Nanocomposite.....	20
2.2.3	Selection of Co-Solution of In-Situ Polymerization.....	23
2.3	Optical Swelling Test.....	24
2.4	Electrical Conductivity Characterization .....	26
2.5	Cross-Linking Density Characterization.....	26
2.6	Digital Imaging .....	26
2.6.1	Cryo-microtoming.....	26
2.6.2	TEM .....	27
2.6.3	SEM .....	27
2.6.4	HIB.....	27
2.6.5	XRD .....	28
2.7	Tensile Testing.....	28
3	EXPERIMENTAL RESULTS & DISCUSSION .....	30
3.1	Swelling Dimensional Characterization.....	30
3.1.1	Graphene Nano-Platelets .....	30
3.1.2	Carbon Black .....	35
3.1.3	Graphene Nano-Scrolls.....	41
3.1.4	Pure PDMS with Different Manufacturing Solutions.....	46
3.1.5	GNP/PDMS with Various Manufacturing Parameters .....	49
3.2	Cross-Linking Density .....	53
3.2.1	GNP/PDMS.....	53
3.2.2	CB/PDMS .....	54
3.2.3	NS/PDMS .....	55

3.2.4	Different Curing Parameter of PDMS .....	57
3.2.5	Different Curing Parameter of 1% GNP .....	58
3.3	Exfoliation Characterization .....	59
3.3.1	Electrical Resistance .....	59
3.3.2	Microscopy .....	65
3.3.3	X-Ray Diffraction .....	73
3.4	Tensile Testing .....	77
3.4.1	Stroke Length vs. Optical Measurement .....	77
3.4.2	GNP/PDMS .....	80
3.4.3	CB/PDMS .....	83
3.4.4	NS/PDMS .....	86
3.4.5	Different Curing Solutions for PDMS .....	89
4	CONCLUSIONS .....	92
5	EXTENDED WORK .....	97
	REFERENCES .....	99
	APPENDICES .....	114
	APPENDIX A – SAMPLE XRD CHARACTERIZATION SHEETS .....	115
	APPENDIX B – ADDITIONAL MODULUS CORRELATION GRAPHS .....	117

## LIST OF FIGURES

Figure 1-1: In-situ polymerization process with solution mixing.....	7
Figure 1-2: Visualization of nano-particles in their solution with corresponding quality of distribution and/or dispersion.....	9
Figure 2-1: Sonication process of tri-phase solution in 5 °C cooling bath .....	22
Figure 2-2: Curing setup for nanocomposite with 100 °C Teflon coated granite plate. ....	23
Figure 2-3: Optical swelling measurement setup in glass petri dish .....	25
Figure 2-4: Sample image measurement of 2% GNP/PDMS after 8 hours of submerged after 8 hours.....	25
Figure 2-5: Dog bog sample of Type V dimension of ASTM D638-14 with white paint marking for digital strain measurement.....	29
Figure 2-6: Tensile Experiment setup with optical measurement system. ....	29
Figure 3-1: Transient swelling ratios of GNP/PDMS with 0%-4% filler volume in acetone.....	31
Figure 3-2: Transient swelling ratios of GNP/PDMS with 0%-4% filler volume in chloroform .....	31
Figure 3-3: Transient swelling ratios of GNP/PDMS with 0%-4% filler volume in toluene.....	32
Figure 3-4: Equilibrium (12 hr) swelling ratios of GNP/PDMS with corresponding filler volume percentage.....	33
Figure 3-5: Equilibrium swelling data of GNP/PDMS correlated to Kraus equation .....	34
Figure 3-6: Transient swelling ratios of CB/PDMS with 0%-4% filler volume in acetone .....	36
Figure 3-7: Transient swelling ratios of CB/PDMS with 0%-4% filler volume in chloroform .....	37
Figure 3-8: Transient swelling ratios of CB/PDMS with 0%-4% filler volume in toluene.....	37
Figure 3-9: Equilibrium (12hrs) swelling ratios of CB/PDMS with corresponding volume filler percentage .....	38
Figure 3-10: Equilibrium swelling data of CB/PDMS correlated to Kraus equation .....	40
Figure 3-11: Transient swelling ratios of NS/PDMS with 0%-4% filler volume in acetone .....	41
Figure 3-12: Transient swelling ratios of NS/PDMS with 0%-4% filler volume in chloroform .....	42
Figure 3-13: Transient swelling ratios of NS/PDMS with 0%-4% filler volume in toluene.....	42

Figure 3-14: Equilibrium (24hrs) swelling ratios of NS/PDMS with corresponding volume filler percentage .....	43
Figure 3-15: Equilibrium swelling data of NS/PDMS correlated to Kraus equation .....	45
Figure 3-16: Equilibrium swelling ratios for various pure PDMS curing parameter .....	47
Figure 3-17: Equilibrium swelling ratios for 1% GNP/PDMS with alternative manufacturing parameters .....	50
Figure 3-18: Equilibrium swelling ratios of GNP/PDMS with corresponding crosslinking density. Color of data points corresponds to filler volume percentage: white – 0%, black – 1%, green – 2%, red – 3%, yellow – 4%.....	54
Figure 3-19: Equilibrium swelling ratios of CB/PDMS with corresponding crosslinking density. Color of data points corresponds to filler volume percentage: white – 0%, black – 1%, green – 2%, red – 3%, yellow – 4%.....	55
Figure 3-20: Equilibrium swelling ratios of NS/PDMS with corresponding crosslinking density. Color of data points corresponds to filler volume percentage: white – 0%, black – 1%, green – 2%, red – 3%, yellow – 4%.....	56
Figure 3-21: Resistivity of GNP/PDMS, CB/PDMS and NS/PDMS with corresponding filler volume percentages .....	62
Figure 3-22: Resistivity of 1% GNP/PDMS with corresponding percent filler volume for alternative manufacturing parameters .....	63
Figure 3-23: A.) 1% GNP/PDMS without charging effect; B.) 1% GNP/PDMS with charging effect; C.) 4% GNP/PDMS without charging effect; D.) 4% GNP/PDMS with charging effect; with working distance of 9.724 mm and field of view of 10 $\mu\text{m}$ .....	67
Figure 3-24: A.) 1% CB/PDMS without charging effect; B.) 1% CB/PDMS with charging effect; C.) 4% CB/PDMS without charging effect; D.) 4% CB/PDMS with charging effect; with working distance of 9.724 mm and field of view of 10 $\mu\text{m}$ .....	68
Figure 3-25: A.) 1% NS/PDMS without charging effect; B.) 1% NS/PDMS with charging effect; C.) 4% NS/PDMS without charging effect; D.) 4% NS/PDMS with charging effect; with working distance of 9.724 mm and field of view of 10 $\mu\text{m}$ .....	69

Figure 3-26: SEM images of carbon coated NS/PDMS with filler volume percentages A.) 1%, B.) 2%, C.) 3% and D.) 4%.....	71
Figure 3-27: HIB image of non-carbon-coated treated 1% NS/PDMS .....	71
Figure 3-28: SEM images of A.) 1% volume fraction of NS/PDMS with no sonication and B.) 1% volume fraction of NS/PDMS cured at room temperature .....	72
Figure 3-29: TEM images of 4% filler volume NS/PDMS with standard cure.....	73
Figure 3-30: XRD result of pure GNP with corresponding intensity peak and two-theta diffraction angle .....	73
Figure 3-31: XRD data for 1% to 4% NS/PDMS with corresponding intensity peaks and two-theta diffraction angles.....	75
Figure 3-32: XRD results of 1% to 4% GNP/PDMS with corresponding intensity peaks and two-theta diffraction angles .....	76
Figure 3-33: Stress-strain data based on stroke length and optical measurement from tensile testing of PDMS .....	78
Figure 3-34: (Top) First and (Bottom) last image from optical measurement during tensile testing of pure PDMS.....	79
Figure 3-35: Modulus of elasticity of GNP/PMDS versus filler volume fraction.....	81
Figure 3-36: Linear region of stress-strain curve for 0% to 4% GNP/PDMS. (Only first test for each filler volume percent is displayed).....	82
Figure 3-37: Modulus of elasticity of CB/PMDS versus filler volume fraction.....	84
Figure 3-38: Linear region of stress-strain curve for 0% to 4% CB/PDMS. (Only first test for each filler volume fraction is displayed) .....	86
Figure 3-39: Crosslinking-density of CB/PMDS to corresponding modulus of elasticity .....	86
Figure 3-40: Modulus of elasticity of NS/PDMS versus filler volume fraction.....	87
Figure 3-41: Linear region of stress-strain curve for 0% to 4% NS/PDMS. (Only first test for each filler volume percent is displayed) .....	88
Figure 3-42: Crosslinking-density of NS/PDMS to the corresponding modulus of elasticity .....	89
Figure 3-43: Modulus of different co-solution cured GNP/PDMS samples.....	90
Figure 3-44: UTS of different co-solution cured GNP/PDMS samples .....	91

Figure B-1: Swelling ratios in chloroform, toluene, and acetone of GNP/PDMS to corresponding modulus of elasticity.....117

Figure B-2: Crosslinking-densities of GNP/PDMS to corresponding modulus of elasticity .....117

Figure B-3: Swelling ratios in chloroform, toluene, and acetone of CB/PDMS to corresponding modulus of elasticity.....118

Figure B-4: Swelling ratios in chloroform, toluene, and acetone of NS/PDMS to corresponding modulus of elasticity.....118

## LIST OF TABLES

Table 1-1: Summary of literature review on swelling of nanocomposites .....	14
Table 3-1: Equilibrium swelling ratios for GNP/PDMS.....	33
Table 3-2: Equilibrium swelling ratios of GNP/PDMS comparison between Kraus prediction and experiment results.....	35
Table 3-3: Equilibrium swelling ratios of CB/PDMS .....	39
Table 3-4: Equilibrium swelling ratios of CB/PDMS comparison between Kraus predictions and experiment results.....	40
Table 3-5: Equilibrium swelling results for NS/PDMS nanocomposite.....	44
Table 3-6: Equilibrium swelling ratios of CB/PDMS comparison between Kraus prediction and experiment results.....	45
Table 3-7: Equilibrium swelling ratios for NS/PDMS nanocomposites.....	48
Table 3-8: Organic solutions and corresponding solution parameters.....	49
Table 3-9: Equilibrium swelling ratios for 1% GNP/PDMS with alternative manufacturing parameters in acetone, chloroform and toluene.....	50
Table 3-10: Cross-linking percentage of GNP/PDMS, CB/PDMS and NS/PDMS .....	53
Table 3-11: Cross-linking density of pure PDMS cured with alternative of co-solutions.....	58
Table 3-12: Cross-linking density of 1% GNP/PDMS for different manufacturing parameters .....	59
Table 3-13: Resistivity of GNP/PDMS, CB/PDMS and NS/PDMS for percent filler volume ranging from 0% to 4% .....	62
Table 3-14: Resistivity of 1% GNP/PDMS for alternative manufacturing methods.....	63
Table 3-15: Resistivity comparison between pure PDMS and PDMS filled with 1% GNP cured with different co-solutions.....	64
Table 3-16: Modulus of elasticity and UTS for 0% to 4% GNP/PDMS .....	82
Table 3-17: Modulus of elasticity and UTS for 0% to 4% NS/PDMS. “*” indicates only two trials were used for average and standard deviation calculations .....	85
Table 3-18: Modulus of elasticity and UTS for 0% to 4% NS/PDMS. “*” indicates only two trials were used for average and standard deviation calculations .....	87

Table 3-19: Elastic modulus and UTS at 0% and 1% GNP/PDMS for different co-solutions

.....89

## NOMENCLATURE

$\Delta H$	Energy required. J
$V$	Volume, m <sup>3</sup>
$t$	Thickness, m
$E$	Energy (Material Parameter), J
$D$	Diameter, m
$T$	Temperature, K
$R$	Ideal gas constant, 8.3145 J/mol·K
$c$	Material constant
$d$	atomic plane distance between graphene layers, m

### *Greek Symbols*

$\Phi$	Volume fraction of nano-filler
$\delta_H$	Hildebrand Parameter, J <sup>1/2</sup> m <sup>-3/2</sup>
$\delta_X$	Hansen Parameter for X-type of intermolecular force, J <sup>1/2</sup> m <sup>-3/2</sup>
$\rho$	Density, kg/m <sup>3</sup>
$\zeta$	Specific surface area m <sup>2</sup> /kg
$\xi$	Correlation length between nano-fillers, m
$\psi$	Interface Area Function

$\theta$	Diffraction angle
$\lambda$	X-ray radiation wavelength, m

*Subscripts*

c	Cohesive Energy
s	Swelled
us	Un-swelled
filled	Filled with nano-fillers
unfilled	Unfilled with nano-fillers
LD	London Dispersion intermolecular force
DD	Dipole-dipole intermolecular force
H+	Hydrogen bond intermolecular force
mix	Organic solution mixture with carbon-based nanoparticles
sur-p	Surface energy of the nanoparticle
sur-p	Surface energy of the organic solution
vap	Vaporization

# 1 INTRODUCTION

## 1.1 Multifunctional Polymer Composites

Multifunctional polymer composites are polymers with micro- or nano-sized additives to expand the functionality of traditional polymers. Additives/fillers with nano-scale dimensions have a significant surface area to volume ratios and possible quantum effects allowing for non-existing material properties to be introduced into standard polymers [1]. For example, by adding electrically conductive fillers which induce electrical conductivity in an insulating polymer, new methods for electromagnetic shielding [2,3] and conductive paints [1,4] can be realized. Novel applications such as motors, generators and magnetic sensors can utilize magnetic polymers which are made possible with the addition of magnetic fillers [5]. In addition to imparting non-inherent properties to polymers of electrical conductivity and magnetic polarity, nano-fillers may also be used to enhance existing polymer properties. For example, with the addition of carbon-based nano-fillers to polymers, their elastic modulus can be increased and swelling behaviour controlled. The focus of this thesis is to control the swelling behavior of polymers by the addition of carbon-based nano-fillers and understand the effect of carbon-based nano-fillers on the swelling of nanocomposites.

Polymers tend to absorb fluids to a certain extent. In general, this phenomenon is caused by intermolecular forces between the solid and fluid phases. Three principle intermolecular forces of London dispersion, dipole-dipole, and hydrogen bond exists in all materials, but varies in weighted values [6,7]. The combined value of the three forces defines the magnitude of the total intermolecular forces. When the magnitude and type of intermolecular forces between the two phases are both similar, the attraction is strong enough to break the phase bonds and induce

swelling. Some engineering applications require specific polymers to be immersed in a certain fluid environment, which will cause swelling. In many cases, the swelling will inhibit the application of the polymer. For example with polymer seals (e.g. O-rings), swelling of the o-ring results in improper sizing between the seal and the gland which leads to additional internal stress and higher failure rate, especially in dynamic applications [8,9]. In microfluidic applications, unwanted dimensional changes due to swelling of the polymer microfluidic system can lead to improper experimental results [10,11]. One method to control swelling while maintaining the advantages of polymer material is to combine the polymer with nano-fillers. Within microfluidics applications, the addition of nano-fillers can improve technologies of hydrogels which are polymer networks swollen within water. Nano-fillers can expand ranges of pH or temperature while improving mechanical strength and thermal conductivity with hydrogel sensors [12]. In general, by introducing nano-fillers to polymers to control swelling, new opportunities for traditional applications can be explored. Polymer seals, micro-fluidics, and hydrogels are examples of nanocomposite applications for swelling control.

## **1.2 Polymer Matrix and Nano-filler**

A composite material is defined by the physical combination of two or more significantly different materials, both in chemical and physical structure, that remain distinct in the finished product [13]. Combining various different thermoplastic or thermoset matrices with metallic, organic, or inorganic based nano-fillers can result in a countless of alternative composite materials, each with its unique properties. The selection of the studied nanocomposite was based on the composites' adaptability towards the swelling application of polymer seals and/or microfluidics and its ease of manufacturing for efficient research. In the application of polymer seals, rubber thermoset – often fluorocarbon based – are generally used for o-rings due to its wear and chemical resistance. With

the reactivity of fluorine, the manufacturing process of any fluorocarbon based polymers is complex and potentially dangerous. In contrast, microfluidic systems were designed for ease of manufacture and characterization. Hence, polymers chosen for microfluidic components have high machinability [14]. Poly-dimethylsiloxane (PDMS) – a silicon thermoset rubber – was chosen for the polymer matrix in this thesis due its application in both microfluidics and polymer seals [15], ease of manufacturing, and the large reference base of nanocomposites.

### ***1.2.1 Carbon Based Nano-fillers***

Nano-fillers range from metallic particles of gold and silver to inorganic particles of clay or carbon-nano-tubes. Nano-fillers are classified by their morphologies [16] and categorized into classes of layers, particles, and fibres [17]. This study utilized all three categories of nano-fillers with a carbon basis. Graphene nano-platelets (GNP), carbon black (CB), graphene nano-scrolls (NS) – a derivative of GNP based on immersing GNP into isopropanol [18-21] – are the respective three categories of carbon-based nano-fillers with of platelet (or layer), particle and fiber morphology.

#### ***1.2.1.1 Graphene Nano-Platelets***

GNP, the filler with layered morphology in this study, is an atomically thick two-dimensional layer of graphite. Defect-free graphene is mechanically the strongest material ever measured with Young's modulus of 1 TPa and ultimate strength of 130 GPa [22]. Hence, graphene based nanocomposites used to increase mechanical strength have been studied extensively [23-26]. In addition to being the strongest mechanical material, single-layer graphene has a high electrical conductivity of up to 6000 S/cm [28]. Similarly, the usage of graphene to improve the electrical conductivity of nanocomposites has also been explored extensively [23-24]. These unique

properties of graphene coupled with the high surface area and gas impermeability [29] are key aspects of improving mechanical, electrical, and gas barrier properties of polymers. The study of graphene to the swelling application is shown in its combination with hydrogels [30,31], but not towards other microfluidics applications of PDMS. This gap provides the opportunity to expand on current literature and confirm to the effect of graphene on swelling.

#### *1.2.1.2 Carbon Black*

CB fillers, the particle morphology of the study, are technically aggregates and agglomerates of spherical carbon particles with surface modification that form an aciniform (grape shaped groups) cluster [32]. As a product of incomplete combustion of hydrocarbons in a furnace, thermal and furnace carbon black is primarily used to enhance rubbers for wear performance, conductivity, optic visibility and ultraviolet resistibility [33]. Carbon black is one of the oldest and most cost effective nano-filler to date; however, its mechanical property is weaker compared to GNP or carbon nanotubes due to the lower surface area to volume ratio. CBs' application can be seen in prolonging tire-life [33] to conductivity studies [33-37]. The study of the swelling of CB nanocomposite was one of the first swelling studies relating swelling ratio to filler-volume and is still, today, used as a base model [38,39]. Hence, the CB based nanocomposite for the current study serves the purpose of providing a baseline to historical data.

#### *1.2.1.3 Graphene Nano-scrolls*

NS, the fillers with the fibrous morphology of the study, is a derivative of graphene nano-platelets. By immersing GNP in isopropanol, the graphene platelets curl or roll into scrolls [18-21]. While both NS and carbon nanotubes are carbon based nano-fibres, their aspect ratios are drastically different. Carbon nano-tubes generally enhance nanocomposites more efficiently; i.e. less percent

volume of nano-fillers is needed to achieve desired property improvements in terms of mechanical strength [40,41], thermal conductivity [42], and electrical conductivity [43,44]. However, due to the high aspect ratio of carbon nanotubes, it may have similar detrimental effects on human health as asbestos [45-47]. Hence, the required safety protocols and equipment make carbon nano-tubes less effective to study over the lower surface area to volume ratio graphene-nano-scrolls. NSs are one of the least studied carbon based fillers due to the greater efficiency of their counterpart of carbon nano-tubes; hence, limited information is available in the technical literature relating to the electrical enhancement, mechanical strengthening, and swelling effects. This gap provides an opportunity to expand on current knowledge.

### **1.3 Manufacturing of Nanocomposites**

Prior to any applications, nanocomposites must first be synthesized. Typical macro composite manufacturing methods such as wet lay-up, pultrusion, prepreg lay-up and filament winding, do not apply to the challenges of micro/nanofabrication [48]. The manufacturing processes of nanocomposites are not as a trivial as a “mix and stir”. Additional processes must be implemented to aid the dispersion and distribution of agglomerated nanoparticles in a high viscosity pre-polymer or molten polymer. In addition, the comparatively high viscosity of polymer liquids induces additional challenges to dispersion. With the polymer employed in this study being a thermoset, two main methods of thermoset nanocomposite manufacturing can be categorized as high shear mixing [49-56] – i.e. melt compound or three-roll milling – and in-situ polymerization/solution mixing [37, 55-58].

### ***1.3.1 Shear Mixing***

The most economical, scalable, and safe method for dispersing nanoparticles into thermoset polymers is through shear mixing at elevated temperature [59-61]. However, manufacturing graphene-based nanocomposites at elevated temperature have been limited to a few studies because of the thermal instability of most chemically modified graphene fillers. In addition, the distribution and dispersion of nano-fillers are better achieved through in-situ polymerization/solution mixing than purely shear mixing [52]. Since many enhancements of polymers depend on well dispersed and distributed nano-filler, in-situ polymerization is typically advantageous for research purposes.

### ***1.3.2 In-Situ Polymerization/Solution Mixing***

In-situ polymerization has been successfully used to create graphene based composites with a polymers matrix of polyvinyl alcohol [63], poly-methyl methacrylate [64], epoxy [65], polyurethane [66], and PDMS [23, 24, 67]. In-situ polymerization is defined as solely the addition of nano-fillers into the monomer resin, followed by the curing of the resin and nano-filler mixture with the curing agent. However, the increase in viscosity of the monomer resin due to the addition of nano-fillers generally hinders the dispersion and distribution of the nano-fillers. Hence, the in-situ polymerization process is generally coupled with solution mixing, where an additional co-solution is introduced – and later removed via evaporation – into the manufacturing process to decrease the viscosity of the resin. During the tri-phase mixture of the co-solution, polymer resin, and nano-filler, the processes of mechanical and/or sonication mixing can additionally aid in the distribution of nano-fillers [68]. As shown for polyvinylpyrrolidone and N-methylpyrrolidone as the polymer resin, graphite has been directly exfoliated to single- and multiple-layer graphene via sonication [69, 70]. Figure 1-1 depicts the in-situ polymerization process where the polymer resin

and nano-filler are dispersed in a solvent, mixed and then solidified while also removing the solvent.

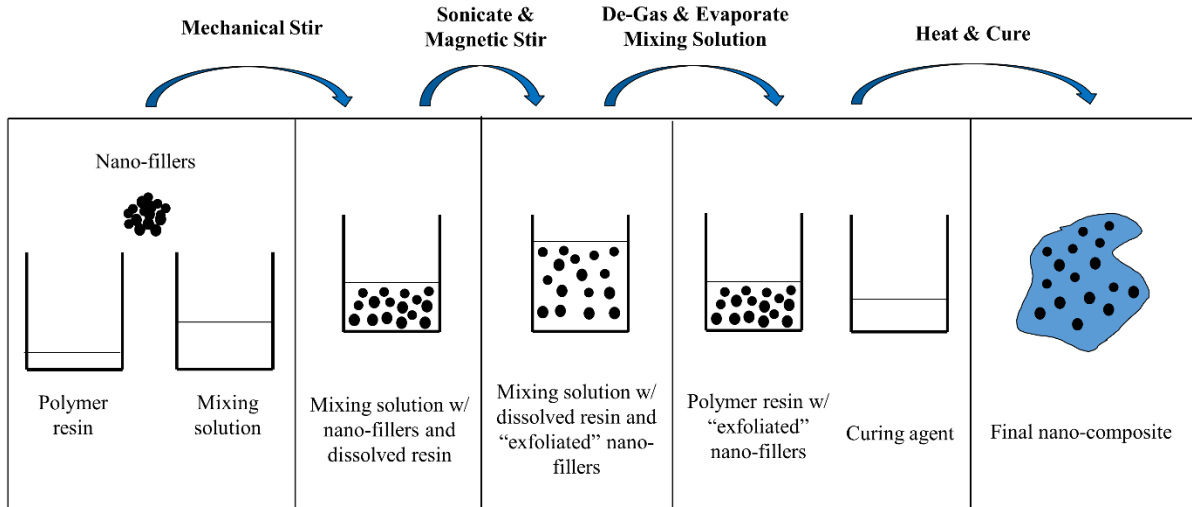


**Figure 1-1: In-situ polymerization process with solution mixing**

### 1.3.2.1 Dispersion and Distribution in Manufacturing

The dispersion and distribution of agglomerated particles are critical for making a quasi-homogenous nanocomposite. As shown in Figure 1-2, both dispersion and distribution are typically needed to enhance the nanocomposite. However, a homogeneous dispersion of nanoparticles in a polymer with existing compounding techniques remains challenging due to the strong tendency of the particles to agglomerate [70,71]. For carbon-based nano-fillers, particles can be exfoliated through oxidization or thermal reduction [71]. Graphene can also be exfoliated through a combination of organic solvents with mechanical and/or sonication mixing. Regardless of the method of exfoliation, the separation between single graphene is ultimately due to the breakage of Van der-Waal attraction force. Hernandez quantified the energy required for exfoliation with the following equation (1):

$$\Delta H_{\text{mix}} \approx 2 \frac{V_{\text{mix}}}{t_{\text{mix}}} \left( \sqrt{E_{\text{sur-p}}} - \sqrt{E_{\text{sur-sol}}} \right)^2 \phi \quad (1)$$

where  $\Delta H_{\text{mix}}$  is the energy difference/required to exfoliate the graphene nano-filler in solution,  $V_{\text{mix}}$  is the volume of the mixed solution with graphene nano-fillers,  $t_{\text{mix}}$  is the thickness of the graphene,  $E_{\text{sur-p}}$  is the surface energy of the graphene-fillers,  $E_{\text{sur-sol}}$  is the surface energy of the solution, and  $\phi$  is the volume fraction of graphene filler in the solution mixture. Equation (1) demonstrates that when the surface energy of the immersed solution,  $E_{\text{sur-sol}}$ , is the same as that of the surface energy of graphene/nano-tube 70-80 mJ/m<sup>2</sup> [70,72,73] the additional energy to exfoliate approaches zero and exfoliation occur naturally. In addition, any difference between the surface energy can be induced by prolonging mechanical and/or sonication mixing which ultimately exfoliates the graphene aggregates [68,74-76]. By combining both common PDMS in-situ polymerization solution of toluene ( $E_{\text{sur-sol}} = 61.15$  mJ/m<sup>2</sup>), isopropanol ( $E_{\text{sur-sol}} = 44.90$  mJ/m<sup>2</sup>), chloroform ( $E_{\text{sur-sol}} = 63.50$  mJ/m<sup>2</sup>), and cyclohexane ( $E_{\text{sur-sol}} = 58.61$  mJ/m<sup>2</sup>) with mechanical and sonicated mixing, a well dispersed and distributed quasi-homogenous nanocomposite can be achieved.

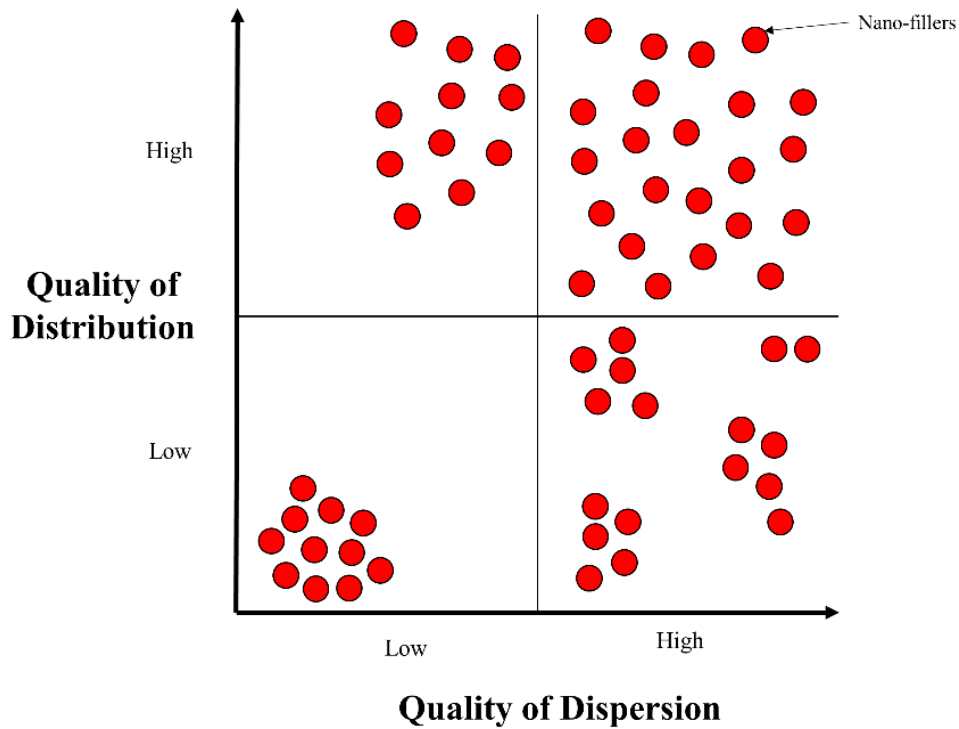


**Figure 1-2: Visualization of nano-particles in their solution with corresponding quality of distribution and/or dispersion**

### 1.4 Swelling Theory

The focus point of this research is to determine the effects of carbon-based nano-filler addition on swelling of PDMS. The fundamentals of swelling link to solubility. Typically, solubility is thought of a solid – i.e. the solute – dissolving into a liquid – i.e. the solvent. However, for materials such as cross-linked polymers that cannot be dissolved, solubility is measured by the degree of swelling where ultimately the liquid “dissolves” into the solid. For this phenomenon to occur, the cohesive energy between the solid and liquid phase must be similar. As seen in equation (2), the cohesive energy,  $E_c$ , is defined as the heat of vaporization per volume:

$$E_c = \frac{\Delta H_{\text{vap}} - RT}{V_{\text{molar}}} \quad (2)$$

where  $\Delta H_{\text{vap}}$  is the heat of vaporization,  $R$  is the ideal gas constant,  $T$  is the temperature, and  $V_{\text{molar}}$  is the molar volume. Cohesive energy corresponds to vaporization energy and relates to solubility because the energy required to break the intermolecular forces for solubility is similar to the energy required to change a liquid to a vapour phase. [6,7]. Cohesive energy for polymers, which ultimately relates to intermolecular forces, can be quantified via a solubility parameter: the Hildebrand Solubility Parameter and the Hansen Parameter. The Hildebrand Solubility Parameter, which equals to the square root of the cohesive energy density,  $\delta_H = E_c^{1/2}$ , measures the total magnitude of the intermolecular forces [77,78]. The Hansen Parameter, i.e. the expansion of the Hildebrand Parameter,  $\delta_H^2 = \delta_{LD}^2 + \delta_{DD}^2 + \delta_{H+}^2$ , measures the distribution of the three primary intermolecular forces of London Dispersion, dipole-dipole, and hydrogen bond [79,80]. Hence, when the magnitude ( $\delta_H$ ) and the type of intermolecular forces ( $\delta_{LD}$ ,  $\delta_{DD}$ ,  $\delta_{H+}$ ) between the polymer and the solvent are similar, then swelling occurs.

The Hildebrand parameter is frequently used in the Hildebrand-Scatchard equation (3) which is used to predict swelling for a binary solid and liquid system:

$$\Delta H_{\text{mixing}} = (\delta_{\text{solid}} - \delta_{\text{liquid}})^2 \phi_{\text{solid}} \phi_{\text{liquid}} \quad (3)$$

where  $\Delta H_{\text{mixing}}$  is the enthalpy change on mixing,  $V$  is the volume of mixture,  $\Phi_i$  is the volume fraction of the respective constituent  $i$ , and  $\delta_i$  is the Hildebrand parameter for the respective  $i$ . However, the following assumptions are made for equation (3) “(a) the components mix with no volume change on mixing at constant pressure; (b) the interaction forces act between the center of the molecules and the interaction between a pair of molecules is not influenced by the presence of

other molecules; (c) the mixing is random and the distribution is temperature independent; (d) no reaction occurs between the components; and (e) there is no complex formation or special association” [7]. While the swelling of a nanocomposite system can be assumed to be a binary solid and liquid system, the assumption of paired molecules between solid and liquid not influenced by the presence of other solid molecules is not fully understood. The attraction between the liquid solvent and polymer matrix will be significantly different than the attraction between the nano-fillers.

By assuming the bond between the polymer and filler remains intact, the Kraus equation (4) takes consideration of the filler material and estimates the swelling effect around a radius,  $R$ , of the filler particle, then integrates this estimation to the whole system. The Kraus equation is given as:

$$\frac{V_{\text{unfilled}}}{V_{\text{filled}}} = 1 - m \frac{\phi}{1 - \phi} ; m = (3c - 1) - 3cV_{\text{unfilled}}^{\frac{1}{3}} - V_{\text{unfilled}} \quad (4)$$

where  $V_{\text{unfilled}}$  is the swelling volume without nano-fillers,  $V_{\text{filled}}$  is the swelling volume with nano-fillers,  $\phi$  is the volume fraction of graphene filler in the solution mixture, and  $c$  is a material constant, is a widely used model for the prediction of swelling effects in a nanocomposite with a spherical filler [38, 82]. While the Kraus equation was derived assuming spherical fillers only and aggregates of particles as simply larger particles, Kraus explicitly stated that “non-spherical particles may obey an equation of the form of [Kraus] ... and that the shape and aggregation effects can be lumped into the constant  $c$ ” [38].

To increase accuracy and with the rise in popularity of platelet and fibrous nano-fillers, a modified version of the Kraus equation, the Interface Area Function (IAF), was proposed to accommodate other filler shapes [84]:

$$\frac{V_{\text{unfilled}}}{V_{\text{filled}}} = 1 - m \frac{\psi\phi}{1 - \psi\phi} ; \psi = \rho\zeta\xi\phi \quad (5)$$

where  $\psi$  is the IAF,  $\rho$  is the density of the nano-filler,  $\zeta$  is the specific surface area of filler, and  $\xi$  is the correlation length between nanoparticles. Even though the modified Kraus equation accounts for the nano-filler morphology and shows the same trend as the original Kraus equation, it still does not take consideration of aggregates of nanoparticles. However, the modified Kraus equation is the most prominent equation to estimate swelling of nanocomposites.

## **1.5 Swelling Experiment and Characterizations of Nanocomposite**

### ***1.5.1 Swelling Equilibrium***

Swelling experiments and characterizations are mostly recorded during the steady state or the equilibrium of the swelling process. Equilibrium in swelling of a polymer network is the balance of elastic polymer network force to the osmotic pressure exerted on the polymer by the swelling agent [83]. Swelling of a polymer occurs at the crosslink junctions where each network strand is being stretch and untangled. The force needed to stretch and untangle these network strand correlates directly to the elastic modulus. Hence, at the equilibrium swelling each network strand is balance by the stretch of the osmotic pressure and the pull of the material elasticity.

### ***1.5.2 Existing Experimental Studies of Nanocomposite Swelling***

Kraus' derivation and experimentation of CB filled vulcanizates in 1963 was the first and foundational work toward understanding swelling of nanocomposites [38]. The Kraus relationship was still used and proven valid 40-years later by Bandyopadhyay *et al.* [84] and Burnside *et al.* [85,86] in their study on swelling of non-carbon based silica nanocomposites. As mentioned before, in 2008, Bhattacharya *et al.* revised and improved the Kraus relationship by incorporating

the shape of the nano-fillers with the IAF [84]. However, Bhattacharya's experimentation utilized clay particles instead of CB. Studies specific to swelling of CB based nanocomposites are rare. Swelling characterization is generally a secondary objective in most CB nanocomposite studies with primary focus towards the enhancement of resistivity and mechanical properties. For example, Marquez *et al.* tested the swelling of an elastomer as a secondary objective to their primary objective of characterizing conductive variations of a CB and graphite filled polybutadiene composite [88]. Similarly, Mostafa *et al.* related the effect of swelling towards the compression strength only after characterization the compression strength of various CB filled styrene butadiene and nitrile butadiene [89]. Similar to CB nanocomposites, studies of GNP nanocomposites characterizing swelling are secondary to the main objective of either electrical conductivity or mechanical strength. Swelling measurements were generally performed to characterize the crosslinking density of the polymer. For example, in both of Araby *et al.*, swelling studies were performed to evaluate cross-linking density, but its primary objective was on using GNP to enhance the electrical and thermal properties of styrene-butadiene [90,91]. The only GNP nanocomposites studies that treat characterization of swelling as a primary objective are applications toward hydrogels. GNP combined with polyvinyl alcohol, polyacrylic acid, and polyacrylamide used as hydrogels were studied for their mechanical and thermal properties. Due to the hydrogels' function as absorbent of water, swelling in H<sub>2</sub>O were extensively characterized [92-96]. All of the mentioned studies used a gravimetric methodology to characterize the swelling of nanocomposites. In addition, shown in Table 1-1, the general trend for all nano-filled composites signifies an increase in resistance to swelling as filler content increased. Lastly, no studies exist for swelling of NS composites.

**Table 1-1: Summary of literature review on swelling of nanocomposites**

Reference	Composition	Statement of Swelling change W.R.T. increase filler content
Kraus [38]	Rubber/Carbon Black	<i>“the restricted swelling in solvents of crosslinked elastomers containing reinforcing fillers”</i>
Bandyopadhyay <i>et al.</i> [85]	Acrylic rubber, epoxidized natural rubber, and poly (vinyl alcohol) with silica	<i>“Swelling of filled polymers is suppressed by the presence of filler.”</i>
Burnside <i>et al.</i> [86]	PDMS/Silicate	<i>“Solvent uptake (swelling) in dispersed nanocomposites was dramatically decreased”</i>
Burnside <i>et al.</i> [87]	PDMS/Organo-Silicate	<i>“the nanocomposites exhibit a substantial decrease in solvent uptake compared to the unfilled PDMS matrix”</i>
Mostafa <i>et al.</i> [89]	Styrene Butadiene/carbon black, nitrile butadiene/carbon black	<i>“the swelling percentage of both CB-filled styrene butadiene rubber and CB-filled nitrile butadiene rubber vulcanizates decreased with increasing carbon black loading”</i>
Zhang <i>et al.</i> [92]	Polyvinyl alcohol/graphene oxide	<i>“The maximum swelling ratio of the polyvinyl alcohol/graphene oxide hydrogels decreased when graphene oxide was increased from 0.6 to 1.0 wt%”</i>
Shen <i>et al.</i> [93]	Poly(acrylic) acid /graphene oxide	<i>“with the increasing of graphene oxide content, the equilibrium swelling ratio of the graphene oxide – poly(acrylic) acid-gels decrease.”</i>
Huang <i>et al.</i> [94]	Poly(acrylic acid-co-acrylamide)/graphene oxide	<i>“the swelling capacities ... went up with increasing graphene oxide loadings to 0.30 wt% and then decreased with further increasing graphene oxide loadings”</i>

### 1.5.3 Swelling Experiment: Gravimetric vs Optical

Swelling measurements are generally completed by two methods: gravimetric and optical. Gravimetric measurements take into account the ratio of the mass between the swollen network and solvent to that of the dry extracted solid [97-101]. By considering the mass, gravimetric measurements utilize the whole sample volume and anisotropy are taken into consideration.

However, the disadvantage of measuring mass is its-inaccuracy. The swollen network must be measured in an equilibrium state which provides the maximum surface area for the solvent to evaporate. Hence, when volatile organic solutions are used as the swelling solution, the mass measurements of the swollen network are lower than the actual mass of equilibrium in the swelling solution. The second disadvantage is the requirement of extra steps to account for the uncross-linked oligomers. Practically, polymers are not 100% cross-linked. Hence, with gravimetric measurements, if the floating oligomers or uncross-linked polymer is not removed, the mass measurement will include the polymer network, the swelling solution, and the floating oligomer.

Optical measurements measure dimensional changes instead of a mass change [102]. Optical swelling measurements typically only quantify two dimensions of a sample, and the swelling volume needs to be extrapolated with an isotropic assumption. However, with an optical measurement system, equilibrium swelling can be measured in the swelling solution; hence, unlike gravimetric measurements, the evaporation of the swelling solution can be avoided during the swelling measurement. In addition, unlinked oligomers do not affect optical swelling measurements since oligomers do not affect dimensional swelling of the polymer network.

#### ***1.5.4 Characterization of Dispersion and Distribution***

##### ***1.5.4.1 Microscopy Digital Imaging***

Exfoliation of nano-filler agglomerates is critical for any enhancement of the nanocomposites. Microscopy with transmission electron microscope (TEM), scanning electron microscope (SEM), or helium ion beam microscope (HIB) can be a means for characterizing the exfoliation state of the processed nanocomposites [71,103]. The microscope images can give a visual qualitative evidence of exfoliation. However, there are limitations with microscopy. First, the image field of view is limited and does not always reflect the bulk sample. Even if the viewed image does not

contain agglomerates, there is no guarantee that the bulk is free of agglomerates. Therefore, microscopy is a method to assess dispersion, but not distribution. Second, the prepared sample for microscopy can be altered during the preparation process which then does not reflect the bulk sample. With TEM microscopy, the thickness of sample slices needs to be on the order of a micro or nanometer scale. The preparation for micro or nanometer thick samples, using a cryo-microtome, can change or deteriorate the property of the original bulk sample [104,105]. Lastly, TEM, SEM, and HIB all utilize a high voltage electric field; hence, the quality of the images heavily depends on the electric conductivity of the material. Since not all nanocomposites with carbon-based nano-fillers are conductive, charging effects on samples during microscopy can damage the sample and/or deteriorate image quality. Therefore, microscopy by itself is not enough to characterize both the state of distribution and dispersion of nanocomposites.

#### *1.5.4.2 Electrical Conductivity*

Electrical conductivity is an indirect method of characterization the state of filler dispersion and distribution. While a conductive nanocomposite does not necessarily guarantee a high degree of exfoliated/dispersed nano-fillers, the nano-fillers needs to be dispersed sufficiently well for the nanocomposites to become conductive. In a nanocomposite, conductivity is induced predominantly by electrons tunneling through the insulative polymer matrix between fillers, rather than by direct particle-to-particle contact. As the distance increases between fillers, the probability of electron tunneling decreases. At a certain distance between two fillers, the resistance induced by the polymer matrix reaches a level at which tunneling effects effectively cease to exist. This critical distance is frequently termed electron tunneling distance: the maximum distance between nano-fillers where electrons can pass through the matrix [27]. If the distance between two or more fillers is less than the electron tunneling distance, then the two or more fillers form a cluster [27].

Eventually, the cluster will grow and span the size of the composite bulk making it conductive. The clustering effect of nano-fillers is the key to the electrical conductivity of these composites. Hence, coupling microscopy with conductivity measurement is a possible means for assessing both the state of filler dispersion and distribution.

#### 1.5.4.3 X-Ray Diffraction

X-ray diffraction is commonly used to characterize the state of filler dispersion and distribution in a nanocomposite structure due to its simplicity and availability [105,106]. For a material with a periodic spatial structure, such as a crystal or layered nano-filler, a diffraction peak at a specific X-ray incident angle will be recorded by a detector according to Bragg's law. The latter states that the smaller the angle, the greater is the distance between periodic features of the structure until the periodic structure no longer exists and the diffraction peak vanishes. As shown by Bhattacharya et al., as nano-fillers inside the polymer matrix progress from an agglomerated to intercalated to then exfoliated morphology, the peak of the plain nano-filler will shift towards the left (i.e. smaller angles) until a fully random and exfoliated nanocomposite morphology is achieved [108]. Even though, Bhattacharya et al. utilized clay based nano-fillers, this shift is also observed in carbon-based nanocomposites such as GNP. According to Szabo *et al.*, a peak of plain graphite exists at  $2\theta = 26.3^\circ$  (Cu K $\alpha$  radiation, X-ray wavelength = 0.154 nm) and will shift to  $14.1^\circ$ - $14.9^\circ$  as the graphite becomes oxidized creating more spacing between layers graphite oxide [109]. In addition, as seen in Schniepp *et al.* and McAllister *et al.* study, the XRD graph for fully exfoliated graphene resulted in no major peaks [110, 111].

## **1.6 Thesis Objectives**

This thesis research focuses on carbon-based nano-fillers of various morphologies and their effect on swelling of poly-dimethyl siloxane polymer matrices. Through swelling experiments and the assessment of polymer cross-linking density, nano-filler exfoliation and mechanical strength, the thesis objective is to determine the effects of carbon-based nano-fillers on the swelling behaviour of PDMS. Co-objectives of this thesis are a.) manufacturing of various carbon filler modified PDMS nanocomposites, b.) assessing the optical swelling test methodology, and c.) evaluate published models for swelling prediction such as the Kraus relationship [38].

## **1.7 Thesis Organization**

Following Chapter 1, which includes background information and reasoning behind the chosen materials and experimental methodology, Chapter 2 details the experimental process. Experimental results are presented in Chapter 3. The first part of Chapter 3 (Section 3.1) examines the results of the first set of swelling experiments. This first phase of experimentation was completed with three different PDMS nanocomposites containing sphere shaped carbon black, disk shaped graphene nano-platelets, and rod-shaped carbon nano-scrolls, with filler volume fraction ranging from 0% to 4%. Results pertaining to the equilibrium swelling time, the effect of nano-filler morphology on swelling ratio, and validate the Kraus theory are presented. It will be shown that the results from first experiment phase contradicted the thesis hypothesis that was based on Kraus; hence, the original plan of continuing to validate the modified Kraus equation with IAF was terminated. The focus was shifted to discovering the reason behind the contradiction to the original hypothesis. Hence, Section 3.1 continues by discussing the second phase of swelling experiments, which describes the testing of nanocomposites made with different co-solutions and

manufacture parameters. This second phase aims to explain the contradictory results obtained in the first set of experiment. Section 3.1 concluded with an updated thesis hypothesis of nano-filler exfoliation being the major factor affecting the swelling ratio of a nanocomposite. Section 3.2 to 3.3 explain the nanocomposite characterization needed to support the updated thesis hypothesis. The cross-linking density of the polymer matrix and the degree of agglomeration of the embedded nano-fillers are discussed. Section 3.4 then relates swelling, degree of cross-linking and exfoliation to the mechanical strength of the studied nanocomposites. Chapter 4 summarizes the results and states the major conclusions. Finally, in Chapter 5 possible future work extending from this thesis is discussed.

## **2 EXPERIMENTAL METHODOLOGY**

### **2.1 Materials**

XG Science (Grade M, Lansing, MI, USA) and Cabot Corporation (Vulcan XC72, Boston, MA, USA) supplied the respectively GNP and CB fillers for the study. Poly-dimethyl siloxane was supplied Dow Corning (Slygard 184, Auburn, MI, USA). Cyclohexane, toluene, and chloroform, acetone and isopropanol were all supplied from Fisher Scientific with 99.9% purity.

### **2.2 Manufacture**

#### ***2.2.1 Safety***

Safety precautions were considered and taken into actions during the manufacturing and experimentation of this study. All manufacturing and experimentation were completed with standard lab safety wearables under proper ventilation or fumehood. In addition, due to the presence of nano-fillers and hazardous solutions used in the in-situ polymerization and optical swelling experimentation, all processes were completed with the user wearing a fitted repertory mask with Organic Vapors/P100 combo filters (S-Series, Honeywell, Morris Plains, NJ).

#### ***2.2.2 Manufacture of Bulk Nanocomposite***

The manufacture of the bulk nanocomposites was completed with the following procedure. A mass of 25 g to 30 g of PDMS part A, weighted with a 0.001g resolution weight scale (AV213 Adventure Pro from OHAUS, Parsippany, NJ, USA), was first placed into a 500 ml beaker. The desired volume fraction (1% to 4%) of nano-particle was calculated according to the recorded PDMS part A weight and placed into the same beaker. The maximum of filler loading considered in this study was 4% volume fraction. A volume fraction past 4% increased the viscosity of the resin/filler

mixture to a point where the mixture was unprocessable with the given experimental setup. Co-solution of either toluene, isopropanol, chloroform, or cyclohexane, weighted at 400% of the resin/filler mixture weight, was then poured into the beaker. The mixture was then stirred with a mechanical stir (BDC 2002 Variable-speed Stirrer from Caframo, Wiaraton, ON, Canada) at 500 RPM for 5 minutes to achieve a uniform distribution of the tri-phase solution.

As seen in Figure 2-1, a tapered ultrasonic tip (Q500 Sonicator from QSONICA, Newtown, CT, USA) was immersed in the tri-phase solution. The solution was placed in a refrigerated water cooling bath set a 5 °C (NESLAB RTE-17 Digital Plus Refrigerated Bath from Thermo Scientific, Newington, NH, USA) to slow the evaporation of the co-solution and to reduce heat from sonication. The solution was sonicated in the cooling bath for 10 hours at 40% of power of 500W at 20 kHz. The solution was then placed on a heated magnetic stir at 65 °C for 24 hours to evaporate the co-solution. To ensure all co-solution was evaporated after a magnetic stir, the solution was placed in an in-house made heated vacuum system at 15 kPA and 65 °C for 2 hours. The weight of the remaining PDMS part A and nano-fillers were weighed to ensure the co-solution was evaporated. The target mass of the remaining mixture was to be approximately one gram less of the starting total. The loss of mass was due to residue mixture remaining on different mixing tools – stir stick, mechanical stir, sonication tip, and magnetic stir.

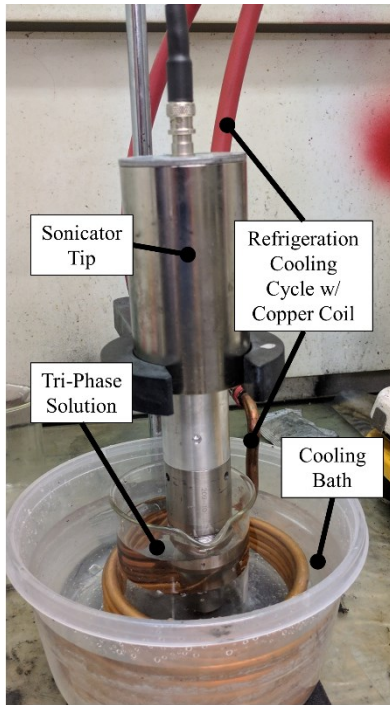


**Figure 2-1: Sonication process of tri-phase solution in 5 °C cooling bath**

Following the solvent removal process, 1:10 of PDMS part B curing agent was added to the resin/nano-filler mixture and mixed with the mechanical stir at 250 RPM for 10 min. The nanocomposite mixture was then degassed with the vacuum system at 15 kPa and room temperature for 15 min, during which no air bubbles were extracted from the nanocomposite mixture. The nanocomposite mixture was then brought up from room temperature to 40 °C which decreased the viscosity to ensure proper pouring out of the beaker. As seen in Figure 2-2, the composite mixture was then poured onto a Teflon coated (ToolMates Dry Film Lubricant 6075 from AERVOE Industries, Gardnerville, NV, USA) granite surface plate (88N85.01 from Lee Valley Tools, Edmonton, AB, Canada) that was pre-heated to 100 °C. Spacers with a thickness of 1 mm were placed at the sides of the granite plate and a second granite plate was pressed on top of the base. The sample was cured overnight for 12 hours at 100 °C in an oven.

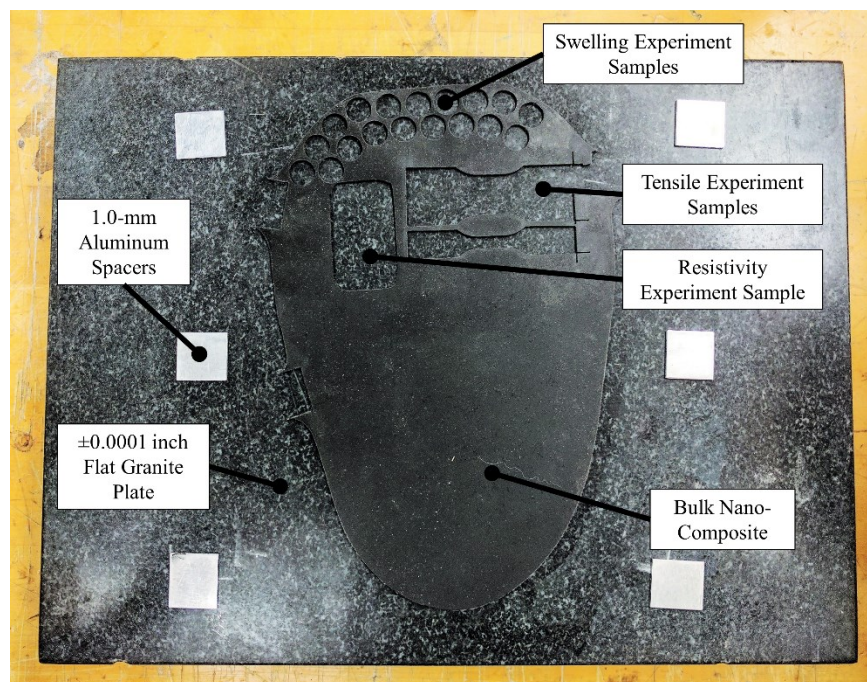


**Figure 2-2: Curing setup for nanocomposite with 100 °C Teflon coated granite plate.**

The bulk sample was carefully removed from the granite plates as a whole and left at room temperature to cool and reach equilibrium for 24 hours. A 1.0 cm stainless steel punch was used in conjunction with a hand press to extract circular testing samples from each bulk sample.

### ***2.2.3 Selection of Co-Solution of In-Situ Polymerization***

The selection of co-solutions for in-situ polymerization was based on availability, previous studies, and surface energy compatibility with graphene exfoliations as previously explained in Section 1.3.2.1. Previously, Filippidou *et al.* used a 30:70 mixture of isopropanol/cyclohexane as the co-solution to make GNP/PDMS functional strain sensor [23]. Lee *et al.* used a 30:70 mixture of isopropanol/Stoddard solvent as the co-solution to make GNP/PDMS biocompatible strain sensors [67]. Lastly, Loomis *et al.* used only isopropanol to create GNP/PDMS test samples for mechanical characterization [24]. Based on these studies, isopropanol and cyclohexane - both of which have similar surface energy to that of graphene – were the selected co-solutions for the in-situ

polymerization manufacturing process. In addition, toluene and chloroform – both of which also have similar surface energy to graphene – were also selected as alternative co-solutions to test for manufacture variability. While no previous studies have used these co-solutions, Johnson *et al.* state that the dispersion of graphene is most commonly achieved through sonication by creating shear stresses and cavitation in the solvent [112]. Hence, the co-solution should aid in dispersing the nano-fillers as long as sonication was applied.

### **2.3 Optical Swelling Test**

As shown in Figure 2-3, 5 sample disks were placed on top of a stainless-steel mesh in a glass petri dish. Each sample disks were then secured under a stainless steel ring. By using the mesh and the ring, the sample was ensured to stay stationary during any movement of the petri dish during the experiment while exposing maximum and consistent surface area of the sample disk to the solution.

Prior to the submerging of the samples, Toupview's digital image scale was calibrated with a 0.1mm and 0.01mm microscope calibration slide (Model A36CALM7, Microscope Net). Three solvents were used as the swelling agent: toluene, chloroform, and acetone. The solvent solution was poured into the petri dish until the top of rings were submerged. Digital images were immediately captured for each sample disks as the 0-hour timestamp with the 9.0 MP Camera (2X-270X Simal-focal Zoom Stereo Microscope, Microscope Net). Images were then captured at times of 0.25, 0.5, 1, 2, 4, 8, 12 and 24 hours after immersion. Each image was then measured with the software ToupView x64 v3.7.4594 of the sample image is shown in Figure 2-4.

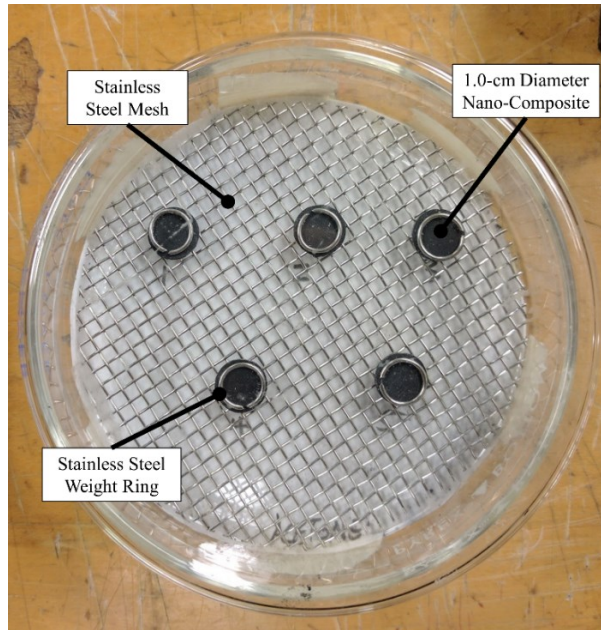


**Figure 2-3: Optical swelling measurement setup in glass petri dish**

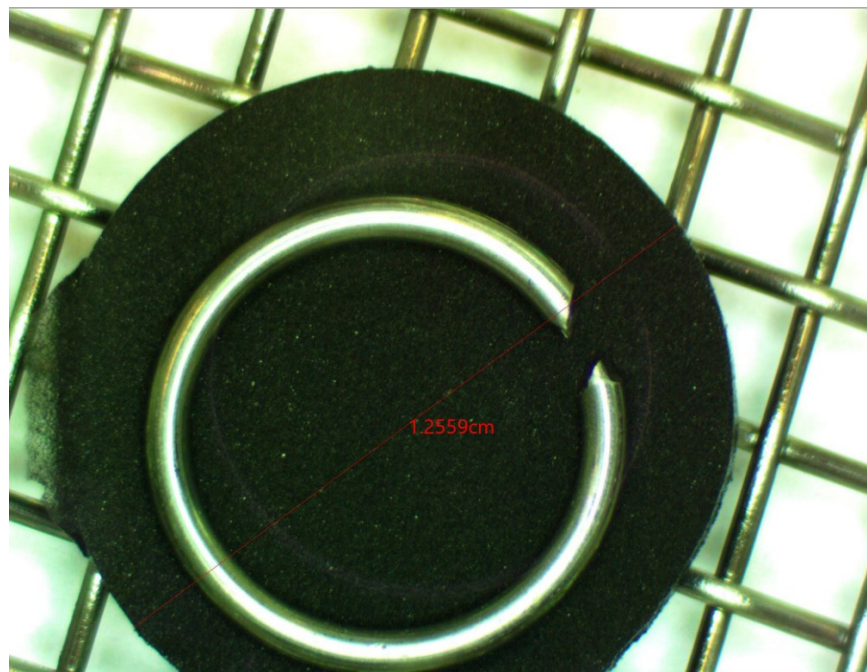


**Figure 2-4: Sample image measurement of 2% GNP/PDMS after 8 hours of submerged after 8 hours**

## **2.4 Electrical Conductivity Characterization**

Electrical conductivity test of nanocomposites was conducted in association with the University of Calgary Polymer Processing Group. Two electrode connectors with 90 V as the applied voltage were employed to measure the DC electrical conductivity of a rectangular sample (25 mm x 42 mm x 1 mm) of the nanocomposite. Due to the innate low conductivity of the nanocomposite, the measurements were conducted according to the ASTM 257-75 standard with a Keithley 6517A electrometer connected to a Keithley 8009 test fixture (Keithley instruments, Beaverton, OR).

## **2.5 Cross-Linking Density Characterization**

Cross-linking density characterization was gravimetrically completed. Using the 1.0 cm punch and hand press, 3-disk samples were cut and weighed. Similar to the swelling measurement setup, the three samples were placed in a petri dish on top of a stainless steel mesh. The disk samples were then submerged in toluene for 24 hours. The toluene would swell the polymer sample and flush the polymer network for any oligomers. The nanocomposite disks were then removed from the solution and dried under a fume hood for 24 hours, followed by drying under vacuum at 15 kPA and 100 °C for 1 hour. Mass measurements were taken after the final dry. The difference in mass between before and after swelling in toluene is the total uncross-linked polymer. Hence, the ratio between the after and before mass is the cross-linking percentage.

## **2.6 Digital Imaging**

### ***2.6.1 Cryo-microtoming***

Digital imaging of PDMS cross-section samples needed additional preparation due to the softness of the polymer matrix. A cryo-microtome was needed to section the PDMS nanocomposite. Cryo-microtoming was completed in association with the Cross-Cancer Institution

at the University of Alberta. A diamond knife with a microtome (LEICA Microsystems, EM UC6/EM FC6, Concord, ONT) was used for the sectioning the nanocomposite samples to a thickness around 80 nm. The parameters for Cyro-microtoming of GNP/PDMS samples were based on Ibrahim [113] and Camenzind [114] at 120 °C; however, during the sectioning, the material was still soft until temperature of -160 °C.

### **2.6.2 TEM**

TEM imaging was performed at the Cross Cancer Institute at the University of Alberta using a 200 kV JEOL JEM 2100 TEM (JEOL USA Inc, Peabody, MA) with GIF Filter. The imaged sample was prepared using the previous mentioned cryo-microtome technique with the focus of observing the cross-section of the specimen. TEM imaging was only completed on one sample specimen and was discontinued due to the low conductivity of the sample which resulted in poor image resolution.

### **2.6.3 SEM**

SEM imaging was completed at the NanoFab at the University of Alberta with the Zeiss Sigma FESEM w/ EDX & EBSD (Zeiss Canada, Toronto, ONT) microscope. No additional microtome process was needed to prepare bulk sample for SEM imaging. However, due to the insulative nature of the PDMS based nanocomposites, carbon coating was applied to the samples which introduced surface features that were inconsistent with the rest of the samples. The SEM imaging process was discontinued after the initial imaging of the NS/PDMS sample.

### **2.6.4 HIB**

HIB imaging was performed at the NanoFab at the University of Alberta with the Orion NanoFab HiM w/ Galion FIB (Zeiss Canada, Toronto, ONT). The imaging samples were prepared using the

previous cryo-microtome technique with the focus on observing the cross-section of the samples. HIB images were completed with both “charging” and “non-charging” effects with results discussed later section. HIB imaging was performed for all of the 1% and 4% carbon-filled PDMS based nanocomposite.

### **2.6.5 XRD**

X-ray diffraction characterization was completed in association with the Earth and Atmospheric Science Lab at the University of Alberta. A Rigaku XRD Ultimate IV with settings of Co/38 kV/38 mA (Rigaku American Corp., The Woodland, TX) was used for the XRD characterization. All samples were scanned from 10 to 180 degrees with a scanning rate of 2.00 degrees/min.

### **2.7 Tensile Testing**

Tensile testing of nanocomposites followed the standard of ASTM D638-14. The tensile samples of Type V, as shown in Figure 2-5, were produced from the same bulk sample from the swelling experiments and cut via water jet. Tensile testing was completed with MTS Synergie 300 (Eden Prairie, MIN, USA) controlling the tensile force until break. The strain of the test was measured by both the stroke length of the clamps and using an optical system. The tensile setup and optic system are shown in Figure 2-6. The stroke length measurement was completed via the TestWorks 4, and the optical measurement was completed via an open source software of OSM-Classic that was developed in University of Alberta. OSM-Classic calculates the strain on a sample by determining the change in distance between two high contrasting marks. The software utilizes two error functions to determine the positions of the two edges and directly measures the distance between them. OSM-Classic was used in publications of Raasch [115] and Ivey [116].



**Figure 2-5: Dog bog sample of Type V dimension of ASTM D638-14 with white paint marking for digital strain measurement**

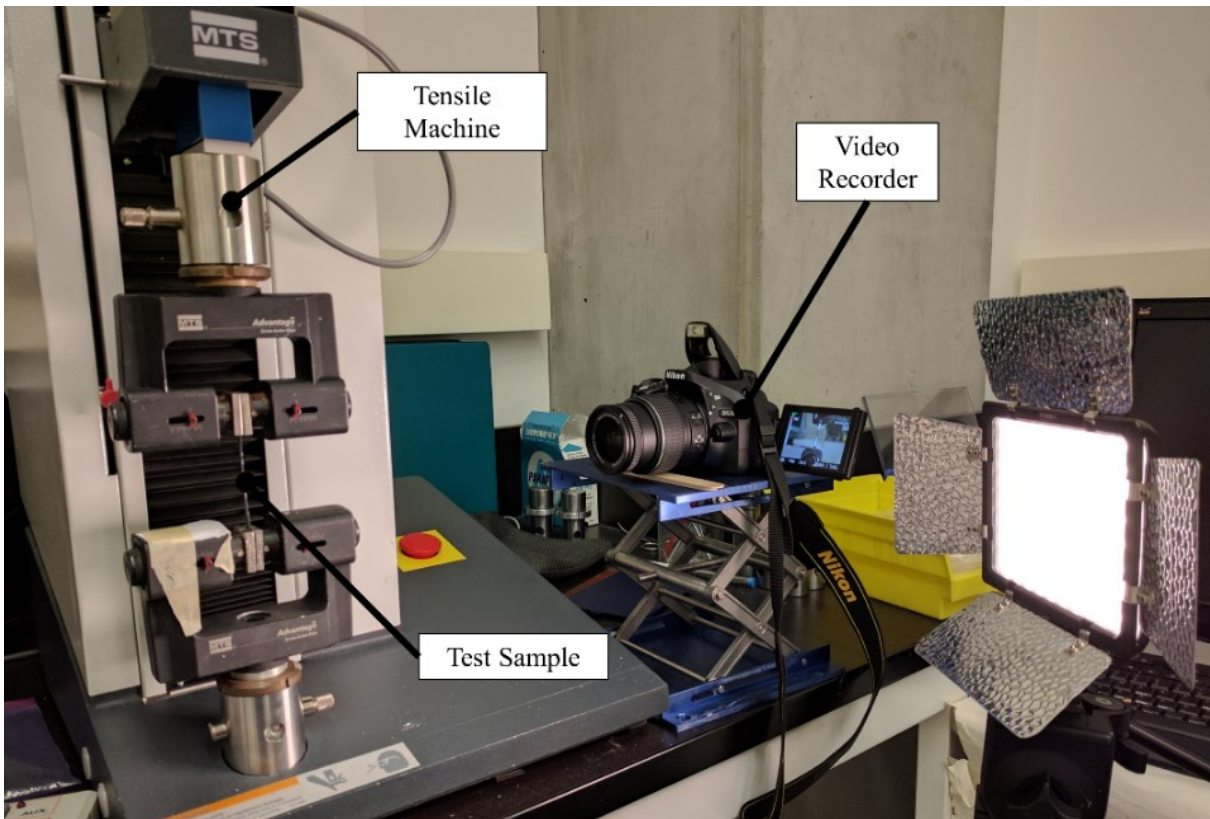


**Figure 2-6: Tensile Experiment setup with optical measurement system.**

## 3 EXPERIMENTAL RESULTS & DISCUSSION

### 3.1 Swelling Dimensional Characterization

Prior to the swelling experiments of nanocomposites, a baseline swelling measurement of un-filled PDMS (i.e. 0% filled PDMS or pure PDMS) was conducted. The equilibrium swelling ratio – defined as the diameter of swelled nanocomposite samples to non-swelled nanocomposite samples – were found to be 1.08, 1.30, and 1.25 respectively for samples immersed in acetone, chloroform, and toluene. Lee *et al.* had swelling ratio results in the same swelling agents of 1.06, 1.39, and 1.31 [102]. The repeatability of each sample was high among all samples, that is, all sample points had a standard deviation of approximately 0.01 except for the 0-hour time stamp. The higher standard deviation at the 0-hour time stamp was attributed to the transient swelling process. The five trials at 0-hour images were captured sequentially; therefore, there was an elapsed time of approximately 1 minute between the first and fifth sample. Though small, the elapsed time caused an increase of 0.133 in swelling ratio between the first, 1.04, and the fifth, 1.188, samples of pure PDMS submerged in chloroform.

#### 3.1.1 Graphene Nano-Platelets

Transient and steady-state results for GNP/PDMS were graphed and are shown in Figures 3-1 to 3-4. Each data point consists of five repeated trial measurements. The objectives of transient graphs were to confirm the onset of steady-state conditions and to observe any abnormality from the typical transient trend. In Figures 3-1 to 3-3 the transient graph of GNP/PDMS swelled by acetone, chloroform and toluene, showed that a steady state condition was reached around the 4-hour mark. This steady state time was 3 hours longer compared to that of Lee *et al.* [102]. The overall trend of transient swelling for chloroform and toluene followed a typical transient process;

however, the trend of transient swelling in acetone exhibited a decrease after an initial peak and minor fluctuation (Figure 3-1). These effects were assumed to be caused by experimental error due to the small fluctuations.

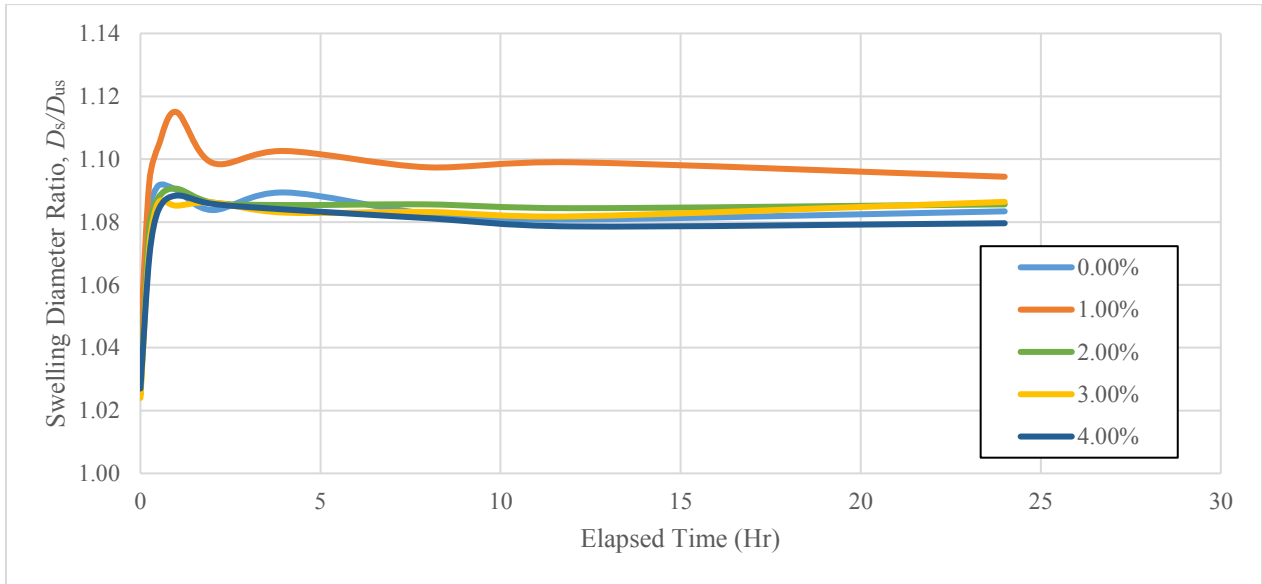


**Figure 3-1: Transient swelling ratios of GNP/PDMS with 0%-4% filler volume in acetone**

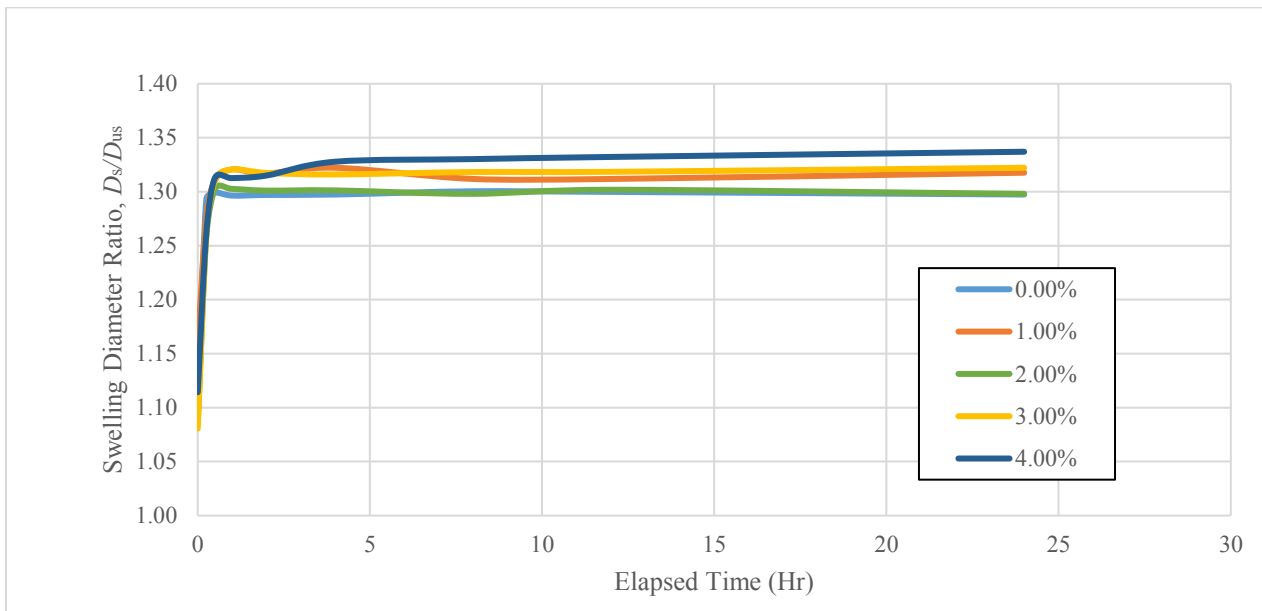


**Figure 3-2: Transient swelling ratios of GNP/PDMS with 0%-4% filler volume in chloroform**

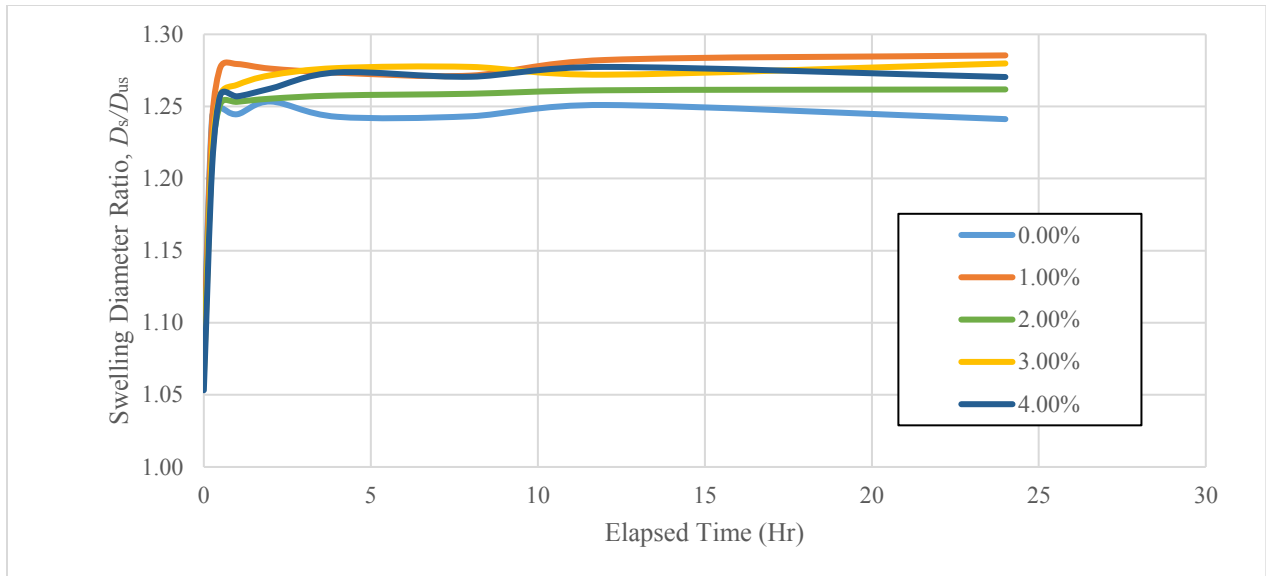


**Figure 3-3: Transient swelling ratios of GNP/PDMS with 0%-4% filler volume in toluene**

The equilibrium swelling ratio was computed and is displayed in both Figure 3-4 and Table 3-1. The data shows an overall increase in swelling percentage as the GNP-filler volume fraction increased for nanocomposites swelled with chloroform and toluene, but not acetone. The overall increase in swelling ratio as GNP volume increased was opposite in trend compared to previous studies with regards to hydrogels. In addition, carbon-based nano-fillers generally increase the swelling resistivity. Even though a decrease in swelling ratio occurred at a volume fraction of 2%, the small decrease of 0.01 for chloroform and 0.02 for toluene can be considered experimental error; hence, the overall trend was still increasing. Acetone as a swelling agent was unique in that the swelling of PDMS was independent of filler volume and the swelling ratio was constant at 1.084.

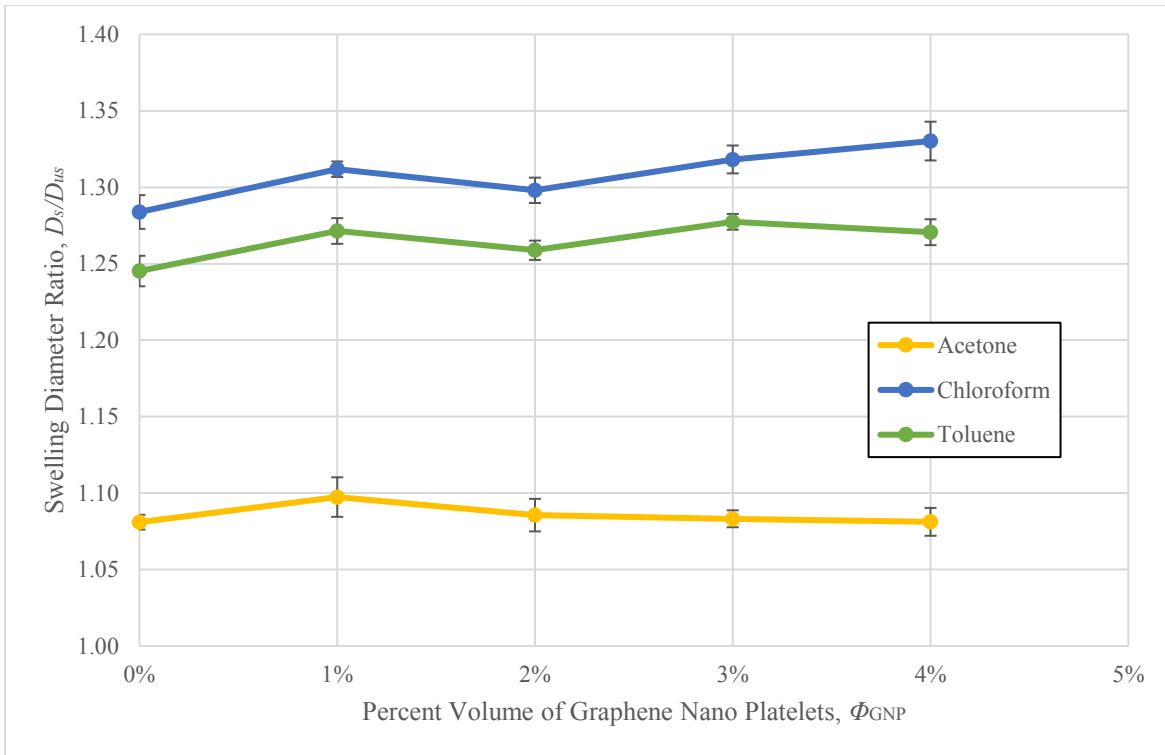


**Figure 3-4: Equilibrium (12 hr) swelling ratios of GNP/PDMS with corresponding filler volume percentage**

**Table 3-1: Equilibrium swelling ratios for GNP/PDMS**

Percent Filler Volume	Percent Filler Mass	Swelling Ratio w/ Acetone, $D_s/D_{us}$	Swelling Ratio w/ Chloroform, $D_s/D_{us}$	Swelling Ratio w/ Toluene, $D_s/D_{us}$
0%	0.0%	1.078 +/-0.0048	1.283 +/-0.0110	1.242 +/-0.0100
1%	2.2%	1.099 +/-0.0129	1.312 +/-0.0051	1.282 +/-0.0084
2%	4.4%	1.084 +/-0.0106	1.302 +/-0.0083	1.261 +/-0.0063
3%	6.6%	1.082 +/-0.0055	1.318 +/-0.0091	1.272 +/-0.0052
4%	8.8%	1.079 +/-0.0091	1.332 +/-0.0127	1.277 +/-0.0085

The equilibrium swelling ratio was used to validate the Kraus equation and is shown in Figure 3-5.

Since the study used an optical swelling measurement, only one dimension of the sample was

measured; hence, the swelling volume was extrapolated from the equilibrium swelling diameter measurements with the following derivation:

$$\frac{V_{\text{unfilled}}}{V_{\text{filled}}} = \frac{\pi \left( \frac{D_{\text{unfilled}}}{2} \right)^2 t_{\text{unfilled}}}{\pi \left( \frac{D_{\text{filled}}}{2} \right)^2 t_{\text{filled}}} \quad (6)$$

However,  $D_{\text{unfilled}} = \frac{D_{s,0\%}}{D_{us}} D_{us}$ ,  $D_{\text{filled}} = \frac{D_{s,x\%}}{D_{us}} D_{us}$ ,  $t_{\text{unfilled}} = \frac{D_{s,0\%}}{D_{us}} t_{us}$  and

$$t_{\text{filled}} = \frac{D_{s,x\%}}{D_{us}} t_{us}$$

$$\text{Therefore, } \frac{V_{\text{unfilled}}}{V_{\text{filled}}} = \left( \frac{D_{s,0\%}}{D_{us}} \right)^3 \left( \frac{D_{s,x\%}}{D_{us}} \right)^3 \quad (7)$$

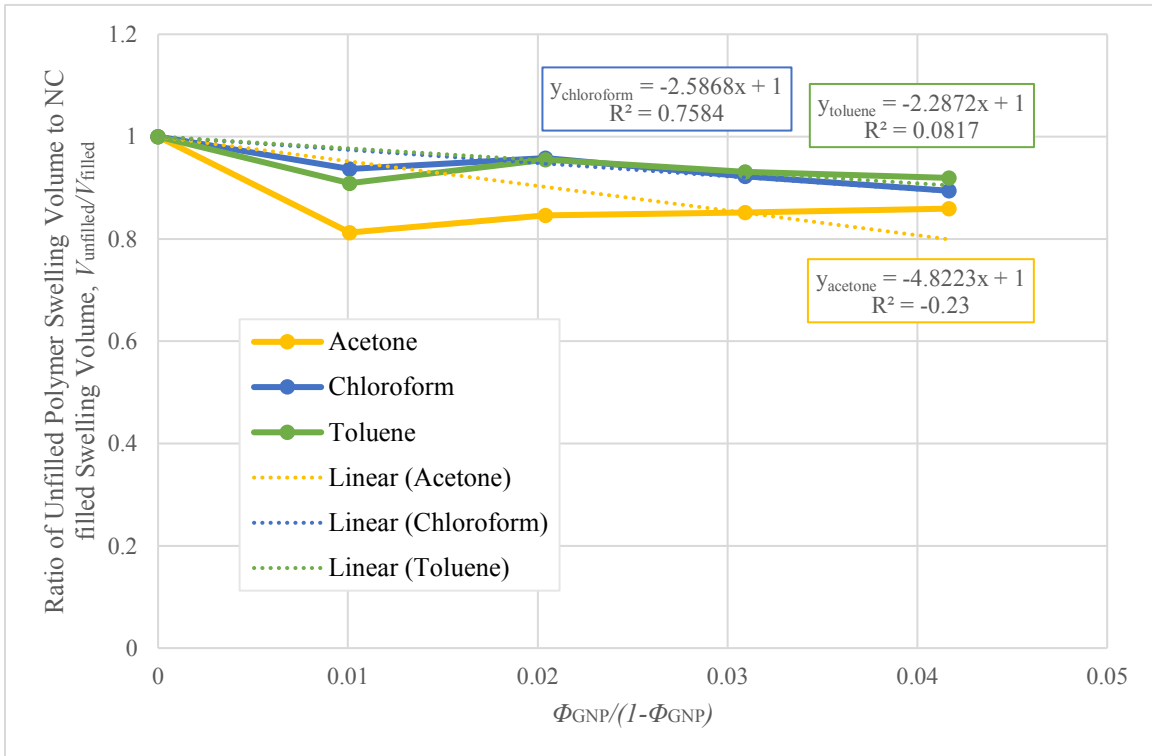


**Figure 3-5: Equilibrium swelling data of GNP/PDMS correlated to Kraus equation**

The equilibrium results of GNP/PDMS for swelling in acetone, chloroform, and toluene did not correlate with the Kraus equation with  $R^2$ -values for a linear correlation being -0.23, 0.75, and 0.08. However, the predicted Kraus equation assumed the adhesion between the filler and polymer. If adhesion was not fully present [38], Kraus predicts the swelling of nanocomposite as

$$\frac{V_{\text{filled}}}{V_{\text{unfilled}}} = \frac{V_{\text{unfilled}}^{-1} - \phi}{1 - \phi} \quad (8)$$

Table 3-2 displays the comparison between the predicted swelling ratio with Equation (8) and the experimental results. The smallest percent difference between the predicted and experimental swelling ratio was 29%.

**Table 3-2: Equilibrium swelling ratios of GNP/PDMS comparison between Kraus prediction and experiment results**

Percent Filler Volume	Swelling Ratio Predicted w/ Equation (8)			Swelling Ratio from Experiments		
	Acetone	Chloroform	Toluene	Acetone	Chloroform	Toluene
0%	0.779	0.925	0.803	1.078	1.283	1.242
1%	0.777	0.924	0.801	1.099	1.312	1.282
2%	0.774	0.924	0.799	1.084	1.302	1.261
3%	0.772	0.923	0.797	1.082	1.318	1.272
4%	0.770	0.922	0.795	1.079	1.332	1.277

### 3.1.2 Carbon Black

Transient and steady-state swelling ratios for CB/PDMS were calculated and are shown in Figures 3-6 to 3-9. The baseline swelling ratio of pure PDMS was different from previous GNP/PDMS experiments due to the change in co-solution used with the in-situ polymerization process. For GNP/PDMS, cyclohexane was used as the co-solution, while isopropanol was used

for the manufacture of CB/PDMS. The baseline swelling ratio of 0% PDMS for isopropanol co-solution cured samples were 1.081, 1.300, and 1.251 for respective swelling agents of acetone, chloroform, and toluene. The results were similar to the baseline swelling ratios of GNP/PDMS and Lee *et al.* [102]. Standard deviations were also similar to that of the GNP/PDMS data, with all errors being below 0.03.

For the transient swelling ratio, the objective was again to determine equilibrium time. Similar to the GNP filled nanocomposites, a steady state swelling ratio for CB filled samples were reached around the 4-hour mark. This steady state time was a longer than what was stated by Lee *et al.*, where typically equilibrium swelling was reached within 1 hour [102]. Similar to the GNP filled nanocomposites, the chloroform and toluene transient swelling results appeared to follow a standard transient process, but, in the case of acetone, the same visible decrease presented itself as time prolonged.

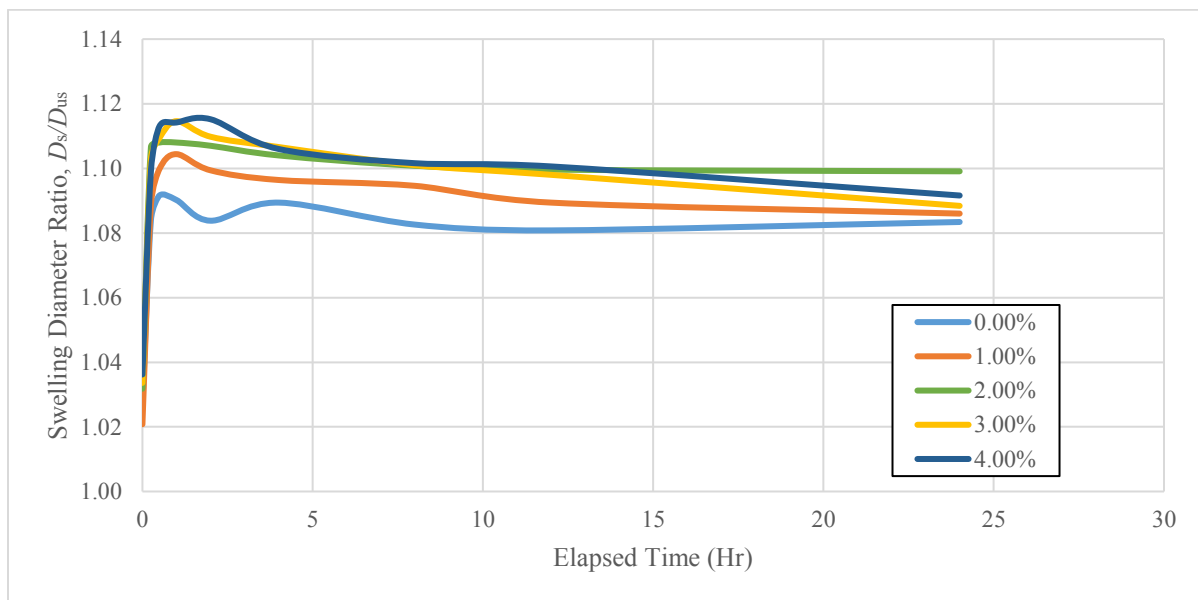


**Figure 3-6: Transient swelling ratios of CB/PDMS with 0%-4% filler volume in acetone**

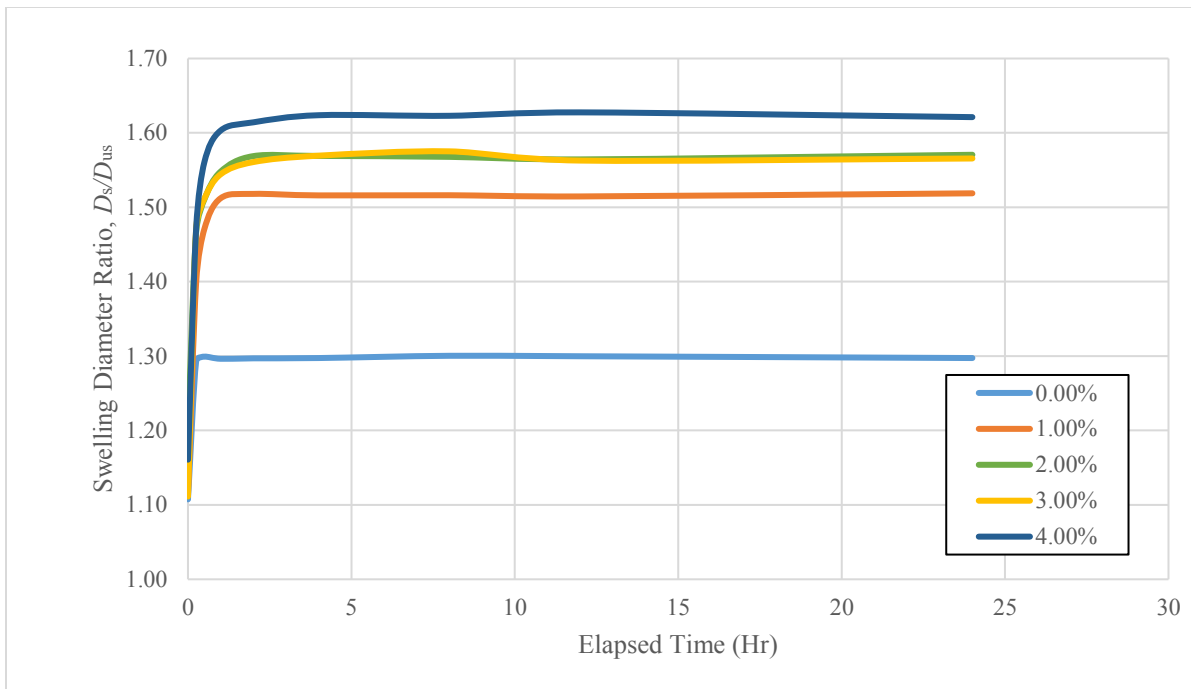


**Figure 3-7: Transient swelling ratios of CB/PDMS with 0%-4% filler volume in chloroform**

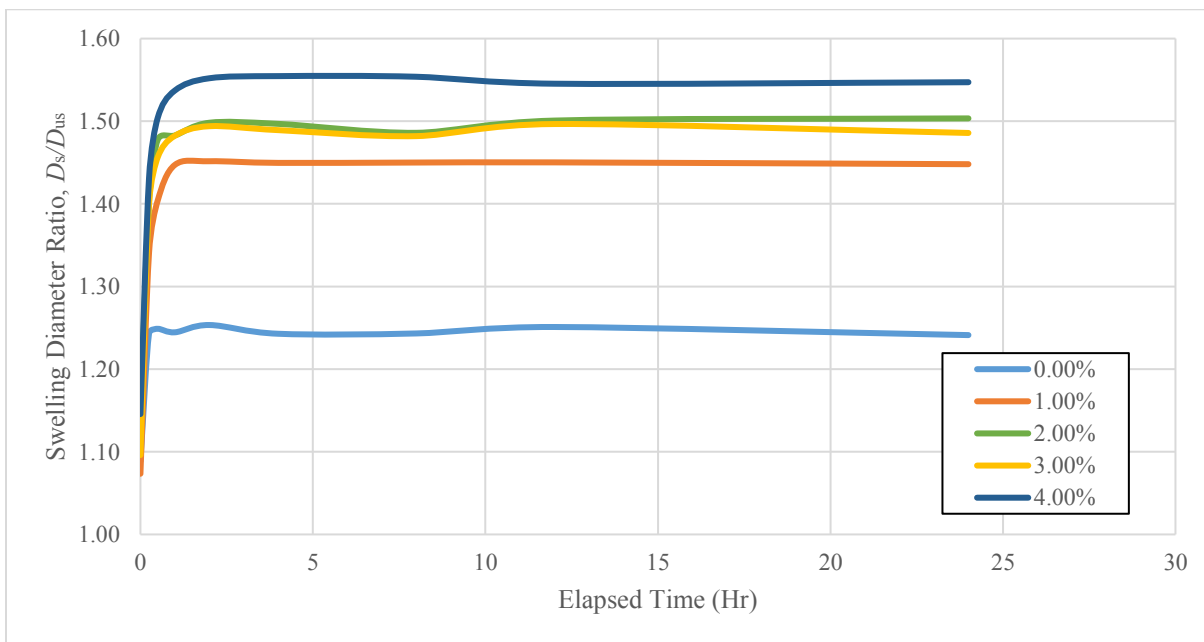


**Figure 3-8: Transient swelling ratios of CB/PDMS with 0%-4% filler volume in toluene**

The equilibrium swelling ratios depicted in Figure 3-9 and Table 3-3 show that the swelling ratio of CB/PDMS in acetone remained at 109.3% and did not change with increasing filler volume

fraction. However, CB/PDMS in the swelling agents chloroform and toluene exhibited a significant change, that is, the swelling ratio increased by 25.2% and 23.6% respectively from 0% to 4% volume fraction CB. For comparison, corresponding values for GNP/PDMS were only 3.8% and 2.8% in swelling agents chloroform and toluene, respectively. It should be mentioned that there is a difference between the percent mass content between GNP ( $\rho = 2.2\text{g/cm}^3$ ) and CB ( $\rho = 1.8\text{ g/cm}^3$ ). However, by accounting for the density different at approximately 7% mass content – 6.6% mass of GNP and 7.2% mass of CB, the swelling ratio had a percent difference of 26% in chloroform and 25% in toluene.

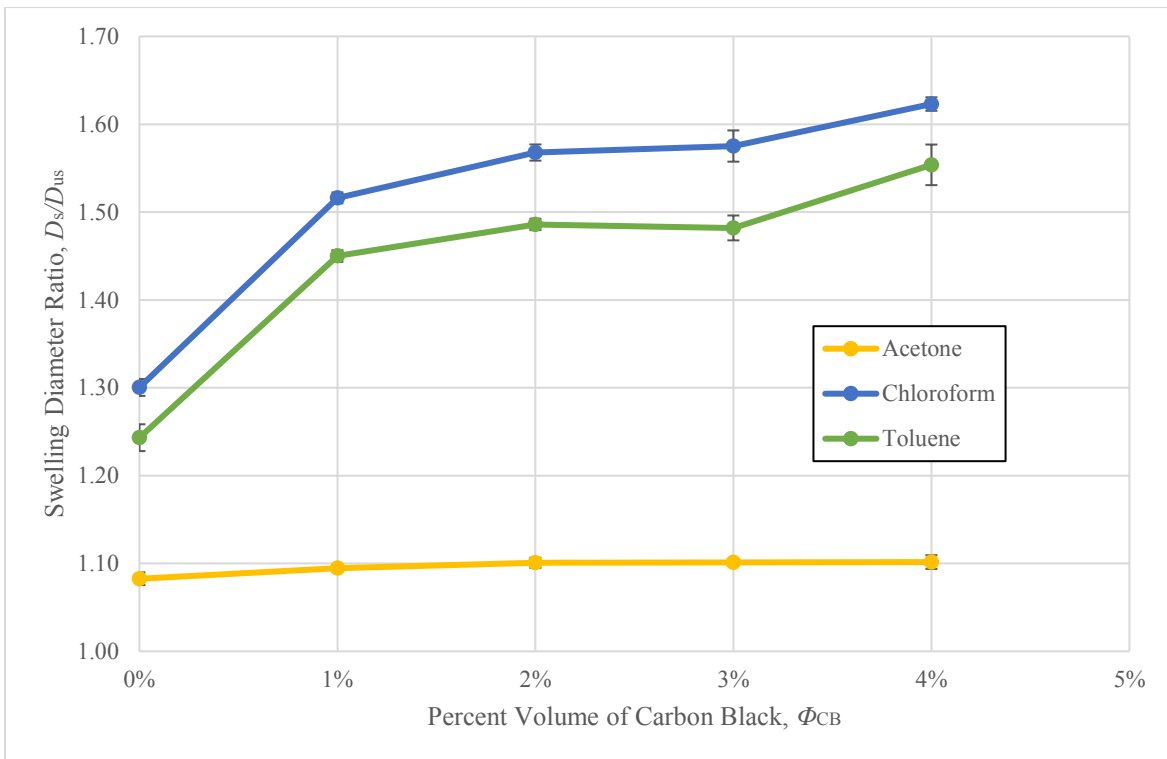


**Figure 3-9: Equilibrium (12hrs) swelling ratios of CB/PDMS with corresponding volume filler percentage**

**Table 3-3: Equilibrium swelling ratios of CB/PDMS**

<b>Percent Filler Volume</b>	<b>Percent Filler Mass</b>	<b>Swelling Ratio w/ Acetone, <math>D_s/D_{us}</math></b>	<b>Swelling Ratio w/ Chloroform, <math>D_s/D_{us}</math></b>	<b>Swelling Ratio w/ Toluene, <math>D_s/D_{us}</math></b>
0%	0.0%	1.081 +/-0.079	1.300 +/-0.096	1.251 +/-0.0069
1%	1.8%	1.089 +/- 0.034	1.515 +/-0.062	1.450 +/-0.0066
2%	3.6%	1.100 +/- 0.057	1.564 +/-0.092	1.501 +/-0.0065
3%	5.4%	1.098 +/- 0.022	1.563 +/-0.178	1.497 +/-0.0142
4%	7.2%	1.101 +/- 0.078	1.628 +/-0.077	1.545 +/-0.0231

The equilibrium results of CB/PDMS for swelling agents of acetone, chloroform, and toluene were again used to validate the Kraus equation. Recall that the Kraus equation was derived from CB filled vulcanizates; hence, the CB/PDMS was the closest composition in this study to the equation's original derivation. However, as seen in Figure 3-10, there was no linear fitted correlation to the Kraus equation with  $R^2$ -value of 0.73, 0.45, and 0.48. In addition, the non-adhesive Kraus equation (8) was used to predict the swelling ratio of CB/PDMS; however, shown in Table 3-4, the results vary drastically with the smallest percent difference between the predicted and experimental value of 31%.

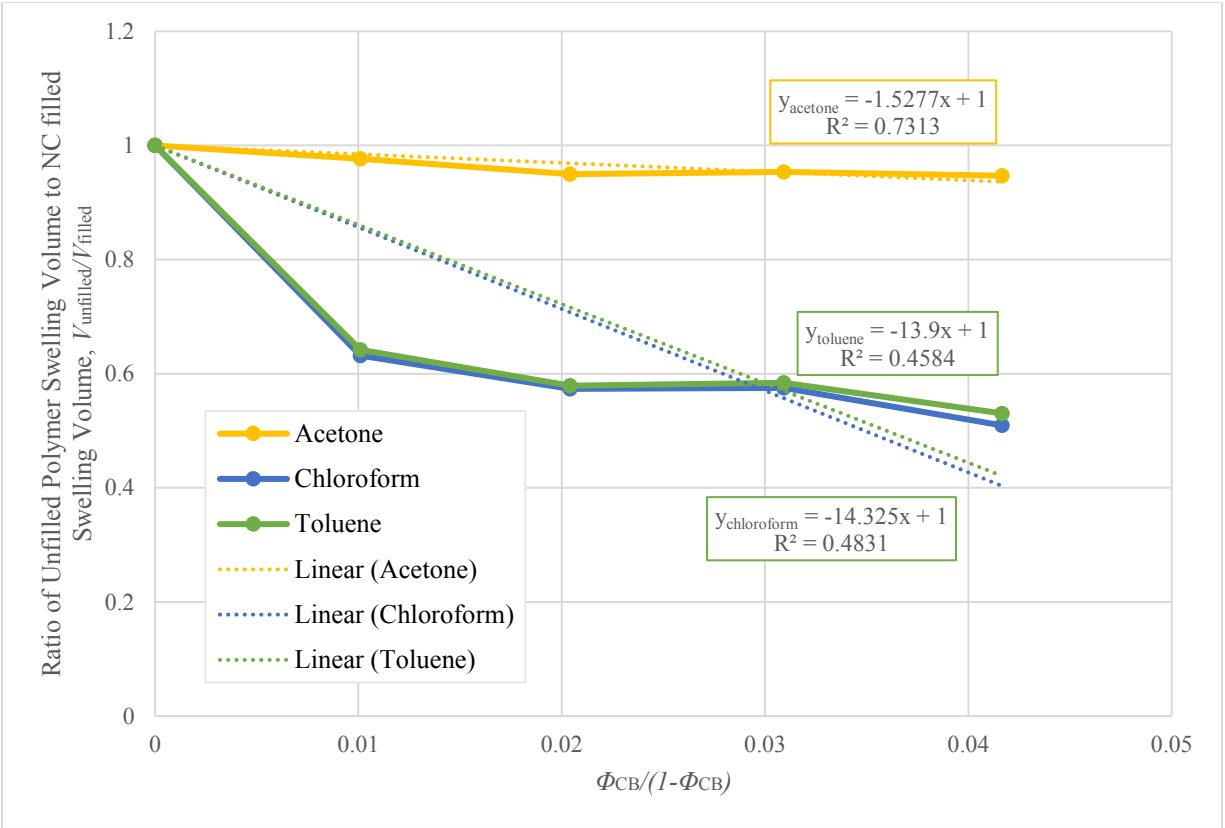


Figure 3-10: Equilibrium swelling data of CB/PDMS correlated to Kraus equation

Table 3-4: Equilibrium swelling ratios of CB/PDMS comparison between Kraus predictions and experiment results

Percent Volume Filler	Swelling Ratio Predicted w/ Equation (8)			Swelling Ratio of Experimentation		
	Acetone	Chloroform	Toluene	Acetone	Chloroform	Toluene
0%	0.780	0.914	0.801	1.081	1.300	1.251
1%	0.778	0.913	0.798	1.089	1.515	1.450
2%	0.776	0.912	0.796	1.100	1.564	1.501
3%	0.773	0.911	0.794	1.098	1.563	1.497
4%	0.771	0.910	0.792	1.101	1.628	1.545

### 3.1.3 Graphene Nano-Scrolls

Steady-state and transient swelling results for NS/PDMS were graphed and are shown in Figures 3-11 to 3-15. With NS produced by immersing GNP in isopropanol, the NS/PDMS samples were made in the same manufacture process as the GNP/PDMS with the exception of using isopropanol as the co-solution in the in-situ polymerization process. Therefore, the baseline swelling ratio 0% PDMS was the same as the CB/PDMS. Similar to the GNP/PDMS, each data points consist of five repeated trials. The standard deviations were also similar to those of the GNP/PDMS tests, with all errors being below 0.03.

Similar to the other transient swelling results, the transient data for NS/PDMS showed that swelling equilibrium was reached at around 4 hours. Both the chloroform and toluene transient swelling results appear to follow a typical transient process, but the acetone presented a visible decrease as time progressed.

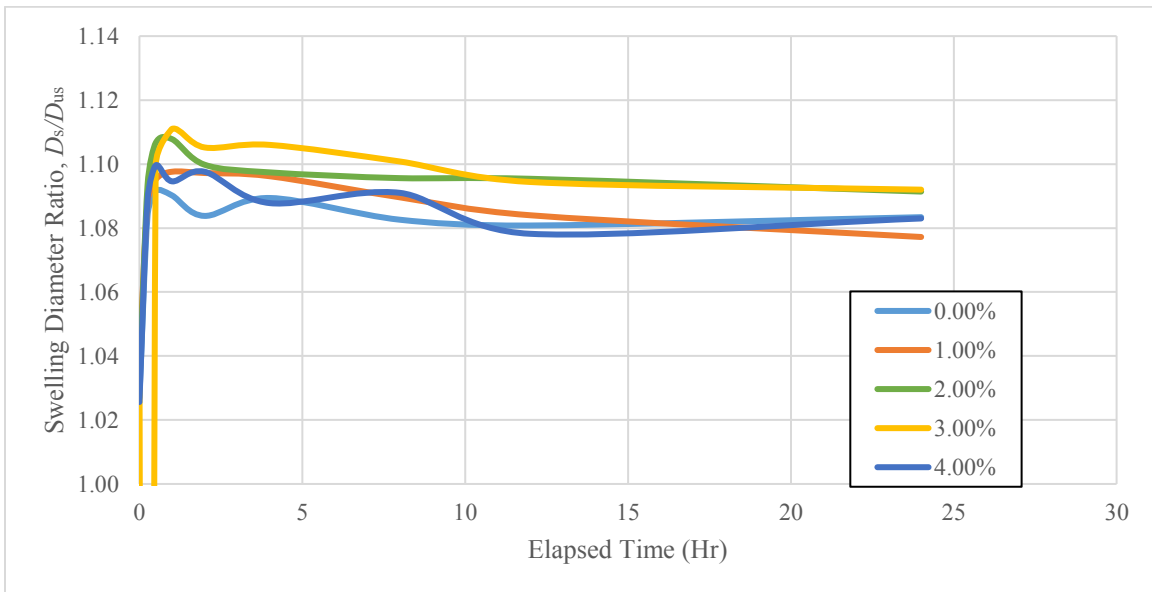


**Figure 3-11: Transient swelling ratios of NS/PDMS with 0%-4% filler volume in acetone**

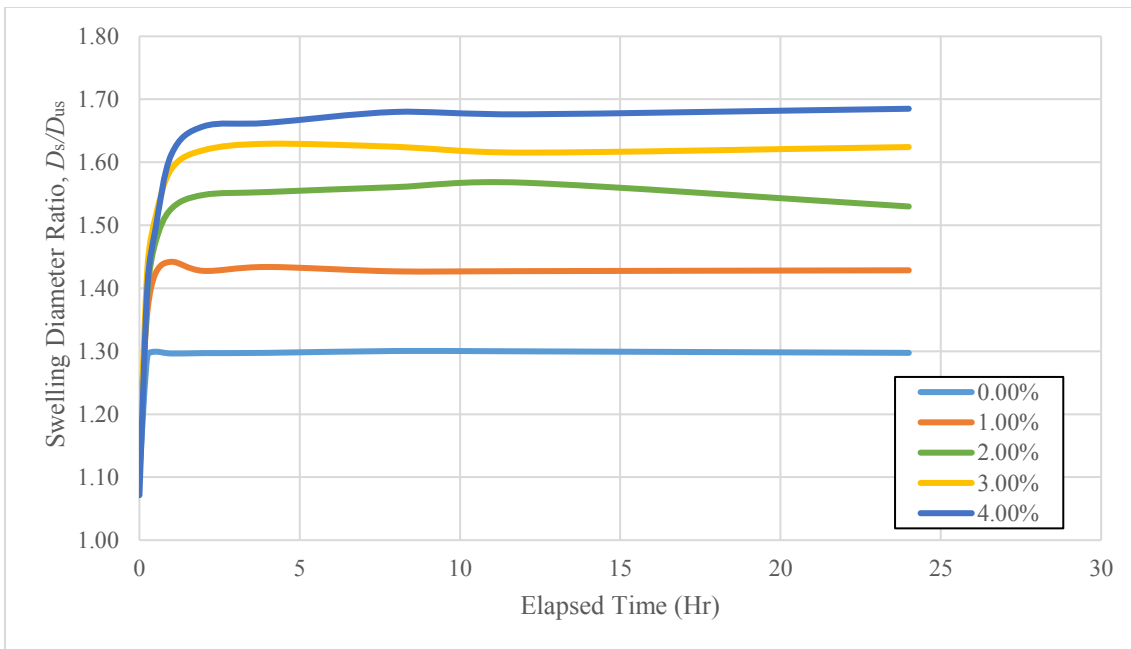


**Figure 3-12: Transient swelling ratios of NS/PDMS with 0%-4% filler volume in chloroform**

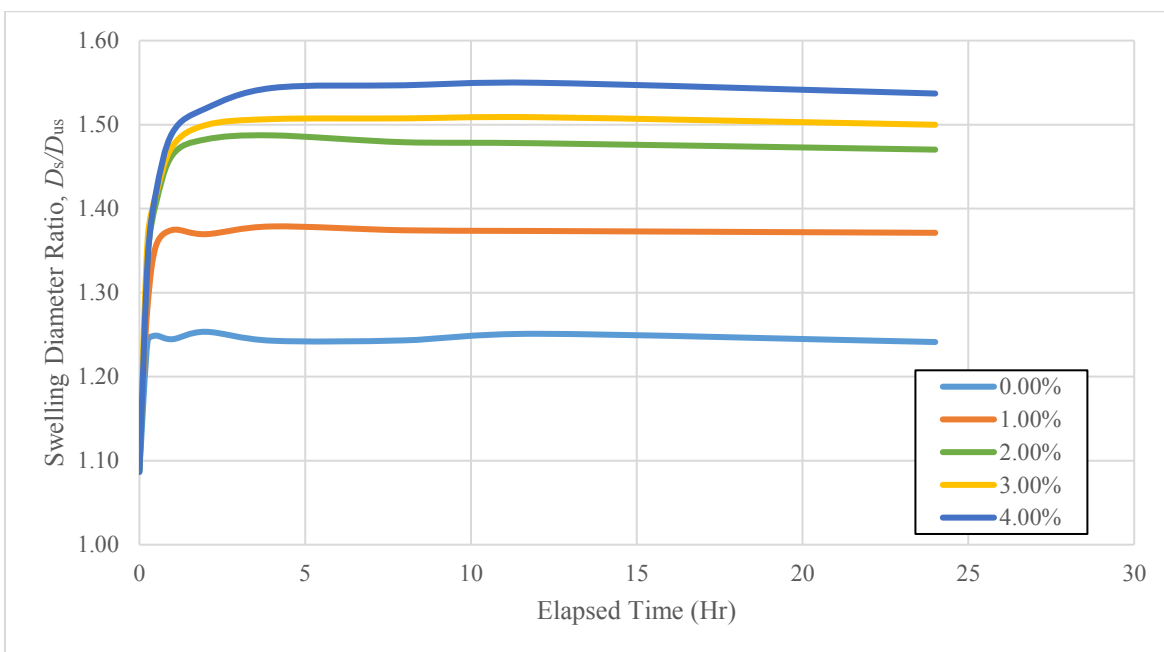


**Figure 3-13: Transient swelling ratios of NS/PDMS with 0%-4% filler volume in toluene**

The equilibrium data in Figure 3-14 and Table 3-5 indicates that an increase in filler volume percentage caused an increase of swelling ratio with swelling agents of toluene and chloroform.

However, similar to both GNP/PDMS and CB/PDMS, the swelling of NS/PDMS remained at

1.086 and did not change as filler volume increased when immersed acetone. With the swelling of NS/PDMS, a linear trend appears to be present between the filler volume and the swelling ratio. This trend was not seen in either the GNP or the CB based composites. The overall swelling ratio of NS/PDMS increased respectively by 28.9% and 22.8% from 0% to 4% volume fraction in chloroform and toluene. These values were similar to that of CB/PDMS which increased by 25.2% and 23.6%, yet differed from its parent filler of GNP/PDMS which increased by only 3.8% and 2.8%.

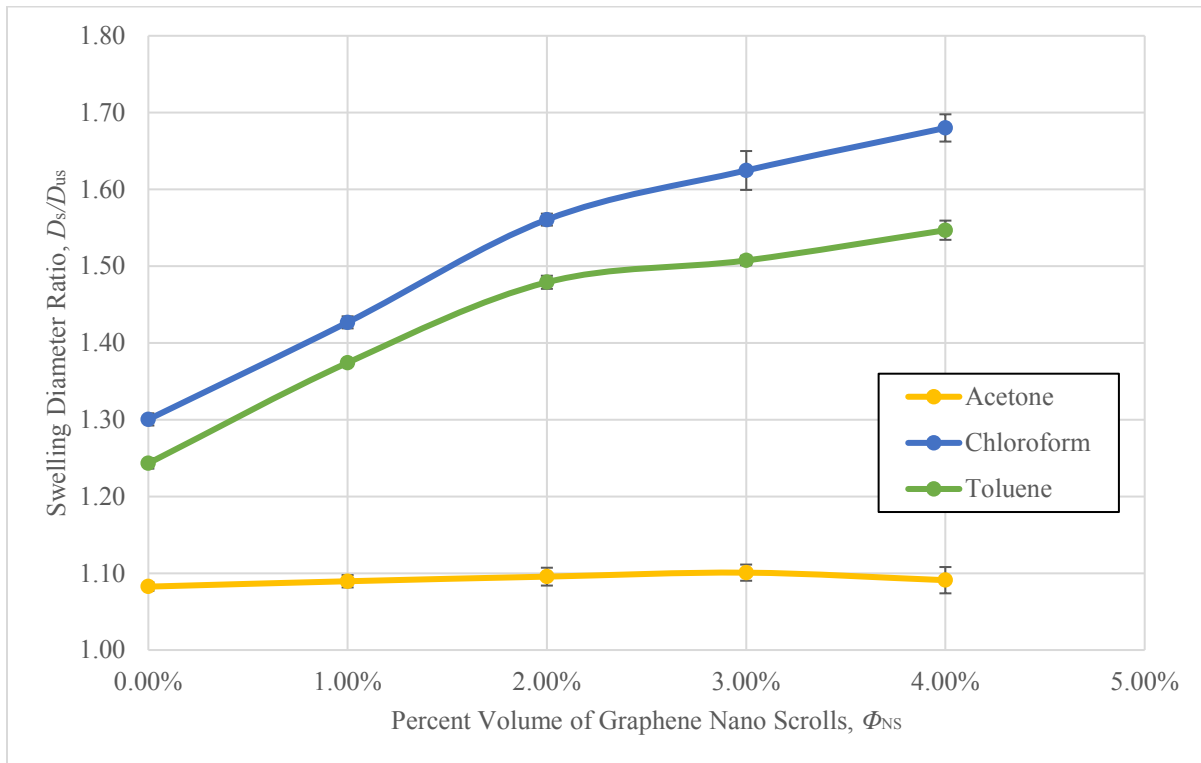


**Figure 3-14: Equilibrium (24hrs) swelling ratios of NS/PDMS with corresponding volume filler percentage**

**Table 3-5: Equilibrium swelling results for NS/PDMS nanocomposite**

<b>Percent Filler Volume</b>	<b>Percent Filler Mass</b>	<b>Swelling Ratio w/ Acetone, <math>D_s/D_{us}</math></b>	<b>Swelling Ratio w/ Chloroform, <math>D_s/D_{us}</math></b>	<b>Swelling Ratio w/ Toluene, <math>D_s/D_{us}</math></b>
0%	0.0%	1.081 +/-0.079	1.300 +/-0.096	1.251 +/- 0.069
1%	2.2%	1.084 +/-0.095	1.427 +/-0.120	1.373 +/- -0.070
2%	4.4%	1.095 +/-0.067	1.568 +/-0.233	1.470 +/-0.085
3%	6.6%	1.094 +/-0.102	1.615 +/-0.243	1.500 +/-0.062
4%	8.8%	1.078 +/-0.080	1.676 +/-0.252	1.537 +/-0.125

The equilibrium results of NS/PDMS nanocomposites swelling were again used in conjunction with the Kraus equation. Compared to the previous GNP and CB nanocomposites, the NS/PDMS submerged in chloroform and toluene fitted the Kraus equation more closely. As shown in Figure 3-15, the linear chloroform and toluene curve fits resulted in  $R^2$ -values of 0.82 and 0.77, respectively. However, the linear fit for the acetone case was still off with an  $R^2$  value of -0.15. The non-adhesive Kraus equation (8) was also used to predict the value of the equilibrium swelling ratio and compared to the experimental results. Shown in Table 3-6, the predicted versus experimental results had a minimal of 33% difference, which indicated that no correlation exists between the non-adhesive Kraus model to the experimental results.

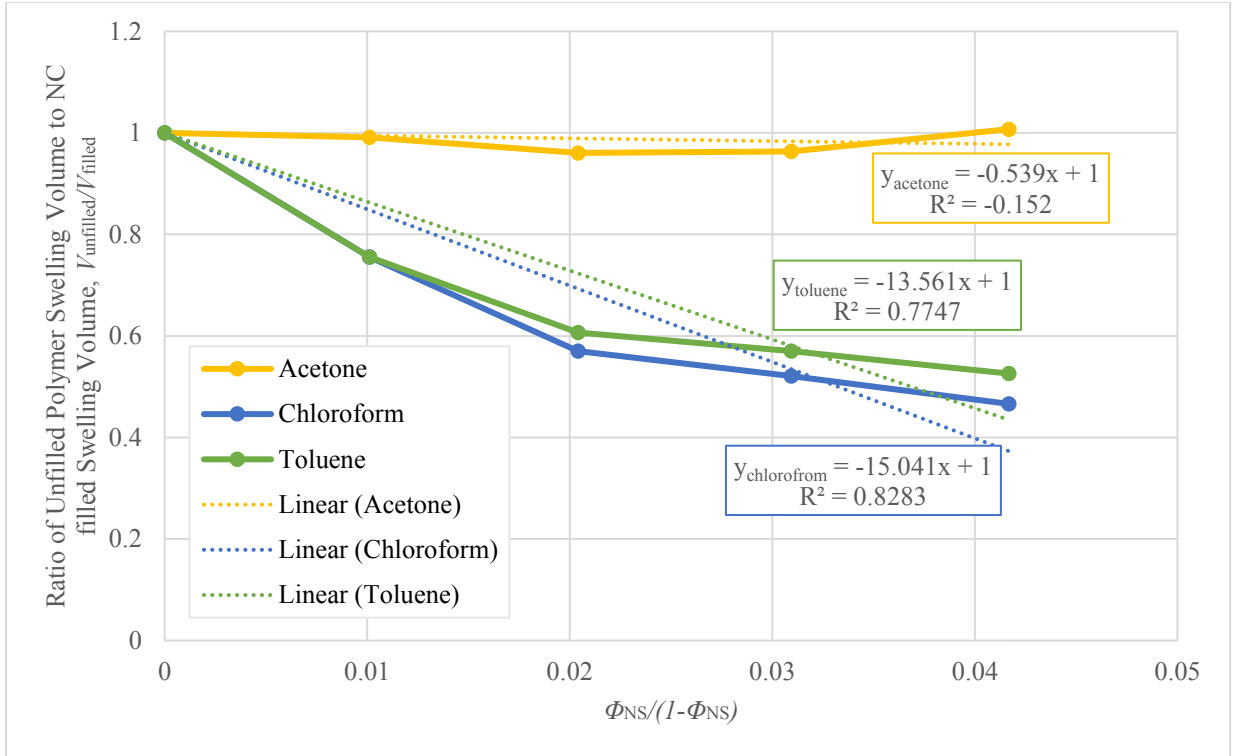


**Figure 3-15: Equilibrium swelling data of NS/PDMS correlated to Kraus equation**

**Table 3-6: Equilibrium swelling ratios of CB/PDMS comparison between Kraus prediction and experiment results**

Percent Volume Filler	Swelling Ratio Predicted w/ Equation (8)			Swelling Ratio of Experimentation		
	Acetone	Chloroform	Toluene	Acetone	Chloroform	Toluene
0%	0.769	0.924	0.804	1.081	1.300	1.251
1%	0.767	0.923	0.802	1.084	1.427	1.373
2%	0.765	0.922	0.800	1.095	1.568	1.470
3%	0.762	0.921	0.798	1.094	1.615	1.500
4%	0.760	0.921	0.796	1.078	1.676	1.537

The transient graphs indicated that swelling equilibrium was reached around the 4-hour mark, and the morphology of the nano-filler did not affect the steady state time. In regards to morphology, the equilibrium results of the initial three carbon-based filler nanocomposites of GNP/PDMS,

CB/PDMS and NS/PDMS displayed conflicting results with respect to the effect of filler morphology on swelling of PDMS nanocomposite. CB/PDMS and NS/PDMS showed significant and similar equilibrium swelling ratios in terms of total increase for the swelling agents of chloroform and toluene, but differed in overall trend and incremental increases. In contrast, GNP/PDMS showed almost no increase in swelling ratio as filler volume increased. All volume percentages of all three carbon-based filler nanocomposites, as well as the original polymer, exhibited the same equilibrium swelling for swelling in acetone.

While the initial swelling experiments were conducted to explore effects that filler morphologies have on nanocomposite swelling, one peculiar finding emerged: the equilibrium results for nanocomposites cured with isopropanol as the co-solution for in-situ polymerization were similar to each other and significantly different than for nanocomposites cured with cyclohexane. This observation motivated studying alternative co-solution cured nanocomposites to explore the effect co-solution on nanocomposites swelling.

#### ***3.1.4 Pure PDMS with Different Manufacturing Solutions***

Prior to characterizing the effect of different co-solutions on the swelling of nanocomposites, the baseline swelling ratio of pure PDMS was re-established with alternative co-solutions. All pure PDMS samples were made with the same manufacturing process as the nanocomposites without the addition of the nano-fillers i.e. all pure PDMS were processed with co-solution, mechanically stirred, and sonicated. Theoretically, the co-solution only breaks the intermolecular bonds of the PDMS part A resin. Hence, once co-solution is fully evaporated, the PDMS resin behaves with no modifications in its monomer structure. However, the similarity in swelling ratio between the CB/PDMS experiments and NS/PDMS experiments, which differs from GNP/PDMS experiments, indicated that the co-solution dissolved the PDMS resins had potential impact.

The newly established baseline swelling ratio of pure PDMS was subjected to four different co-solutions: toluene, cyclohexane, chloroform and isopropanol. Summarized in Table 3-7, the swelling ratio of pure PDMS with swelling agent chloroform and cured with co-solution of chloroform, toluene, cyclohexane, and isopropanol were respectively 1.330, 1.285, 1.283 and 1.300. The swelling ratio of pure PDMS swelling in toluene cured with co-solution of chloroform, toluene, cyclohexane, and isopropanol were respectively 1.301, 1.243, 1.242 and 1.251. The nanocomposite cured with co-solution of isopropanol showed a higher swelling ratio of 1.300 and 1.251 in the respective swelling agent of chloroform and toluene. However, this increase does not explain the significant difference between the previous the swelling ratio between CB/PDMS and GNP/PDMS or NS/PDMS and GNP/PDMS. Lastly, the pure PDMS cured with the co-solution of chloroform showed the largest increase in swelling out of the four with results of 1.330 and 1.301 with swelling agents of chloroform and toluene. The chloroform co-solution cured samples were the closest to that of Lee *et al.* with their results of 1.39 and 1.31.

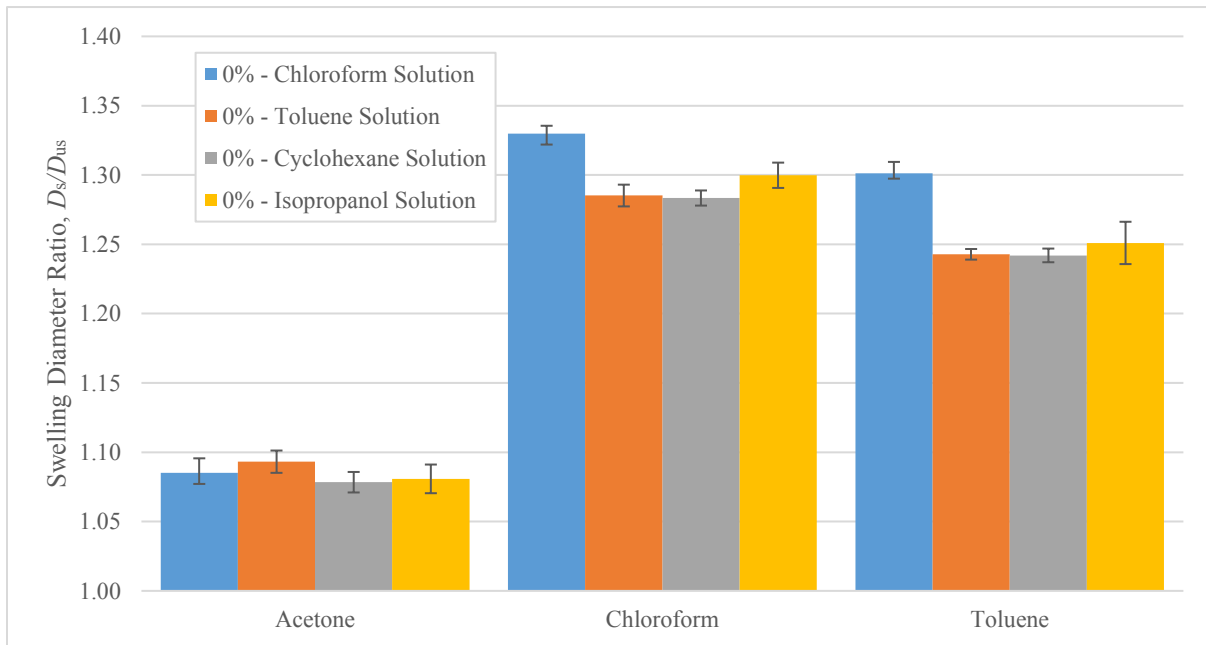


**Figure 3-16: Equilibrium swelling ratios for various pure PDMS curing parameter**

**Table 3-7: Equilibrium swelling ratios for NS/PDMS nanocomposites**

Type of Co-solution	Swelling Ratio w/ Acetone, $D_s/D_{us}$	Swelling Ratio w/ Chloroform, $D_s/D_{us}$	Swelling Ratio w/ Toluene, $D_s/D_{us}$
0% - Chloroform Solution	1.085 +/-0.089	1.330 +/-0.170	1.301 +/-0.093
0% - Toluene Solution	1.093 +/-0.082	1.285 +/-0.052	1.243 +/-0.061
0% - Cyclohexane Solution	1.078 +/-0.048	1.283 +/-0.110	1.242 +/-0.100
0% - Isopropanol Solution	1.081 +/-0.079	1.300 +/-0.096	1.251 +/- 0.069

From the swelling results of alternative co-solution cured pure PDMS, the co-solution showed small effects on the swelling of PDMS. Solution parameter of polarity, Hildebrand parameter, surface energy and surface tension are presented in Table 3-8 to help identify the cause of the increase. No solution parameter clearly indicates the pattern of highest to the lowest swelling ratio of co-solutions chloroform, isopropanol, toluene, and cyclohexane. Cyclohexane has the lowest polarity, but the swelling ratio was similar to that of toluene. Isopropanol has the highest Hildebrand parameter, but was only second in terms of swelling percentage. Lastly, the surface energy and surface tension values of all four co-solutions were similar; hence, no significant relationship exists between the swelling ratio and surface energy and tension. From the swelling experiments with alternative co-solution cured PDMS, no significant effect was found for co-solution cure on the swelling of pure PDMS.

**Table 3-8: Organic solutions and corresponding solution parameters**

<b>Solutions</b>	<b>Polarity Index</b>	<b>Hildebrand Parameter (<math>J^{1/2} m^{-3/2}</math>)</b>	<b>Surface Energy (<math>mJ/m^2</math>)</b>	<b>Surface Tension (<math>mN/m</math>)</b>
Isopropanol	3.9	11.97	52.8	23.0
Toluene	2.4	8.91	58.2	28.4
Cyclohexane	0.2	8.18	54.8	25.0
Chloroform	4.1	9.21	57.3	27.5
Acetone	5.1	9.77	55.0	25.2

### ***3.1.5 GNP/PDMS with Various Manufacturing Parameters***

Four co-solutions for in-situ polymerization, different manufacturing parameters of curing temperature, and sonication time were explored for their effect on the equilibrium swelling ratio of carbon nano-filler composites. From the initial swelling experiments, the equilibrium time was determined to be 4 hours, and all transient swelling was similar. Therefore, no transient effect was recorded, and all samples were swelled for 12 hours.

The steady-state swelling ratio of 1% volume fraction GNP/PDMS with various manufacturing parameters are presented in Figure 3-17 and Table 3-9. The swelling ratio in acetone did not differ with change in the manufacture process. Hence, the swelling change due to the manufacturing process was compared with swelling agents of chloroform and toluene.

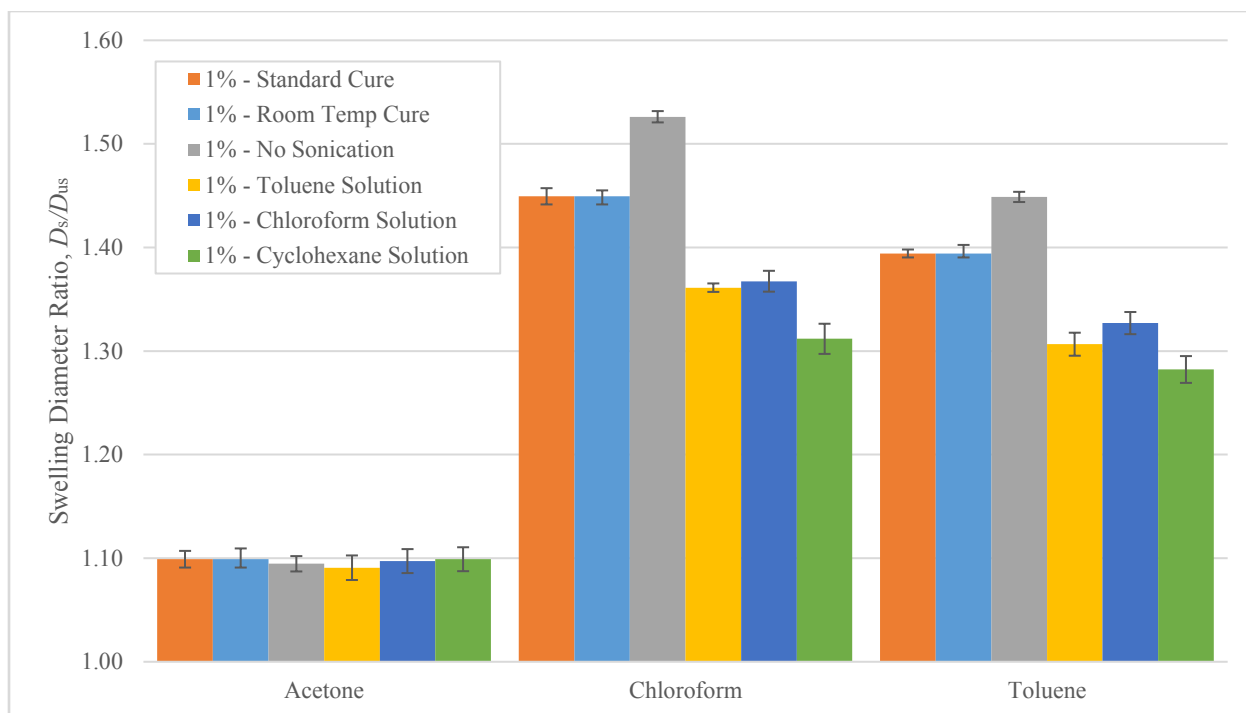


**Figure 3-17: Equilibrium swelling ratios for 1% GNP/PDMS with alternative manufacturing parameters**

**Table 3-9: Equilibrium swelling ratios for 1% GNP/PDMS with alternative manufacturing parameters in acetone, chloroform and toluene**

Type of Cure	Swelling Ratio w/ Acetone, $D_s/D_{us}$	Swelling Ratio w/ Chloroform, $D_s/D_{us}$	Swelling Ratio w/ Toluene, $D_s/D_{us}$
1% - 100 Degree C Cure	1.084 +/-0.095	1.427 +/-0.120	1.373 +/- 0.070
1% - Room Temp Cure	1.099 +/-0.078	1.449 +/-0.055	1.394 +/- 0.088
1% - No Sonication	1.095 +/-0.100	1.526 +/-0.110	1.449 +/- 0.063
1% - Toluene Solution	1.091 +/-0.038	1.361 +/-0.167	1.307 +/-0.117
1% - Chloroform Solution	1.097 +/-0.109	1.367 +/-0.154	1.327 +/-0.140
1% - Cyclohexane Solution	1.099 +/-0.129	1.312 +/-0.051	1.282 +/-0.084

The first comparison was between the standard curing temperature of 100°C and the curing at room temperature. Curing at a higher temperature promotes more cross-linking of the polymer. In addition, preliminary manufacture of nanocomposites showed that at 2% volume fraction or higher, the PDMS nanocomposites did not cure or crosslink at room temperature regardless of time. To ensure complete curing of the GNP/PDMS, the room temperature 1% filled sample was left to cure for 48 hours (24 hours longer than specified). Though this differed from the standard curing time of 12 hours at 100 °C, the focus was to test fully cured nanocomposite. The result was a small increase of 0.022 and 0.021 with swelling agents of chloroform and toluene respectively. Hence, both samples were fully cured and curing temperature does not affect swelling of nanocomposites. However, a lower curing temperature did inhibit cross-linking of the nanocomposite.

Next, the effect of sonication of in-situ polymerization on swelling ratio was tested. Mechanical sonication aids in the exfoliation of the GNP to disperse and distribute the fillers in a homogenous manner. The swelling ratio of the sample with no sonication exhibited significantly more swelling than any other alternative manufacturing parameters. In comparison to the standard cure with 10 hours of sonication, there was a 6.5% and 5.5% increase of swelling in chloroform and toluene. As stated in Chapter 1 with reference Hernandez, exfoliation of GNP is a relation between the total mass of GNP and the total energy input; hence, if the same amount of sonication power and time is applied to two different masses of GNP, the lower mass will exhibit more exfoliation. The swelling result without sonication indicated that the higher presence of agglomeration affected the swelling ratio more than any other parameter.

Lastly, alternative co-solution cured GNP/PDMS of toluene, chloroform, and toluene were compared to the standard cure of isopropanol. The standard cure for isopropanol of the

GNP/PDMS will induce the GNP to curl to NS; hence, the morphology of the filler was different between the four co-solution cured nanocomposites. At the time of testing alternative co-solution cured nanocomposites, the knowledge of isopropanol curling GNP to produce NS was unknown. The use of isopropanol was originally based on Loomis *et al.* [24], Lee *et al.* [102], and Filippidou *et al.* [23], who all used isopropanol as the only or significant part of the co-solution to produce successful exfoliated GNP/PDMS. However, as suggested in the Section 4.1.1 to 4.1.3, the morphology of the filler did not significantly change the swelling ratio. Therefore the results of the four alternative co-solutions for manufacturing process indicated a lack of correlation between co-solution and the swelling ratio. From the highest to lowest, the steady-state swelling ratio with chloroform as the swelling agent was 1.427, 1.367, 1.361, and 1.312 for the respective co-solution of isopropanol, chloroform, toluene, and cyclohexane. The same ranking of swelling ratio was also apparent with toluene as the swelling agent: 1.373, 1.327, 1.307, and 1.382. The alternative co-solution cured GNP/PDMS showed significant effects on the swelling ratio. By eliminating the nano-filler morphology and the effect the co-solution has on the polymer matrix, the co-solution's effect was on either the nano-fillers or the interactions between the nano-fillers and polymer matrix.

The alternative co-solution cured nanocomposite affected the nanocomposites in two possible ways: the effect of the co-solution on the cross-linking/curing of pure PDMS and/or the effect of the co-solution on the nano-fillers. The more likely scenario was the co-solution affecting the nano-fillers due to the results of alternative co-solution cured plain PDMS. With the result of no sonication resulting in significant increase in swelling due to an increase in agglomerations, the different co-solutions were assumed to exfoliate the GNP to different degrees. Hence, the amount of nano-filler agglomeration ultimately provided the most effect of swelling increase.

### 3.2 Cross-Linking Density

Cross-linking density for all the bulk samples were characterized gravimetrically to confirm the cure completion of each polymer and nanocomposite. Cross-linking density characterization was also used to confirm that the co-solution had no significant effect towards the cross-linking of polymer, and its significance was towards the nano-fillers. Specifically, the co-solution was assumed to affect the exfoliation degree of the nano-fillers, which ultimately leads to an increase in swelling. Lastly, the cross-linking density characterization was also conducted to confirm the effect of nano-filler on the swelling of the composite. Since a lack of cross-linking can lead to an increase in swelling, the relationship between cross-linking density to swelling ratio as filler percentage increases was explored. As shown in Table 3-10, the cross-linking percentage or density of PDMS with GNP, CB and NS decreased as the filler percentage increased with the exception of GNP/PDMS.

**Table 3-10: Cross-linking percentage of GNP/PDMS, CB/PDMS and NS/PDMS**

Percent Volume Filler	% Crosslink		
	GNP/PDMS	CB/PDMS	NS/PDMS
0%	95.8%	95.5%	95.5%
1%	95.4%	94.4%	95.2%
2%	95.0%	93.1%	95.2%
3%	95.2%	91.8%	93.1%
4%	95.0%	91.3%	92.0%

#### 3.2.1 GNP/PDMS

GNP/PDMS were the only nanocomposites that did not exhibit a decrease in cross-linking density as filler loading increased. Hence, as shown in Figure 3-18, the relationship between swelling ratio

and cross-linking density resulted in all the data points clustering around 95% crosslinking percentage with no correlation towards swelling ratio. This lack of correlation showed that the presence of GNP does not inhibit the cross-linking of PDMS.

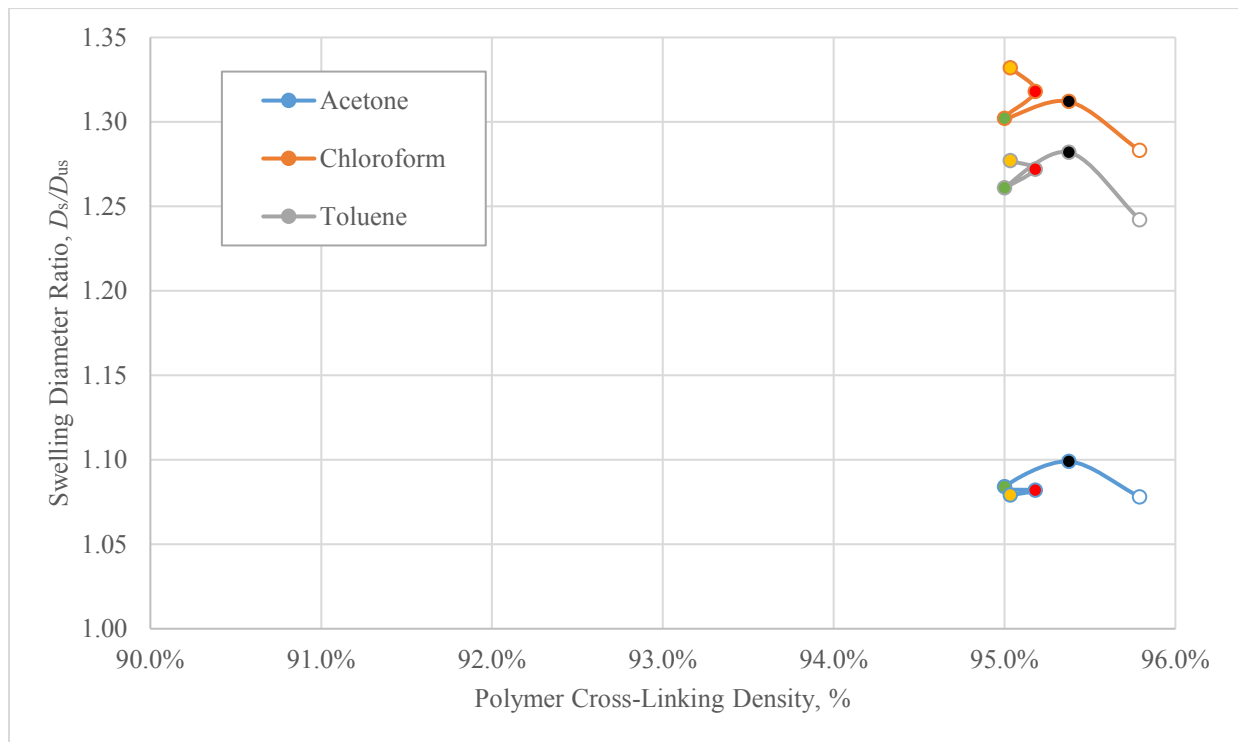


**Figure 3-18: Equilibrium swelling ratios of GNP/PDMS with corresponding crosslinking density. Color of data points corresponds to filler volume percentage: white – 0%, black – 1%, green – 2%, red – 3%, yellow – 4%**

### 3.2.2 CB/PDMS

Much different from the GNP filler, CB/PDMS exhibit a drastically different behavior. Figure 3-19 shows the graphical representation of the relationship between swelling ratio and cross-linking density with data points left to right corresponding to 4%, 3%, 2%, 1%, and 0% of CB filler. Two inflection points were at the beginning at 91.5% and 95.0% of crosslinking percentage. The interest was at the 95% inflection point. The small presence of CB in the system swelled the network

drastically without compromising a full cure to that of pure PDMS. Hence, the effect of CB on filler was seen at 1% filler volume with 20.5% and 19.9% increase in swelling agents of chloroform and toluene. At higher volume percentage, there was a decrease in cross-linking density from the standard ~95% to as low as 91.3%. This decrease in cross-linking contributed to the increase in swelling ratio, but was not the sole factor. However, the lack of cross-linking in the polymer explains the poor correlation with the Kraus equation in Section 3.2.2 since the Kraus equation assumes a fully cured polymer.

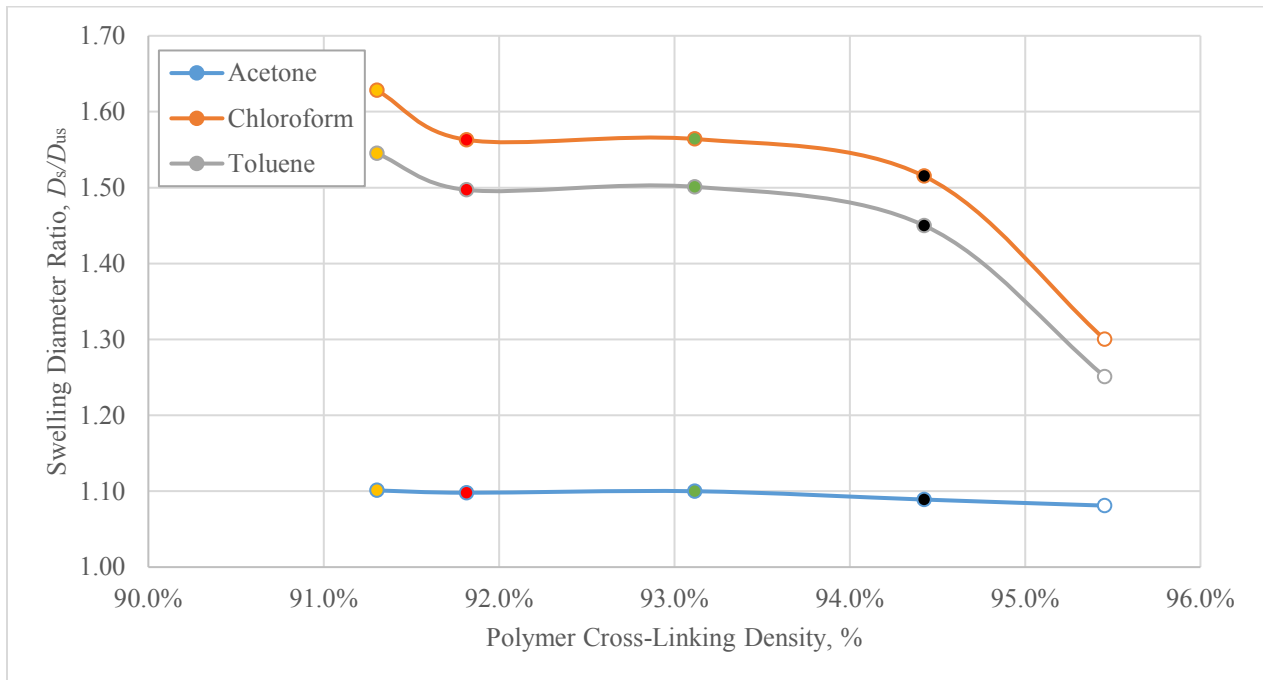


**Figure 3-19: Equilibrium swelling ratios of CB/PDMS with corresponding crosslinking density. Color of data points corresponds to filler volume percentage:**

**white – 0%, black – 1%, green – 2%, red – 3%, yellow – 4%**

### 3.2.3 NS/PDMS

The relationship between the swelling ratio and the crosslinking density for NS/PDMS is shown in Figure 3-20 with percent fillers of 4%, 3%, 2%, 1% and 0% for points going left to right. Similar

to the CB/PDMS, an inflection point appeared with the mere presence of NS at 95.2%. However, different from the NS/PDMS where the increase of filler percentage corresponded to a linear incremental decrease in cross-linking density, the major decrease in cross-linking density occurs between 2% to 3% filler volume.

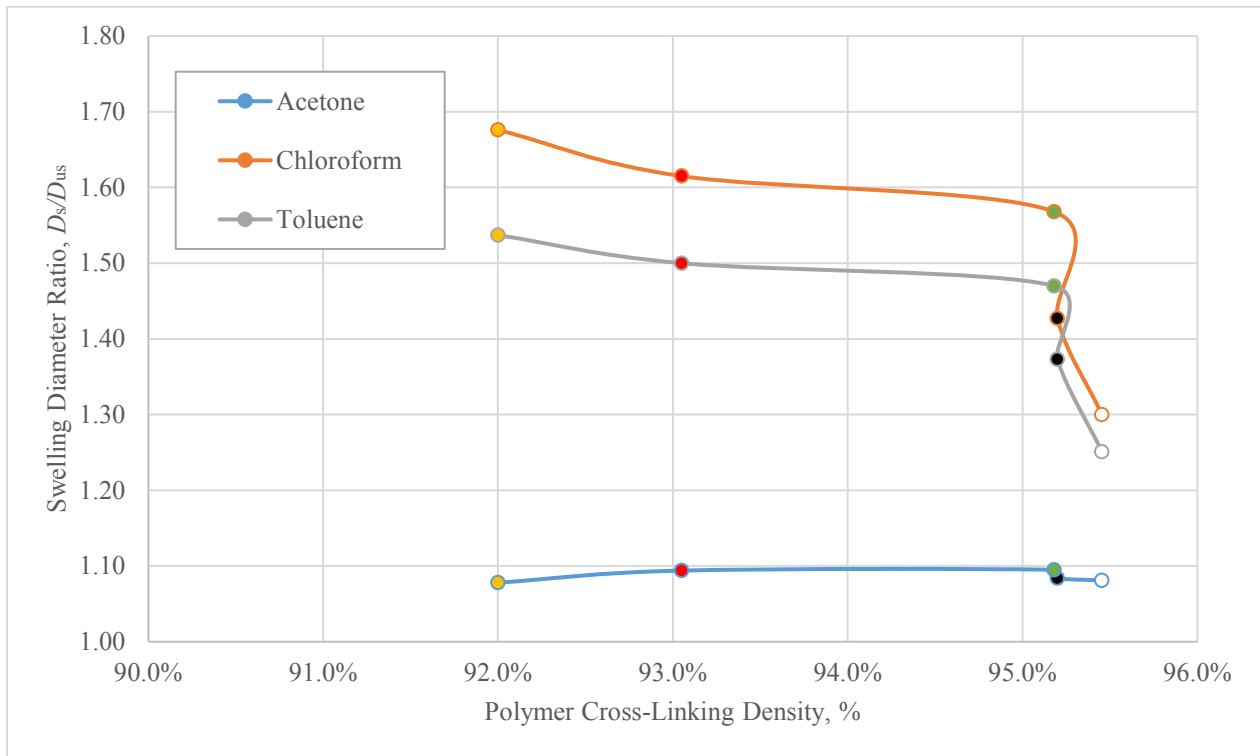


**Figure 3-20: Equilibrium swelling ratios of NS/PDMS with corresponding crosslinking density. Color of data points corresponds to filler volume percentage:**

**white – 0%, black – 1%, green – 2%, red – 3%, yellow – 4%**

An increase of 26.8% and 21.9% of swelling ratio with swelling agents of chloroform and toluene was observed for a filler volume increase from 0% to 2%; however, there was a minimal change of cross-linking density. Hence, the initial increase of swelling ratio was due to solely the presence of NS, while the latter increase in higher filler volume was due to both the presence of NS and the

lack of cross-linking. Similar to CB/PDMS, the lack of cross-linking in polymer explains the lack of correlation with the Kraus equation stated in Section 3.2.3.

From the three correlation graphs between swelling ratio and crosslinking density, the results showed that the swelling ratio increases drastically with similar cure completion to that of the plain polymer at low CB and NS filler volume. On the other hand, the cross-linking density for all GNP/PDMS were similar; hence, the increase in swelling ratio was due to the addition of GNP. Overall, the initial conclusion that the morphology of filler does not have a significant impact on the swelling ratio is still valid. The new insight gained from the cross-linking correlation towards the swelling ratio was that at higher percentages of CB and NS, the swelling increase was due to both the addition of fillers and a lack of cure completion.

#### ***3.2.4 Different Curing Parameter of PDMS***

The main objective of cross-linking characterization was to confirm that alternative co-solutions for in-situ polymerization do not affect the polymer curing process. Table 3-11 shows the cross-linking density of pure PDMS samples that were manufactured through in-situ polymerization. The results showed that all cross-linking density was around 95.5% with the exception of chloroform at 94.8%. In addition, with the chloroform cure, there was a slight yellow tint in the final PDMS. Isopropanol, cyclohexane and toluene had no effect on the cure completion of PDMS while chloroform decreased the cross-linking density slightly. Chloroform was also a co-solution used by Lee *et al.*, who produced GNP/PDMS nano-sensors [67]. Lee *et al.* stated that chloroform was not compatible with their PDMS of MDX-4 4210 Biomedical Grade Elastomer, which was different from the present PDMS of Slygard 184. From the polymer data sheet, there was no mention of chloroform effecting Slygard 184. Therefore, these high cross-linked pure PDMS supported the conclusion of the co-solution used in this study does not affect curing of PDMS.

**Table 3-11: Cross-linking density of pure PDMS cured with alternative of co-solutions**

<b>Co-Solution</b>	<b>% Crosslink</b>
Isopropanol	95.5%
Cyclohexane	95.8%
Toluene	95.6%
Chloroform	94.8%

### ***3.2.5 Different Curing Parameter of 1% GNP***

Along with the pure PDMS, the cross-linking density of GNP/PDMS with alternative co-solutions was tested. In addition, an assessment of the cross-linking density for alternative manufacturing parameters ‘curing temperature’ and ‘sonication time’ was also conducted. As shown in Table 3-12, all results with the exception of curing with chloroform as the co-solution resulted in a cross-linking percentage of slightly above 95%. Recall Figure 3-17 and Table 3-9 where the steady-state swelling ratio was presented for all following alternative manufactured GNP/PDMS, the swelling ratio was significantly different for all samples. Hence, no correlation exists between cross-linking density and swelling ratio for the alternative manufacturing parameters. With chloroform as a co-solution, there was a noticeable effect on the cross-linking density which explains the significant higher swelling ratio compared to isopropanol, toluene, and cyclohexane. However, the most important finding in this context was for the “No Sonication” sample and the cyclohexane cured nanocomposite. Though the cross-linking density of the two samples differed by only 0.3%, the swelling ratio in chloroform and toluene differed by 21.4% and 16.7%. Again, for the No-Sonication sample, the nano-fillers are at the highest degree of agglomeration. Hence, this result further confirms that the effect of a co-solution on swelling revolves around the lack of exfoliation of the nano-fillers instead of the lack of cross-linking in the polymer matrix.

**Table 3-12: Cross-linking density of 1% GNP/PDMS for different manufacturing parameters**

<b>Method of Manufacture</b>	<b>Crosslinking Percentage</b>
1% No Sonication	95.5%
1% Room Temp	95.2%
1% Standard	95.2%
1% Chloroform	93.5%
1% Cyclohexane	95.2%
1% Toluene	95.5%

### **3.3 Exfoliation Characterization**

#### ***3.3.1 Electrical Resistance***

The main methods for the characterization of exfoliation involved digital imaging with TEM, SEM and HIB. However, electrical resistivity can explore exfoliation in a macro scale quantification to support the microscale quantification of digital imaging. For a nanocomposite to be conductive, the amount of conductive nano-fillers needs to spread in the matrix to form a conductive network. This critical amount of conductive nano-filler is called the percolation threshold. The percolation threshold indicates the minimum required mass of the nano-filler which reached a degree of exfoliation that is needed to allow for a conduction of electrical charge via electron tunneling primarily. Typically, complete filler exfoliation is still not present even when electrical conductivity is achieved. Hence, electrical resistance was only one method used to assess the exfoliation state for the previously characterized carbon nano-filler modified PDMS. Electrical conductivity was also used to confirm the assumption that the lack of exfoliation was the leading cause for an increasing swelling ratio. From nanocomposite resistivity theory, a nanocomposite

that has not achieved conductivity but has passed the percolation threshold is subject to substantial filler agglomeration.

### 3.3.1.1 PDMS Nanocomposite with GNP, CB and NS

The percolation threshold for GNP with different polymer matrices was recorded as low as 0.3wt% by Chandrasekaran *et al.* [117] and was estimated as high as 2wt% by Li *et al.* [118]. Chandrasekaran *et al.* used a manufacturing method via three-roll milling, GNP from Punto Quantico S.r.l, and an epoxy polymer matrix. On the other hand, the GNP/PDMS percolation threshold was shown by Filippidou *et al.* to be 5-6wt% [23] and 10wt% by Lee *et al.* [67]. The polymer matrix was critical for defining the percolation threshold of nanocomposites. For CB nanocomposites, Huang *et al.* showed a 2-4wt% percolation threshold for CB/polypropylene and 25wt% for CB/nylon 6 [33]. This drastic difference in percolation threshold was explained by the difference in surface tension between the polymer resins. The higher the polymer surface tension the higher is its percolation threshold. Therefore, with PDMS, which has a lower surface tension than that of polypropylene, a lower or similar percolation threshold of 2-4% was expected. Lastly, electrical conductivity studies for NS nanocomposites are limited, and no documentation for NS nanocomposite percolation thresholds was found; however, NS have a lower conductive than GNP due to the reduction in surface-to-volume ratio. Hence, the percolation threshold of NS/PDMS was expected to be higher than that of GNP/PDMS.

As shown in Figure 3-21 and Table 3-13, the CB and NS composites were not conductive even at the highest nano-filler loading of 8.8wt% and 7.6wt%, respectively. No direct evidence indicates both CB/PDMS and NS/PDMS were past their respective theoretical percolation threshold, but the lack of exfoliation of nano-filler was assumed to cause the composites to be insulative. For GNP/PDMS, the percolation threshold was achieved around 1-3% by volume (2.2-6.6wt%). As

previously stated, the objective of the resistivity characterization was to determine exfoliation in a macro scale sense and relating it back to the swelling ratio. The nanocomposites with GNP were conductive, which indicates that GNP/PDMS had a high degree of exfoliation. In relation to the GNP/PDMS swelling ratio, a high degree of exfoliation leads to the smallest increase in swelling between the three carbon-based nano-fillers. On the other hand, NS and CB nanocomposites were assumed to have passed their theoretical percolation thresholds, but still did not exhibit conductivity. Hence, it can be concluded that the fillers of these nanocomposites were significantly agglomerated and have a low degree of exfoliation. This conclusion correlates to the first set of swelling results where the NS and CB filled nanocomposites were also the two nanocomposites that exhibited the highest swelling ratio increase. With an increase in filler content from 0 to 4% by volume, the amount of agglomeration also increased within these nanocomposites, indicated by the high resistivity, which ultimately resulted in a higher swelling ratio. The state of exfoliation was further investigated by digital imaging, Section 3.3.2, and x-ray diffraction analysis, Section 3.3.3.

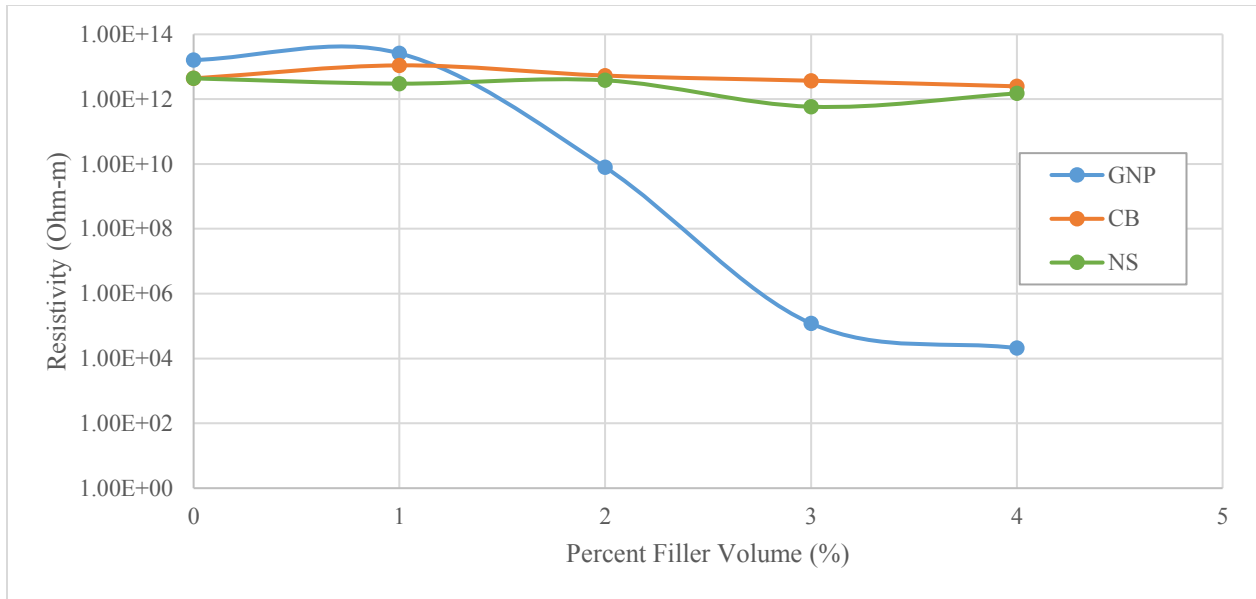


**Figure 3-21: Resistivity of GNP/PDMS, CB/PDMS and NS/PDMS with corresponding filler volume percentages**

**Table 3-13: Resistivity of GNP/PDMS, CB/PDMS and NS/PDMS for percent filler volume ranging from 0% to 4%**

Percent Volume Filler (%)	Resistivity (Ohm-m)		
	GNP	CB	NS
0	1.61E+13	4.37E+12	4.37E+12
1	2.59E+13	1.10E+13	3.01E+12
2	7.92E+09	5.33E+12	3.81E+12
3	1.21E+05	3.71E+12	5.85E+11
4	2.09E+04	2.49E+12	1.50E+12

### 3.3.1.2 Different Manufacturing Parameter

The resistivity of several 1% volume fraction GNP/PDMS samples manufactured with various alternative manufacturing parameters are shown in Figure 3-22 and Table 3-14. Since 1% filler is below the percolation threshold for GNP/PDMS nanocomposites, no samples had sufficient

amount of nanoparticles to achieve a conductive network. Hence, all samples were measured to have high resistivity. A difference in conductivity by two orders of magnitude was apparent between the samples that were cured with cyclohexane and with chloroform. However, the absolute resistivity was high enough to categorize both samples as isolative. In addition, with this high resistivity there was no correlation between resistivity and the steady-state swelling ratio.

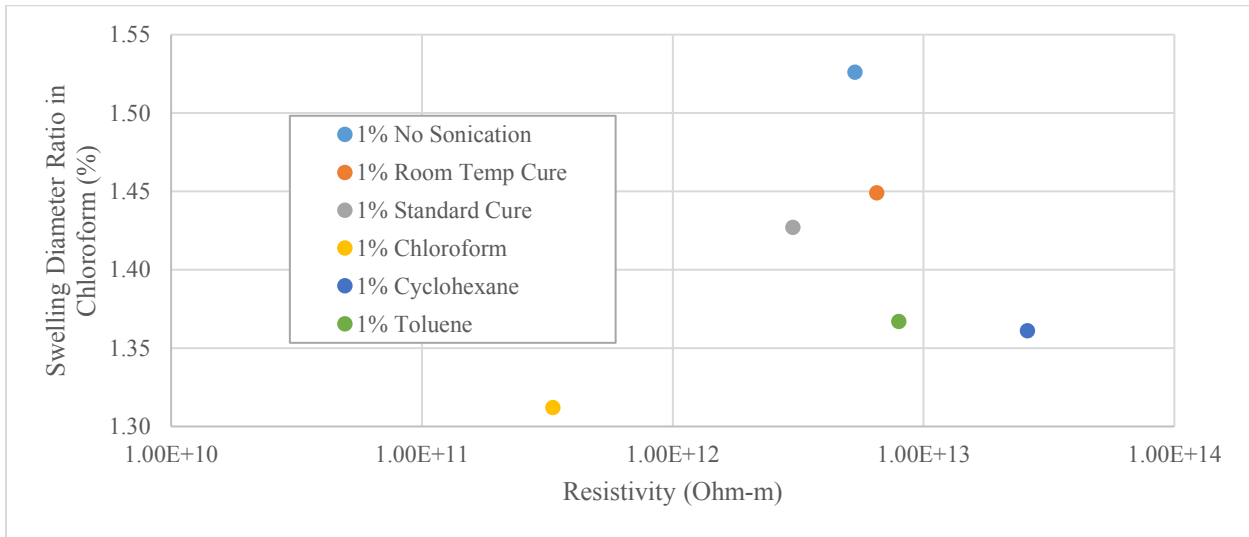


**Figure 3-22: Resistivity of 1% GNP/PDMS with corresponding percent filler volume for alternative manufacturing parameters**

**Table 3-14: Resistivity of 1% GNP/PDMS for alternative manufacturing methods**

<b>Manufacturing Parameter</b>	<b>Resistivity (Ohm-m)</b>
1% No Sonication	5.32E+12
1% Room Temp Cure	6.51E+12
1% Standard Cure	3.01E+12
1% Chloroform	3.33E+11
1% Cyclohexane	2.59E+13
1% Toluene	7.97E+12

### 3.3.1.3 Different Curing Solutions

Lastly, the resistivity between pure PDMS and 1% GNP/PDMS with different co-solutions were tested. As shown in Table 3-15, with the addition of GNP, all samples exhibit a decrease in resistivity. However, percolation thresholds were not exceeded, all samples remained insulative.

**Table 3-15: Resistivity comparison between pure PDMS and PDMS filled with 1% GNP cured with different co-solutions**

Co-Solution	Resistivity (Ohm-m)	
	0%	1%
Cyclohexane	1.53E+13	2.47E+13
Toluene	1.67E+13	7.59E+12
Chloroform	1.23E+12	3.17E+11

Overall, the resistivity characterization supported the notion that the degree of exfoliation was low, which was assumed to be the main cause for steady-state swelling ratio increases. Both the NS and CB nanocomposite exhibited the highest swelling ratio as well as high resistivity even though they passed the assumed percolation threshold. On the other hand, GNP/PDMS exhibited a much less significant increase in swelling ratio while surpassing percolation. As mentioned earlier, the resistivity investigation was performed to explore the degree of exfoliation from a bulk material perspective, and it is important to realize that resistivity and exfoliation are not necessarily correlated. To further explore the exfoliation characteristics of the nano-composites, but on a micro/nanoscale, digital imaging (SEM, TEM and HIB) and X-ray diffraction was performed on a subset of samples.

### **3.3.2 Microscopy**

#### *3.3.2.1 Helium Ion Beam Microscopy*

The clearest and most indicative images were captured by Helium Ion Beam (HIB) microscopy. Traditional SEM and TEM produced images that were deceptive due to the insulative nature of the nanocomposites, see Sections 3.3.2.2 to 3.3.3.3. The cross-sections of selected samples, i.e. 1% and 4% for the standard cure of GNP, NS, and CB filled PDMS, were captured and are shown in Figures 3-23 to 3-25. Images were taken using the same working distance and field of view of 9.724 mm 10  $\mu$ m, respectively. All cross-sections of samples were prepared from the original bulk samples using a cryo-microtome. Figures 3-23 to 3-25 display two identical fields of view captured by the microscope with and without the “charging” input from the Helium Ion Microscope. Charging of the sample was accomplished by bombarding the samples with electrons while the Helium Ion Beam was activated. This bombardment creates more contrast between insulative and the conductive material. The light/white sections of the images are the conductive carbon fillers, while the dark/black sections of the images are the PDMS polymer matrix. No direct correlation to exfoliation was ascertainable from these images; however, large agglomerates were observed in Figure 3-24 for CB/PDMS.

Cross-sections for 1% and 4% GNP/PDMS are shown in Figure 3-23. From the resistivity characterization, both of the 1% and 4% samples were expected to have a high degree of exfoliation, but visual inspection was not able to corroborate this notion. A conductive network can be inferred by comparing the images with and without electron charging. The charging effect from the HIB microscope creates greater contrast in the image by amplifying the conductive sections. Hence, more conductive carbon-based nano-fillers can be observed when charging was applied. More GNP was visible in the charged 1% sample, Figure 3-23B. However, applying

charging in the 4% GNP sample did not reveal any significant increase in the amount of visible filler. Recalling the resistivity characterization, the 4% GNP was conductive while the 1% GNP was not. Consequently, electron charging has a greater effective for the isolative bulk composite displaying more nano-particles.

Nano-particles agglomerates are displayed for 1% and 4% CB/PDMS cross sections in Figure 3-24. Both samples were measured to be electrically insulative. Therefore, the CB/PDMS images with electron charging showed significantly more CB particle in the same field of view, especially for the 4% sample. In addition, a substantial amount of CB agglomerates can be observed in the 4% CB/PDMS sample. Note that technically, CB is defined by aciniform clusters and not individual carbon particles. However, these clusters were too tightly confined (circled in red) to form any conductive network and were visually distinguished to be non-uniformly distributed.

Lastly, HIB images are displayed for NS/PDMS cross-sections in Figure 3-25. For 1% filler loading the charging effect did not display additional fillers comparing Figures 3-25A and 3-25B. However, the image for 4% NS/PDMS with electron charging displayed significantly more nano-fillers. In addition, HIB imaging in Figure 3-25D appears to be the first clear indication of GNP rolling into NS.

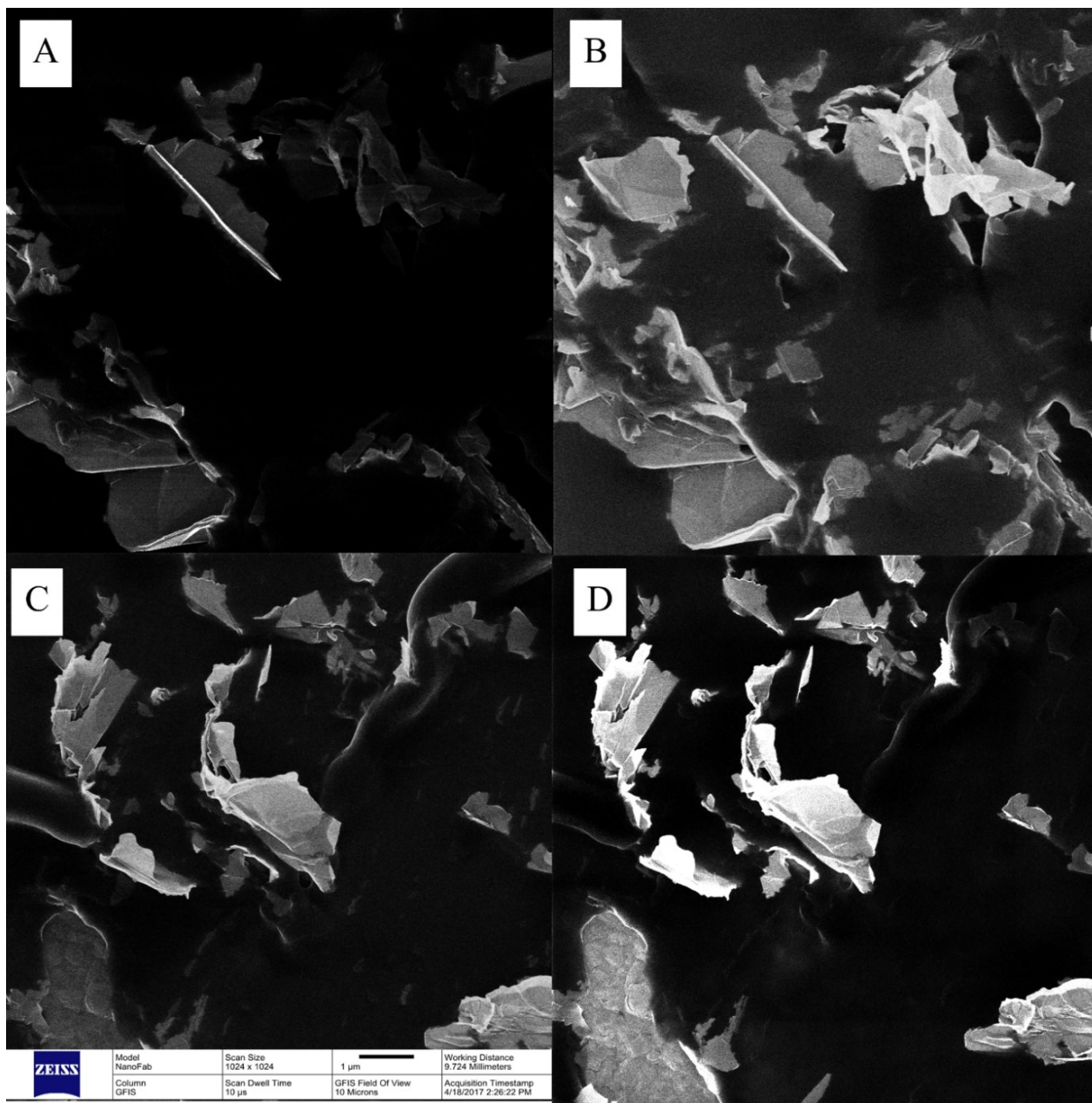


**Figure 3-23: A.) 1% GNP/PDMS without charging effect; B.) 1% GNP/PDMS with charging effect; C.) 4% GNP/PDMS without charging effect; D.) 4% GNP/PDMS with charging effect; with working distance of 9.724 mm and field of view of 10  $\mu$ m**

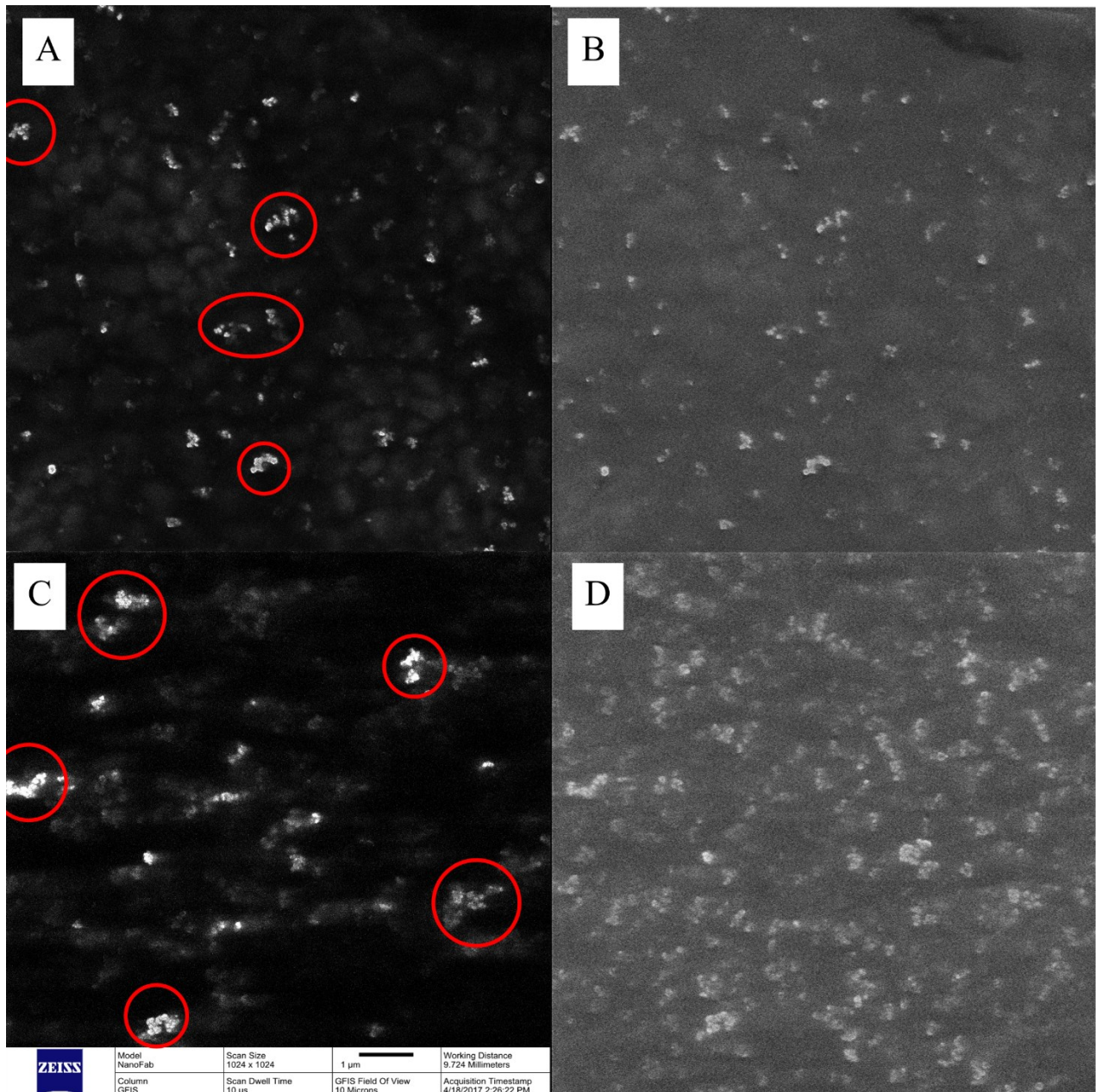


**Figure 3-24: A.) 1% CB/PDMS without charging effect; B.) 1% CB/PDMS with charging effect; C.) 4% CB/PDMS without charging effect; D.) 4% CB/PDMS with charging effect; with working distance of 9.724 mm and field of view of 10  $\mu$ m**

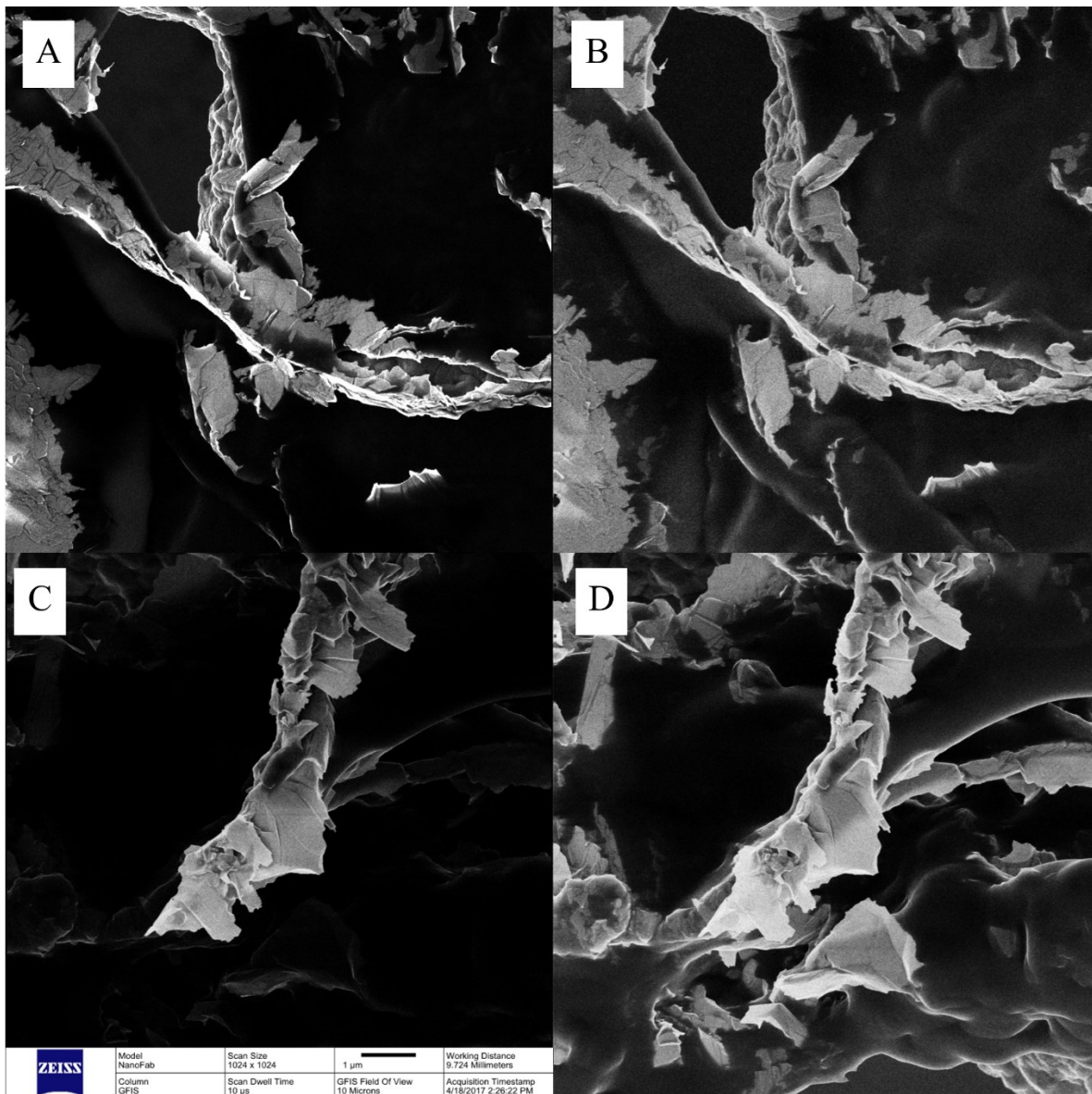


**Figure 3-25: A.) 1% NS/PDMS without charging effect; B.) 1% NS/PDMS with charging effect; C.) 4% NS/PDMS without charging effect; D.) 4% NS/PDMS with charging effect; with working distance of 9.724 mm and field of view of 10  $\mu$ m**

### 3.3.2.2 Scanning Electron Microscopy

Prior to HIB imaging the first attempt of microscopy to identify the exfoliation was with SEM. SEM images were captured on the surface on 1 mm thick bulk samples instead of cross-sections. Figure 3-26 displays SEM images of NS/PDMS with filler volume increasing from 1% to 4%.

These images were the second attempt of SEM imaging with all samples being coated with carbon to induce conductivity. The initial SEM imaging for the non-coated bulk sample resulted in low resolution images due to the insulative nature of the nanocomposites. Figure 3-26 reveals micro-cracks, which were assumed to be the cause of the increase in swelling ratio. Moreover, Kim *et al.* showed similar images with his studies on NS, leading to the assumption that the micro-cracks were NS [119]. However, both assumptions were proven false. Comparing the SEM images of carbon-coated samples to that of HIB images of the cross-sectioned sample, the size of the NS as observed by SEM was thinner and shorter than the NS displayed by HIB microscopy. In addition, as shown in Figure 3-26, the HIB image of the bulk sample surface with 4% NS filler volume without carbon coating showed no indication of any micro-cracks with similar magnification. Therefore, the micro-crack like features shown in the SEM images were in fact cracking of the applied carbon coating as opposed to nano-fillers within the composite.

In addition to the NS/PDMS samples with 1-4% filler loading, SEM images for two alternative manufacturing methods were also captured as shown in Figure 3-27, i.e. No-Sonication and room temperature cure. The SEM image for No-Sonication, Figure 3-27A, shows again micro-crack like features, while image for the room temperature sample, Figure 3-27B, shows additional surface imperfections compared to that cured at the standard temperature of 100°C, Figure 3-26A.

Considering the objective for sample microscopy, that is, the characterization of filler exfoliation, only a limited amount and ambiguous information could be derived using SEM. Hence, the investigation using SEM was discontinued during the study of NS/PDMS.

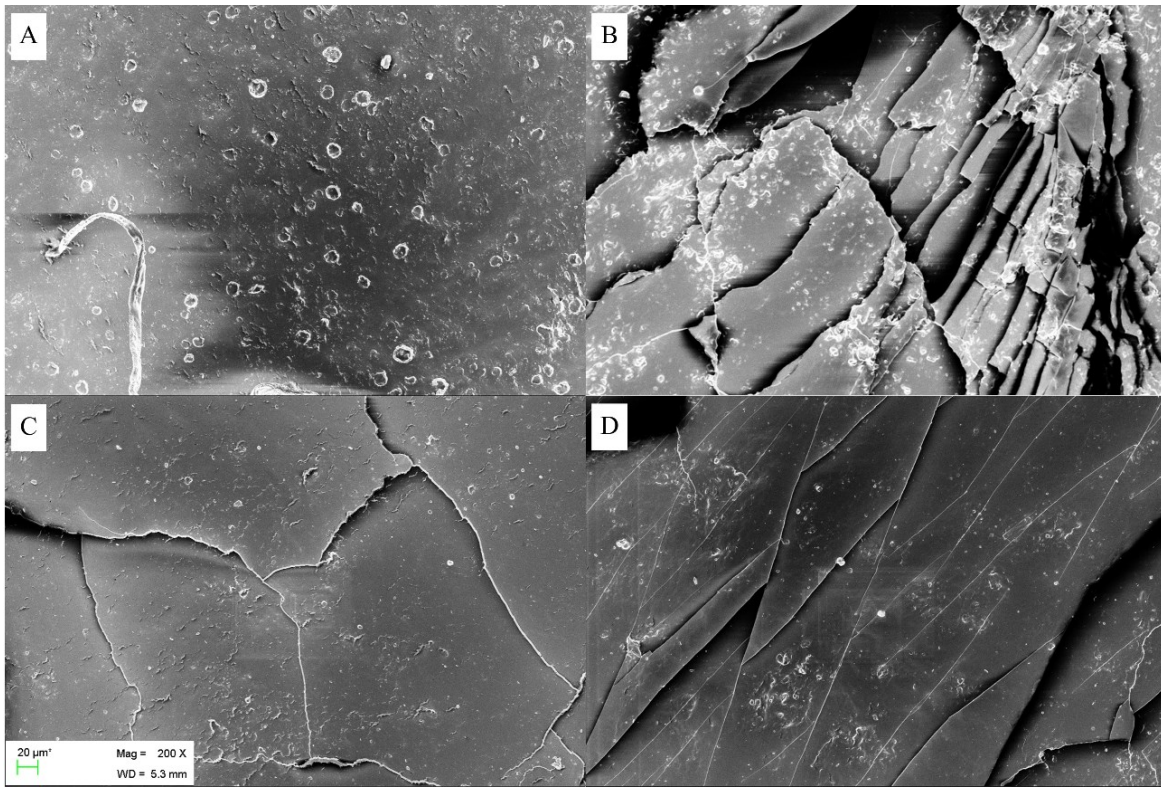


**Figure 3-26: SEM images of carbon coated NS/PDMS with filler volume percentages**

**A.) 1%, B.) 2%, C.) 3% and D.) 4%**

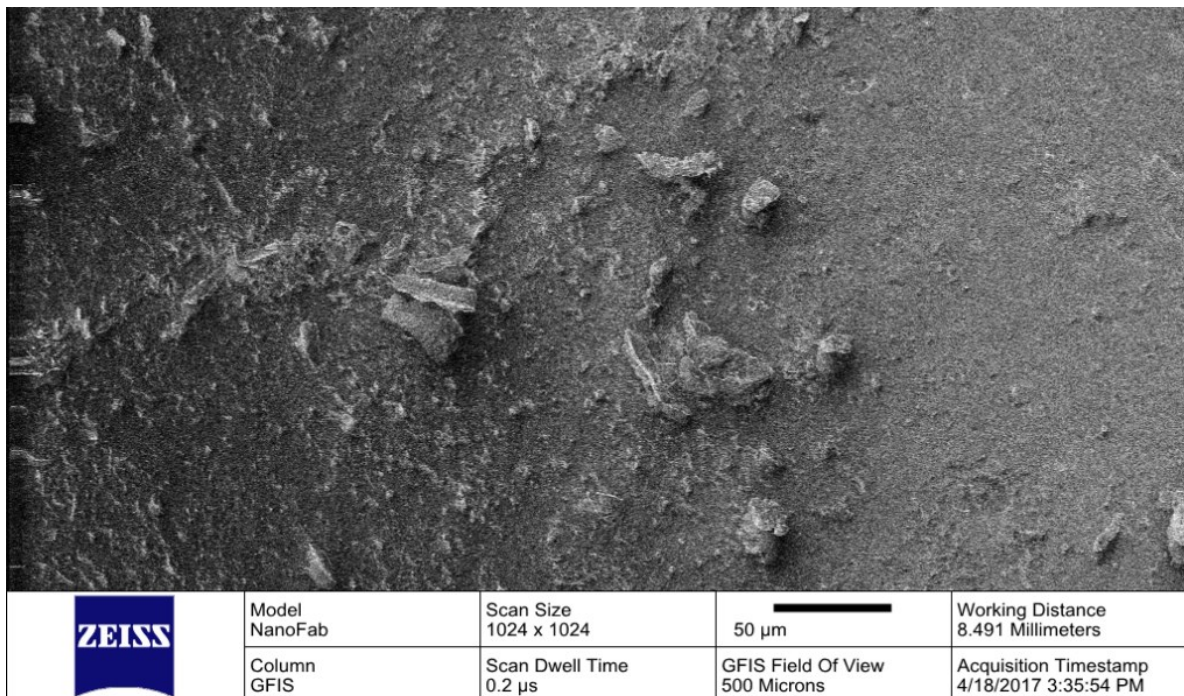


**Figure 3-27: HIB image of non-carbon-coated treated 1% NS/PDMS**

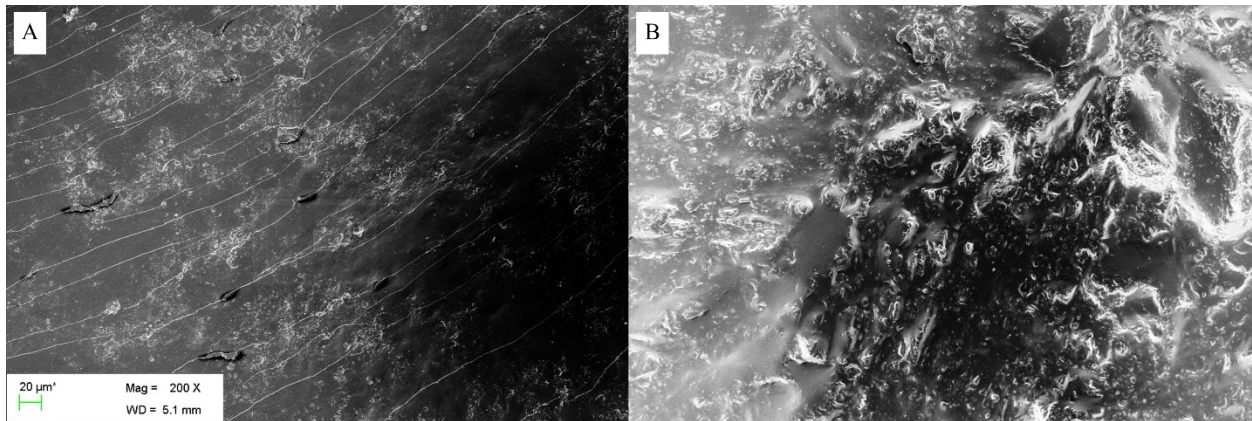


**Figure 3-28: SEM images of A.) 1% volume fraction of NS/PDMS with no sonication and B.) 1% volume fraction of NS/PDMS cured at room temperature**

### 3.3.2.3 Transmission Electron Microscopy

TEM images were captured to further investigate filler exfoliation. Similar to the HIB images, the TEM images were captured on cross-sections of the bulk samples that were prepared using a cryo-microtome. A TEM high voltage of 200 kV was used to investigate NS/PDMS samples. The TEM study only included the 4% NS/PDMS due to the low resolution and instability of the TEM images. The low resolution was due to the low conductivity of the cryo-microtome samples, which made TEM focusing difficult because of the absorption of electrons. The instability and transient behavior of the samples under the TEM is demonstrated in Figure 3-27. As the sample was placed in the 200 kV field, the sample absorbed the energy and electrons. After a few seconds, NS started to split and/or unfold. Only the initial image shown in the far left of Figure 3-27, was similar to that of Xie *et al.* and Maitra *et al.* [119,120]. Splitting of the NS can be interpreted as either the NS unfolding or GNP exfoliating. Hence, due to a low resolution and the instability of the TEM images, the TEM analysis was only completed on one sample of NS, and overall, TEM images were found unsuitable to characterize filler exfoliation.

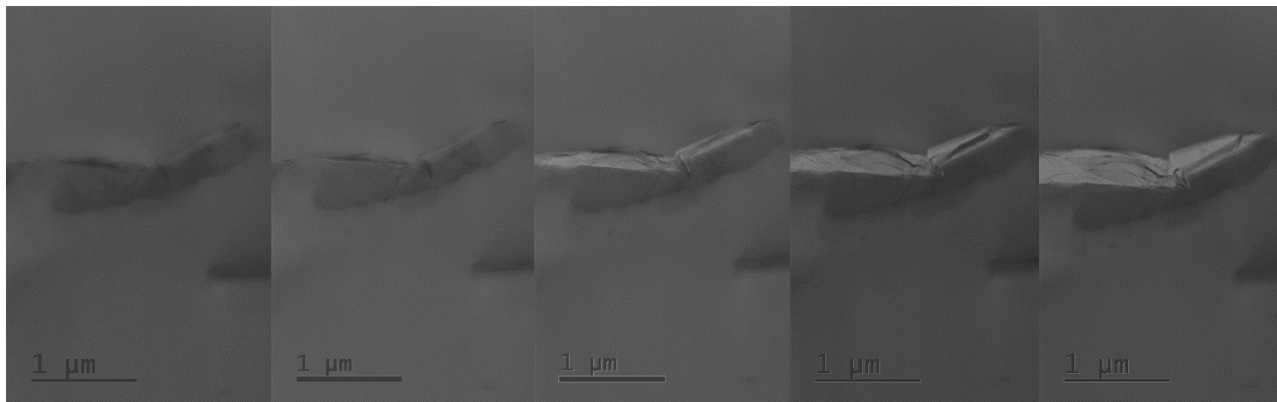


**Figure 3-29: TEM images of 4% filler volume NS/PDMS with standard cure**

### 3.3.3 X-Ray Diffraction

XRD is frequently used to characterize nano-filler exfoliation and was completed in this study to support previous exfoliation claims. However, only samples involving GNP and NS filled nanocomposites were tested to assess a possible increase of the degree of exfoliation. Bulk samples of both NS/PDMS and GNP/PDMS, each with 1-4% filler loading, were tested via XRD. Prior to the characterization the nanocomposites, dry GNP filler was tested first, with results shown in Figure 3-30. The two-theta diffraction angle for GNP was  $30.7^\circ$  with intensity of  $5.8 \times 10^3$ , which is around  $4^\circ$  higher than the value reported by Wang *et al.* [122], Liang *et al.* [123], and McAllister *et al.* [124]. The pure PDMS was also tested, which showed the absence of any intensity peaks.

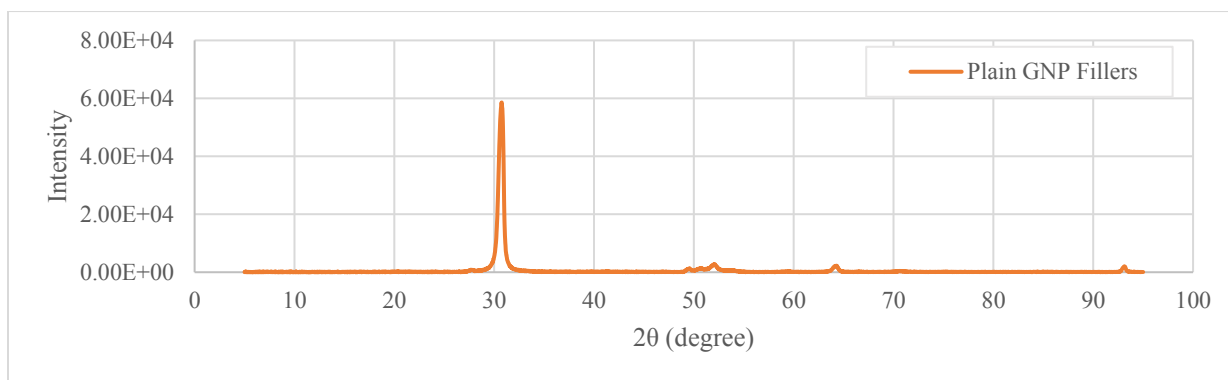


**Figure 3-30: XRD result of pure GNP with corresponding intensity peak and two-theta diffraction angle**

XRD was completed on the bulk material surface for 1% to 4% NS/PDMS. Detailed XRD characterization sheets are shown in Appendix B. Figure 3-31 displays the results for all four filler percentages with two intensity peaks at 12.9° and 30.9° for all four specimens and one additional peak at 10.9° for the 1% and 3% filler percentage. The most indicative peak is at 30.9°, which corresponds to plain GNP, which indicates an agglomeration of nano-scrolls in the bulk samples. At the 30.9° the peak, intensities ( $5.2 \times 10^3$ ,  $6.0 \times 10^3$ ,  $7.9 \times 10^3$ , and  $9.3 \times 10^3$ ) rise with filler volume percentages increasing from 1% to 4%. This increase in filler agglomeration can be ascertained with increasing filler loading. The peaks at 10.9° and 12.9° indicate that portions of the nano-fillers and polymer chains intercalated with one other. As shown by Bhattacharya *et al.* [108], as nano-fillers inside the polymer matrix progressed from agglomerated to intercalated then to exfoliated, the peak of the plain nano-filler shifted towards the left until the nanocomposite became homogenized. This shift is explained further by Bragg's law (9):

$$\sin\theta = n \lambda / 2d \quad (9)$$

where  $n$  is a positive integer,  $\theta$  is the measured diffraction angle,  $\lambda$  is the X-ray radiation wavelength, and  $d$  is the atomic plane distance between graphene layers. As the spacing between graphene layers increases, the diffraction angle decreases until it approaches zero. Therefore, concurrent with the results of both electrical resistance and microscopy, the XRD results for NS/PDMS showed signs of intercalation, but major agglomerates still existed due to the diffraction peaks at 30.9°.

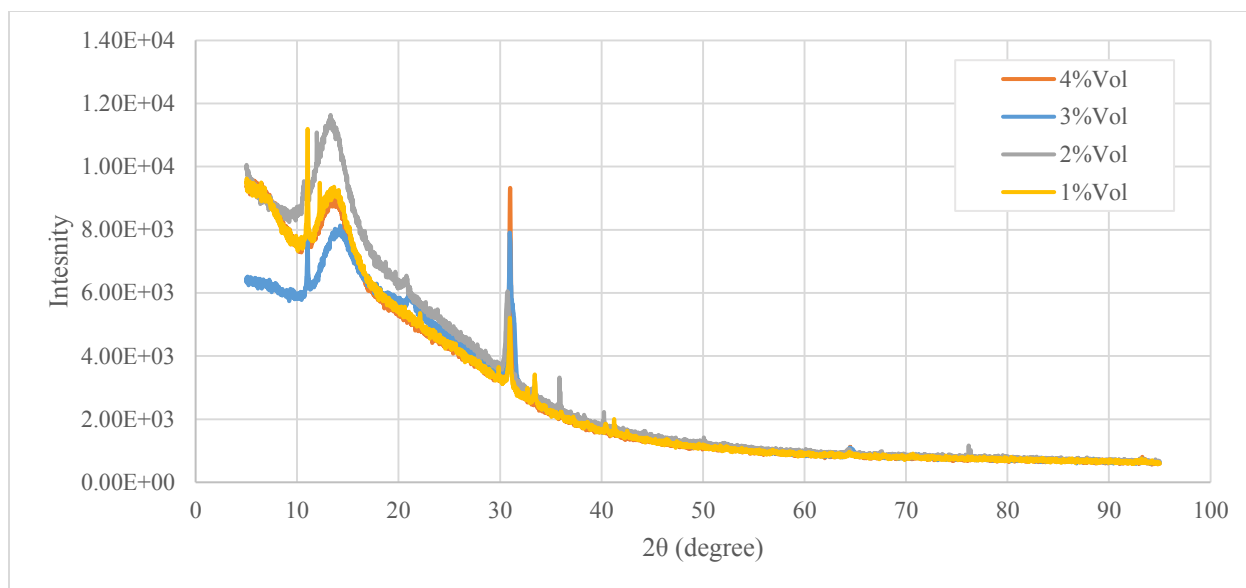


**Figure 3-31: XRD data for 1% to 4% NS/PDMS with corresponding intensity peaks and two-theta diffraction angles**

XRD analyses were also completed for GNP/PDMS which presumably has a high degree of exfoliation. As shown in Figure 3-32, the results for GNP/PDMS revealed different peaks than the NS/PDMS with only one major peak at  $20.1^\circ$  with intensities of  $14.3 \times 10^3$ ,  $15.1 \times 10^3$ ,  $19.6 \times 10^3$ , and  $19.7 \times 10^3$  for the respective volume percentages of 1% to 4%. Compared to the NS/PDMS, the peak at  $12.9^\circ$  for all volume fractions, and the peaks at  $10.9^\circ$  for 1% and 3% volume fraction, all dissipated. However, a minor peak at  $10.4^\circ$  for 2% and 4% arose. The dispersed peak at  $12.9^\circ$  is indicative either of a change in morphology between nano-scrolls to nano-platelets, or a change from previous intercalated fillers to fully exfoliated. The major peak at  $20.9^\circ$  corresponded to the GNP fillers with a  $10^\circ$  shift. The shift indicates substantial intercalation of nano-fillers and polymer chains. Hence, combining the XRD data with previous findings from resistivity measurements and microscopy results, the degree of exfoliation of GNP/PDMS was higher than that of the NS/PDMS. Nevertheless, the GNP/PDMS was not fully exfoliated, which remains the main reason why swelling ratios did not decrease.

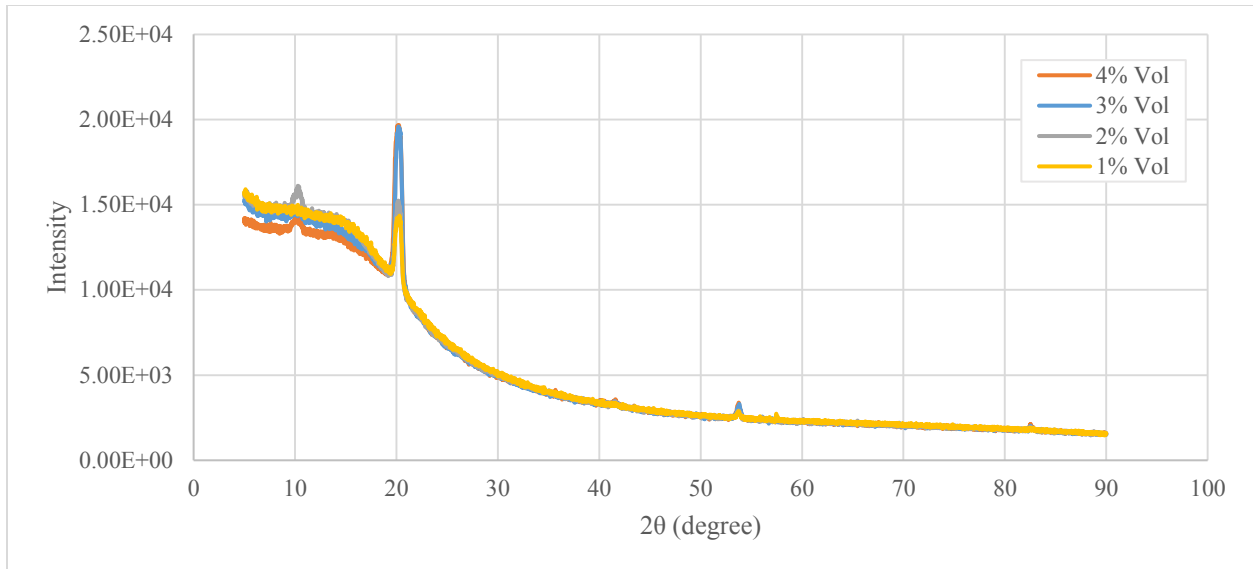


**Figure 3-32: XRD results of 1% to 4% GNP/PDMS with corresponding intensity peaks and two-theta diffraction angles**

The characterization of the degree of filler exfoliation was attempted using four methods: electrical resistivity measurements, HIB imaging, SEM, TEM, and XRD analysis. The electrical conductivity characterization was completed for all manufactured materials. Conductivity testing indicated agglomerations in the insulative bulk material considering theoretical percolation thresholds. HIB imaging was performed on the cross-section of the lowest and highest volume percentage of the three nanocomposites. HIB imaging showed a lack of exfoliation when comparing images with and without electron charging. SEM was inconclusive and was only conducted on a few bulk sample surfaces. TEM of cross-section samples showed agglomerations but was discontinued due to the instability of images. Lastly, XRD patterns indicated filler agglomerations in bulk nanocomposites since intensity peaks were still present at the diffraction angle of plain GNP. All exfoliation characterization approaches support the assumption that the drastic difference in swelling of NS/PDMS and CB/PDMS compared to GNP/PDMS was due to nano-filler agglomeration. In addition, the exfoliation characterization also showed that even

though GNP/PDMS had a higher degree of exfoliation, it was still not homogeneously exfoliated. Hence, due to the lack of homogeneity, the GNP/PDMS did not align with other studies where an increase in nano-filler loading reduced swelling. The lack of exfoliation within the three carbon filled nanocomposites also affected the Kraus correlation between swelling ratio and filler volume percentage. The Kraus relation was derived considering a single nano-particle affecting and holding its polymer surrounding. However, with agglomerated fillers, the bulk nanocomposite does not encompass substantial amounts of isolated particles, and hence, the studied agglomerated nanocomposite did not obey the Kraus equation.

### **3.4 Tensile Testing**

The utility of any nanocomposite lies in its multifunctionality. A suitable nanocomposite should have enhanced properties provided by the fillers (e.g. electrical conductivity), but not suffer a loss of mechanical properties compared to the base polymer. Hence, tensile testing was completed on the bulk samples of all nanocomposites to obtaining both the elastic modulus and ultimate tensile strength (UTS). Moduli and UTS are provided for corresponding filler volume percentages and alternative manufacturing methods in the following section. In addition, graphs correlation the swelling ratio and the modulus of elasticity are shown.

#### ***3.4.1 Stroke Length vs. Optical Measurement***

The present study utilized two methods for calculating strain based on measuring stroke length or using digital imaging. However, as shown in Figure 3-33, the two methodologies yielded drastic different results during tensile experiments. The results from optical measurements were similar to that of Johnston *et al.* [125], while the stroke length measurements resulted in large errors. Errors in stroke length based measurements occurred since strain was computed considering the

whole sample length and not only the gauge section of dog bone samples. Figure 3-33 displays the clamp set up at the first and the final image before failure during a tensile test of pure PDMS cured with isopropanol. Figure 3-33 also shows that, approaching failure, the end of the dog bone sample was not fully covered by the clamp anymore, i.e. to some degree the specimen pulled out of the gripping area. Hence, strain measurements based on stroke length were incorrect. The following section therefore only provides data from optical measurements and stroke length based measurements were discarded.

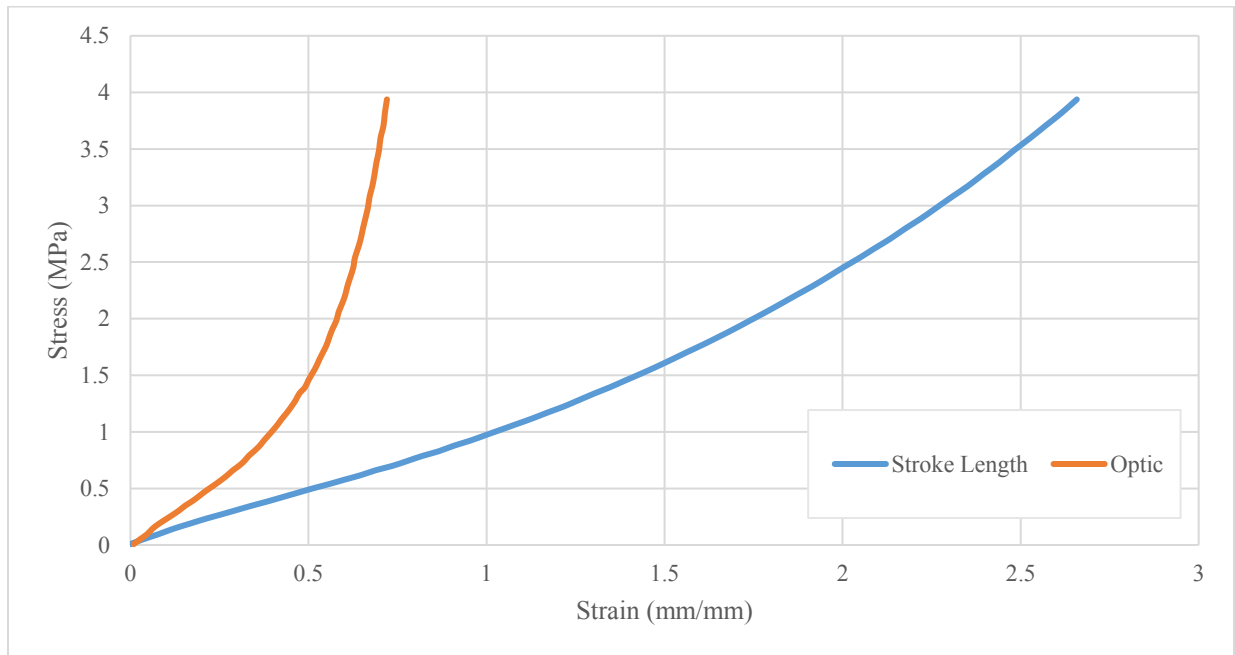


**Figure 3-33: Stress-strain data based on stroke length and optical measurement from tensile testing of PDMS**

The modulus of elasticity was computed within the linear region up to 0.40 mm/mm of strain using Microsoft Excel's linear regression function with a fixed intercept at zero. The optical measurements of pure PDMS yielded a modulus and UTS of 2.46 MPa and 3.96 MPa, respectively. The values obtained by Johnston, *et al.* for a material cured at the same temperature of 100 °C for 53 minutes resulted in 2.05 MPa and 6.25 MPa for modulus and UTS [125]. However, data from

Johnston *et al.* for a 150 °C curing temperature were 2.59 MPa and 5.24 MPa, which are closer to the values obtained in the current study and suggest that the current curing temperature was closer to 150 °C. The current study's optical measurements were also compared to the study by Florian *et al.* [126], where the modulus and UTS were correspondingly 1.76 MPa and 4.5 MPa.

All tensile tests were completed until failure with three trials per sample; however, in certain cases, not all three trials were considered for the average modulus due to a software limitation. The software employed for optical analysis measured the contrast between the black/white markings on the samples and the sample itself. As shown in Figure 3-33, when the sample was elongated during the tensile test, the marking on the samples decreased in intensity which decreased the overall contrast. The software was then unable to detect the difference in contrast and forced closed the program. In addition, due to the program limitation, only the linear regions were plotted for stress versus strain graphs. Though the optical measurement method has its shortcomings, the accuracy of the optical imaging results is still superior to stroke length based measurements.

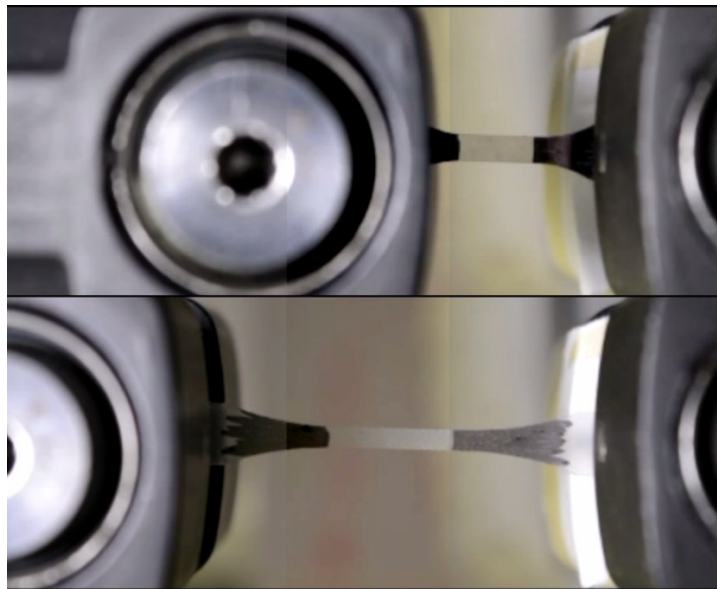


**Figure 3-34: (Top) First and (Bottom) last image from optical measurement during tensile testing of pure PDMS**

### 3.4.2 GNP/PDMS

The modulus of elasticity for a composite material can typically be described by the rule of mixture. The modulus value of the composite is a linear combination of the moduli of the materials of its composition, and the volume fraction of each modulus corresponds to the composition percentage. The rule of mixture basis lies in the continuity of parallel strain between fillers and matrix and its linear elastic response. However, for nanocomposites, the rule of mixture does not generally apply due to the interface interaction between the reinforcing fillers and the matrix material. For macro-fillers, under an applied axial load, the interface region between the bulk and the macro-filler will experience shear stress due to the difference in axial strength. The interfacial shear stress builds along the length of macro-fillers and serves to transfer the load from the surrounding matrix to the macro-fillers. If the interface is strong enough and/or the embedded filler are large enough, the shear stress then translates into tensile fracture of the fillers resulting in the most efficient reinforcement for the composite. However, different from that of macro-fillers, especially fibre reinforcements, nanocomposites do not permit the same interfacial shear transfer due to nano-filler exfoliation, and lack thereof. If the nanocomposite does not reach a homogeneous state, many filler to filler interaction will be present, hence, producing micro/nano-voids inside the composite. If properly dispersed, as shown by Kim *et al.* the value of the nanocomposite modulus with added carbon-based nano-fillers increases, but does not follow the rule of mixture [71].

As shown by the preceding exfoliation assessment, the nanocomposites in the current study did not achieve full dispersion. Therefore, as shown in Table 3-16 and Figures 3-35 to 3-36, GNP/PDMS nanocomposites did not exhibit an increase in modulus nor UTS. With the addition of GNP at 1% volume fraction, an increase in average modulus of 0.1 MPa was ascertained.

However, the increase was less than the measurement error for pure PDMS (0.216 MPa). Overall, when considering measurement errors, the modulus appeared to be constant for increasing filler loading. The UTS decreased with increasing filler volume fraction. The decrease of UTS was similar to that reported by Kim *et al.* where the addition of oxidized graphene flakes decreased the UTS. However, the article also showed an increase in modulus with the addition of oxidized graphene flakes. The major difference between the findings in the articles and present experimental results is the oxidization of the GNP. Oxidized GNP has a higher tendency of exfoliation than the standard GNP used in this study. In addition, the chance of re-agglomeration is lower for oxidized GNP than sonicated GNP. On the other hand, the modulus results for Loomis *et al.*, expressed through the equation of  $E = 1.564 * \%weight^{0.162}$ , at 2% volume fraction or 4.4% weight fraction was approximately 2.0 MPa compared to the present experimental value of 2.6 MPa [127]. This slight increase in polymer properties with regards to GNP was also seen by Kim *et al.*, where thermal reduced graphene sheets were introduced to polyethylene naphthalate and polycarbonate [128]. The authors stated that a lack of increase was due to defects in the sheet structures and the re-agglomeration of particles during manufacturing [128].

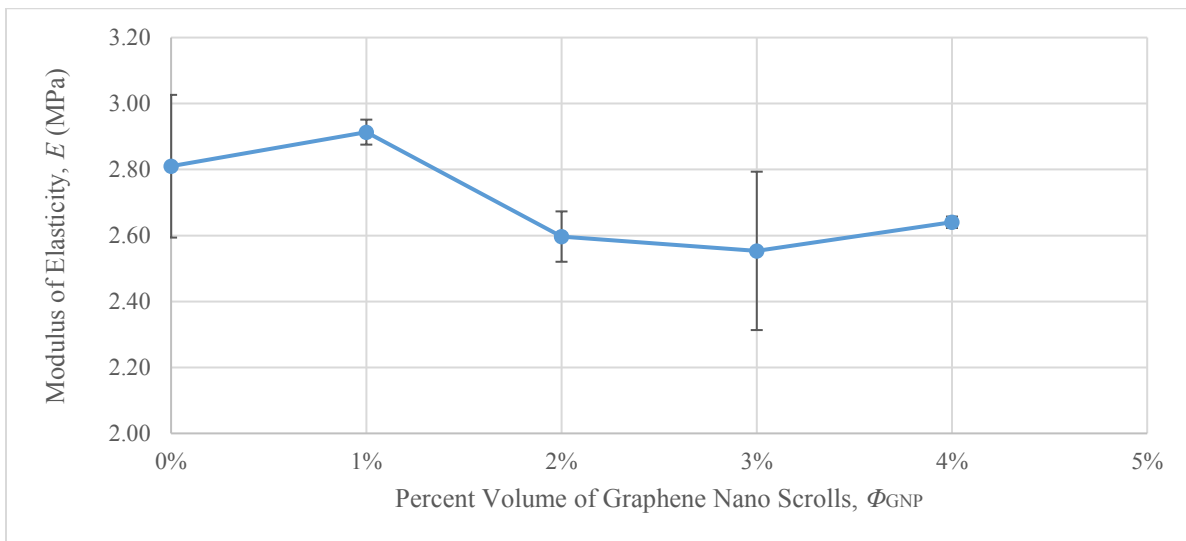


**Figure 3-35: Modulus of elasticity of GNP/PMDS versus filler volume fraction**

**Table 3-16: Modulus of elasticity and UTS for 0% to 4% GNP/PDMS**

Percent Filler Volume	Modulus of Elasticity (MPa)		UTS (MPa)	
	Average	Standard Deviation	Average	Standard Deviation
0%	2.81	0.216	4.08	0.891
1%	2.91	0.038	3.54	0.175
2%	2.60	0.076	2.43	0.203
3%	2.55	0.240	2.77	0.416
4%	2.64	0.017	2.49	0.268

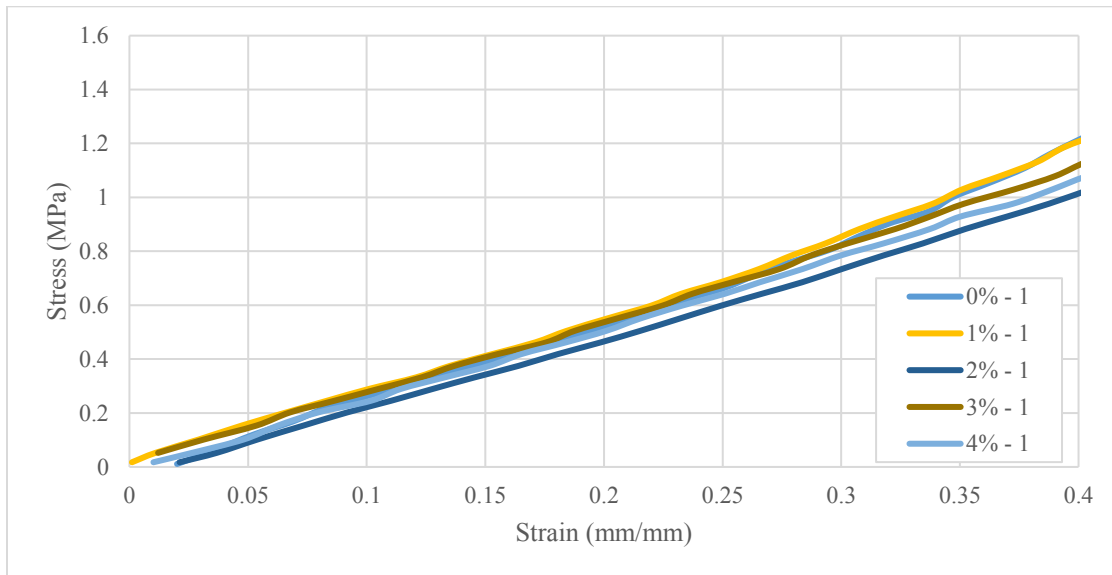


**Figure 3-36: Linear region of stress-strain curve for 0% to 4% GNP/PDMS.**

**(Only first test for each filler volume percent is displayed)**

In regard to a relationship between modulus and swelling ratio, no noticeable trend was observed. Both the swelling ratio and the modulus resulted only in small changes for increasing filler loading, and hence, results are scattered within a narrow range as displayed in Figure B-1 in Appendix B. To ensure that changes in modulus, even though they were small, were due to the addition of GNP instead of a lack of curing, the cross-linking density was contrasted to the modulus. As shown in

Figure B-2 in Appendix B, no correlation was discernable between the modulus and the cross-linking density, that is, the cross-linking density was consistently around 95%. Therefore, any changes in modulus were due to the addition of GNP filler to the polymer.

### **3.4.3 CB/PDMS**

With the addition of CB there was a significant reduction in both elastic modulus and UTS. As shown in Table 3-17 and Figures 3-37 to 3-38, the addition of only 1% CB by volume caused a reduction in modulus and UTS by 246% and 124%, respectively. However, between 1% and 4% volume fraction the modulus reduced to a much lesser degree, i.e., by 7%. For UTS the initial decrease was followed by a fluctuation in UTS with no clear trend for added CB. The maximum decrease was from 3.68 MPa to 1.39 MPa corresponding to pure PDMS and 4% CB/PDMS. A decrease in modulus with the addition of CB was also observed by Huang *et al.* for CB/polypropylene past 5% volume fraction, and was explained by the presence of high amounts of amorphous regions in polypropylene [30]. Roy *et al.* attributed decreasing moduli of CB filled rubber composites to poorly structured CB [29]. As mentioned earlier, carbon black consists of primary grape like chains bonded together by Van der Waals forces to form the secondary chains. In highly structured carbon black, more primary chains of carbon black exist, which eases the dispersion in polymer compared to poorly/low structured CB [127]. Based on these observations the decrease in modulus was attributed to an increase of CB agglomeration within the nanocomposite. These agglomerations acted similar to voids or imperfections inside the material, causing reduced material stiffness and cracking initiation. A similar rationale was reported by Jana *et al.* for silica particles in epoxy [128]. Even though results were for different filler types, the explanation by Jana *et al.*, i.e. aggregates substantially weakened the material integrity and prompted rapid breakage of the specimen, is considered valid in the present case. Consequently,

nano-filler aggregation is seen as reason for both the increase in swelling ratio and the reduction in mechanical properties.

Shown previously, a decrease in crosslinking density corresponded with the increase in CB filler volume. Hence, the decrease in mechanical properties may also be caused by a lack of cross-linking instead of CB agglomeration. However, as shown in Figure 3-39, the relationship between the cross-linking density and modulus was not linear. The 246% decrease in modulus from pure PDMS to 1% volume fraction CB correlated approximately to a 1% decrease in cross-linking density. However, the remaining data for 2% to 4% volume fraction exhibited only a minor linear decrease of modulus to cross-linking density. Hence, it can be inferred that cross-linking had an insignificant effect on modulus in contrast to filler agglomeration. The addition of 1% (agglomerated) CB drastically changed the morphology of the composite compared to the pure polymer, inducing micro-void like features. This change in structure was shown by the extensive decrease in modulus from 0% to 1% filled.

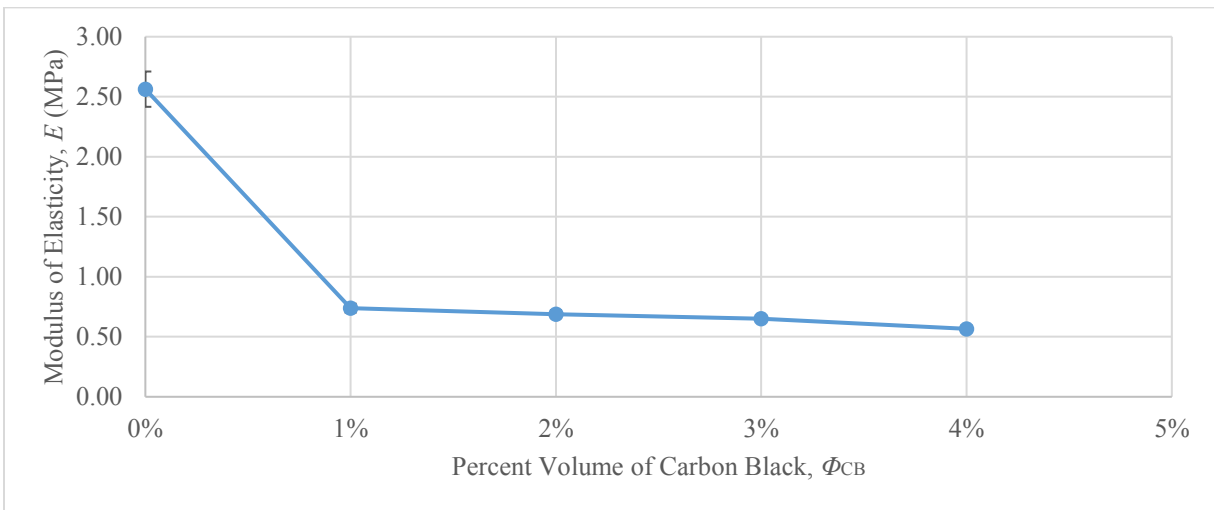


**Figure 3-37: Modulus of elasticity of CB/PMDS versus filler volume fraction**

**Table 3-17: Modulus of elasticity and UTS for 0% to 4% NS/PDMS. “\*” indicates only two trials were used for average and standard deviation calculations**

Filler Percent Volume	Modulus of Elasticity (MPa)		UTS (MPa)	
	Average	Standard Deviation	Average	Standard Deviation
0%	*2.56	*0.147	3.68	0.388
1%	0.74	0.037	1.64	0.139
2%	0.69	0.034	1.93	0.255
3%	0.65	0.018	1.68	0.180
4%	0.57	0.027	1.39	0.171

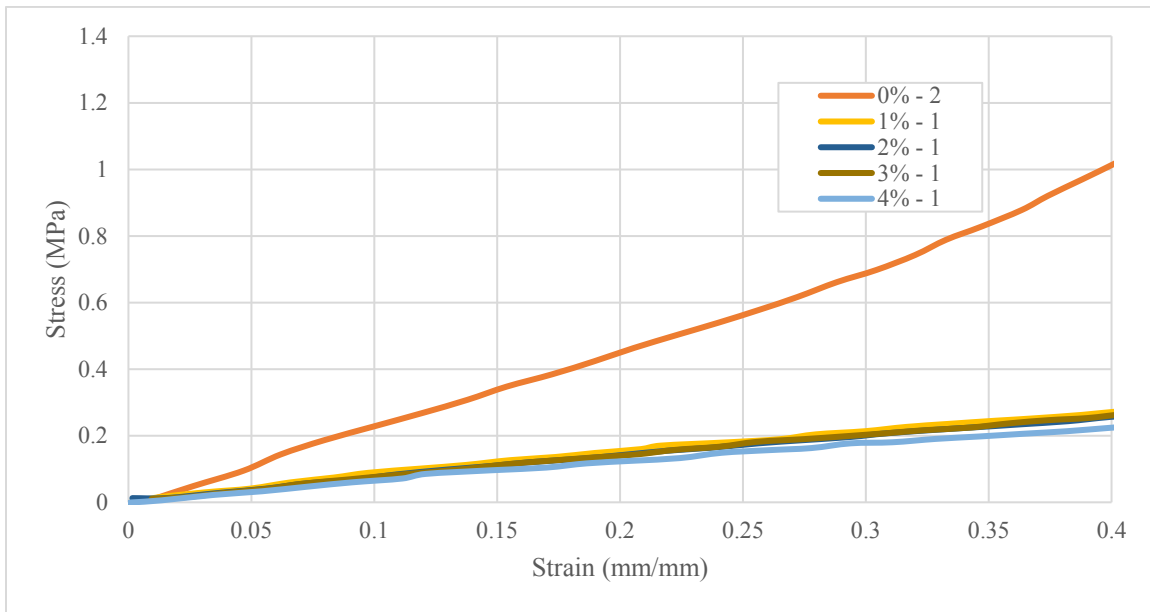


**Figure 3-38: Linear region of stress-strain curve for 0% to 4% CB/PDMS.**

**(Only first test for each filler volume fraction is displayed)**

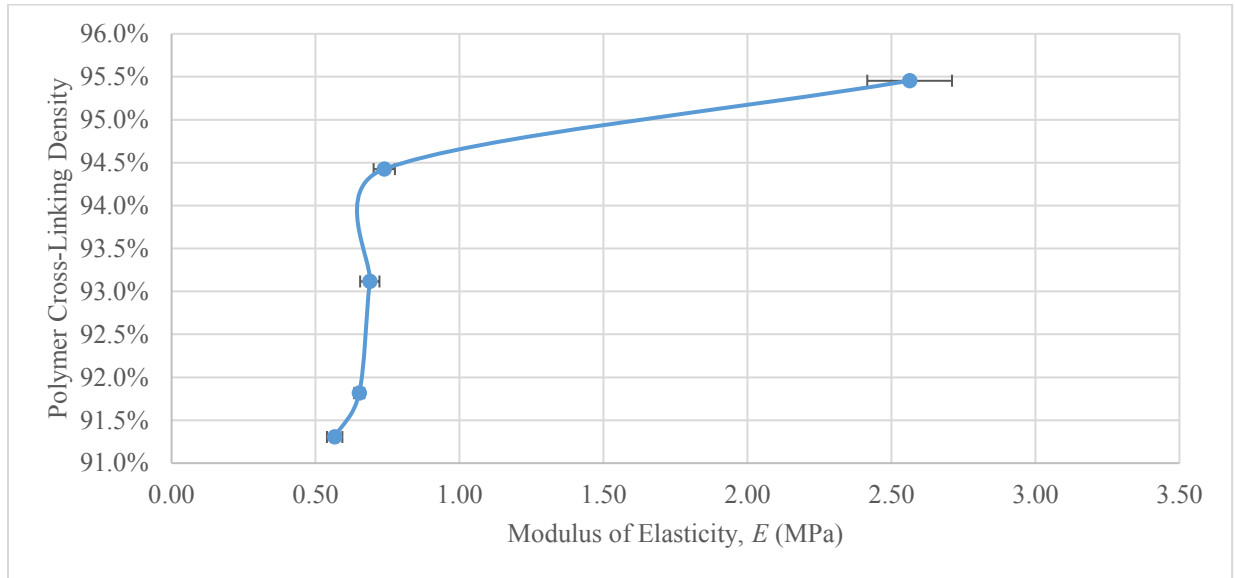


**Figure 3-39: Crosslinking-density of CB/PDMS to corresponding modulus of elasticity**

Lastly, the correlation between modulus and swelling ratio was examined, as shown in Figure B-3 in Appendix B. With the drastic change between the pure PDMS and 1% CB/PDMS an inflection point emerged at the 1% point (modulus of 0.74 MPa). Subsequently, a linear relationship with decreasing slope was observed for the chloroform and toluene cases.

#### **3.4.4 NS/PDMS**

Results for NS/PDMS suggest that similar agglomeration effects were present as observed for CB/PDMS, that is, a low degree of exfoliation caused both an increase in swelling ratio and a reduction in mechanical properties. As shown in Table 3-18 and Figures 3-40 to 3-41, the modulus of NS/PDMS decreased by 97% from pure PDMS to 1% NS volume fraction. This substantial decrease was followed by only small changes in modulus between 1% and 4% NS/PDMS. A similar observation can be made for the UTS. Consequently, an initially large decrease in modulus

resulted from NS filler addition due to a change in material morphology. However, after this initial change, the addition of greater volume fractions of NS only caused minor reductions in mechanical properties.

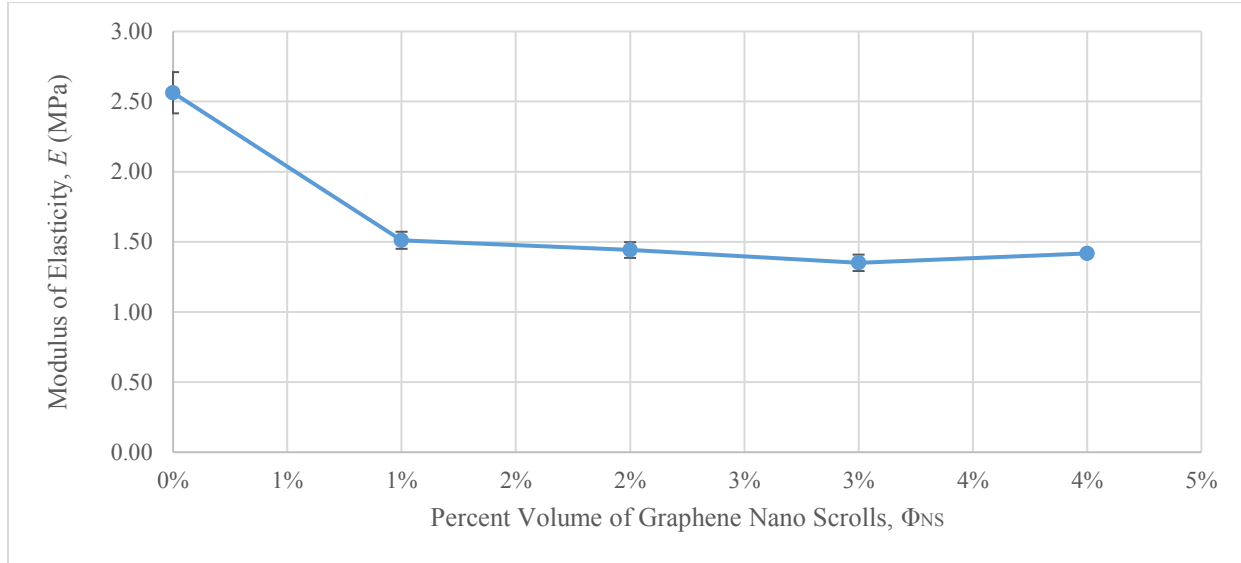


**Figure 3-40: Modulus of elasticity of NS/PDMS versus filler volume fraction**

**Table 3-18: Modulus of elasticity and UTS for 0% to 4% NS/PDMS. “\*” indicates only two trials were used for average and standard deviation calculations**

Filler Percent Volume	Modulus of Elasticity (MPa)		UTS (MPa)	
	Average	Standard Deviation	Average	Standard Deviation
0%	*2.56	*0.147	3.68	0.388
1%	*1.51	*0.061	2.12	0.766
2%	1.44	0.056	1.81	0.164
3%	1.35	0.058	1.57	0.269
4%	1.42	0.016	1.39	0.100

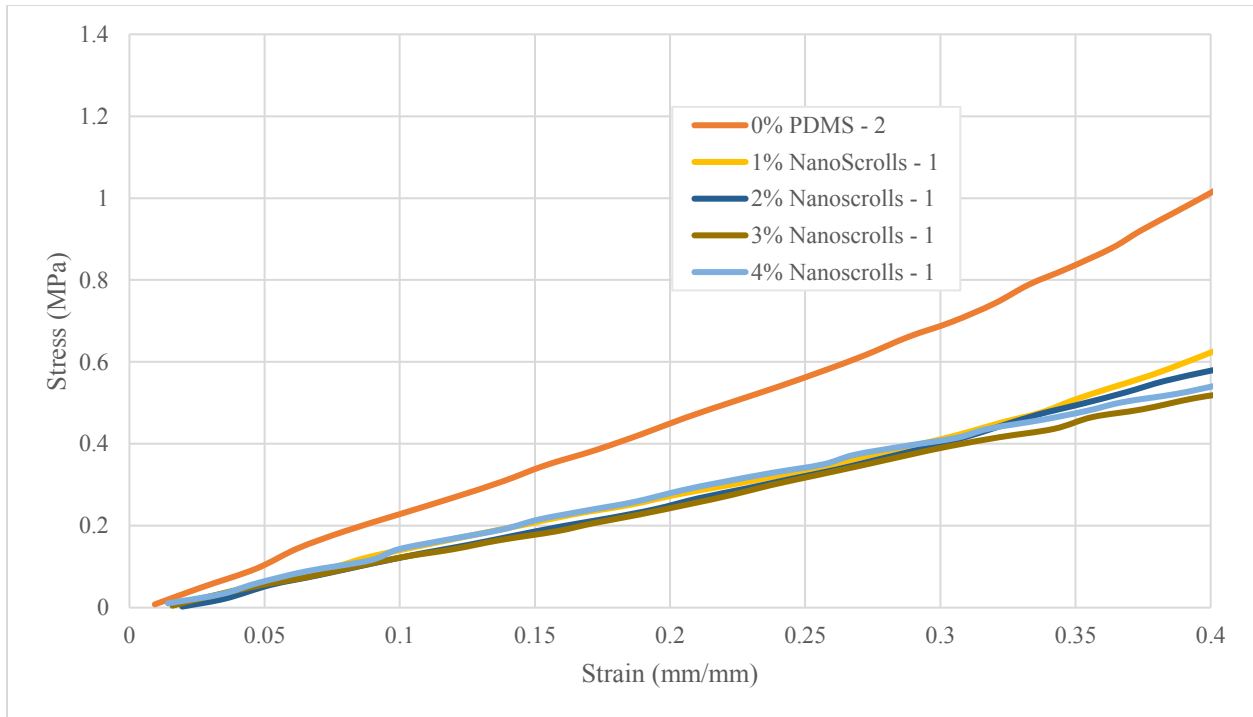


**Figure 3-41: Linear region of stress-strain curve for 0% to 4% NS/PDMS.**

**(Only first test for each filler volume percent is displayed)**

To further corroborate the effect filler agglomeration causing decreased mechanical performance, the cross-linking density was correlated with the elastic modulus as shown in Figure 3-42. Similar to CB/PDMS, NS/PDMS exhibited a large decrease in modulus but only a small reduction in crosslinking density (0.5%) between pure PDMS and 1% NS/PDMS. After this initial decrease in modulus, the modulus remained approximately constant while cross-linking density was further reduced with increased filler content. This result confirms that nano-filler morphology was chiefly affecting mechanical properties, and not cross-linking density.

The correlation between swelling ratio and modulus was also investigated for NS/PDMS. Referring to Figure B-4 in Appendix B, after an initial decrease the modulus stayed approximately constant with increasing in swelling ratio. This trend differs from the behavior observed for CB/PDMS where a linear trend was seen after the initial decrease.

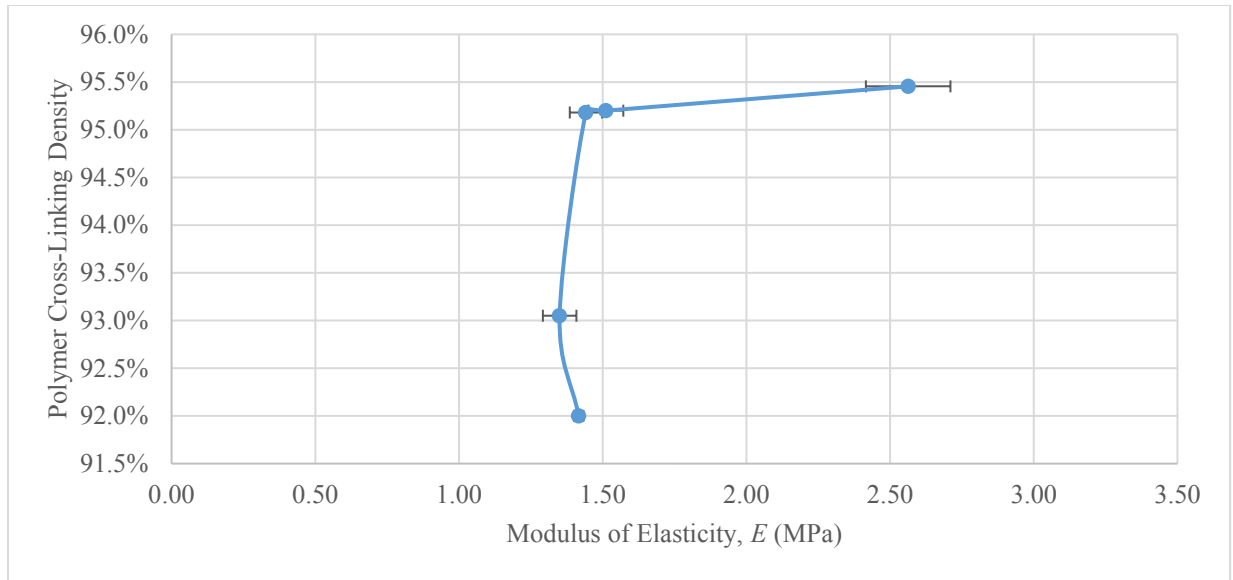


**Figure 3-42: Crosslinking-density of NS/PDMS to the corresponding modulus of elasticity**

### 3.4.5 Different Curing Solutions for PDMS

The mechanical properties of GNP/PDMS samples made with different curing co-solutions were also studied as shown in Table 3-19 and Figures 3-43 to 3-44. With co-solutions chloroform and isopropanol, a large decrease in both the modulus and UTS was observed for the addition of 1% volume fraction GNP. In comparison, for co-solutions cyclohexane and toluene, changes in modulus and UTS were considerably smaller. Base on previous discussions, these differences depending on co-solution are assumed to stem from the state of filler exfoliation, that is, nano-fillers were poorly dispersed for processing with chloroform and isopropanol.

**Table 3-19: Elastic modulus and UTS at 0% and 1% GNP/PDMS for different co-solutions**

Solution	Percentage	Modulus of Elasticity (MPa)		UTS (MPa)	
		Average	Standard Deviation	Average	Standard Deviation
Chloroform	0%	1.58	0.244	3.02	0.354
	1%	0.74	0.004	1.44	0.036
Cyclohexane	0%	2.81	0.216	4.08	0.891

	1%	2.91	0.038	3.54	0.175
Toluene	0%	2.41	0.077	3.72	0.238
	1%	2.09	0.040	3.13	0.087
IPA	0%	2.56	0.147	3.68	0.388
	1%	1.51	0.061	2.12	0.766

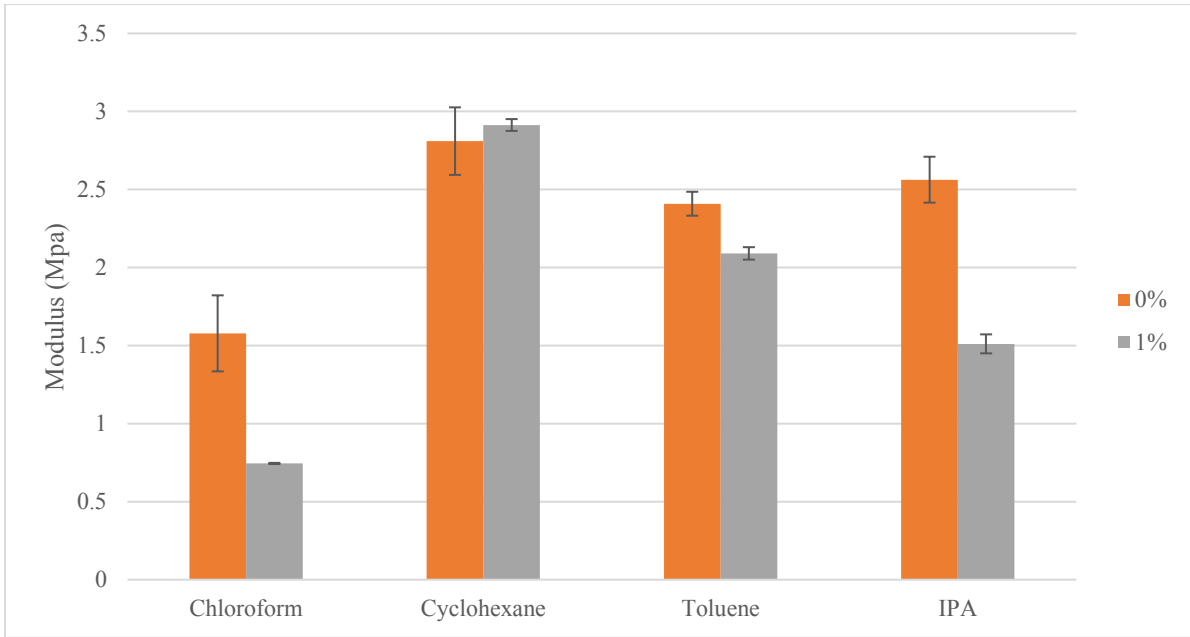


**Figure 3-43: Modulus of different co-solution cured GNP/PDMS samples**

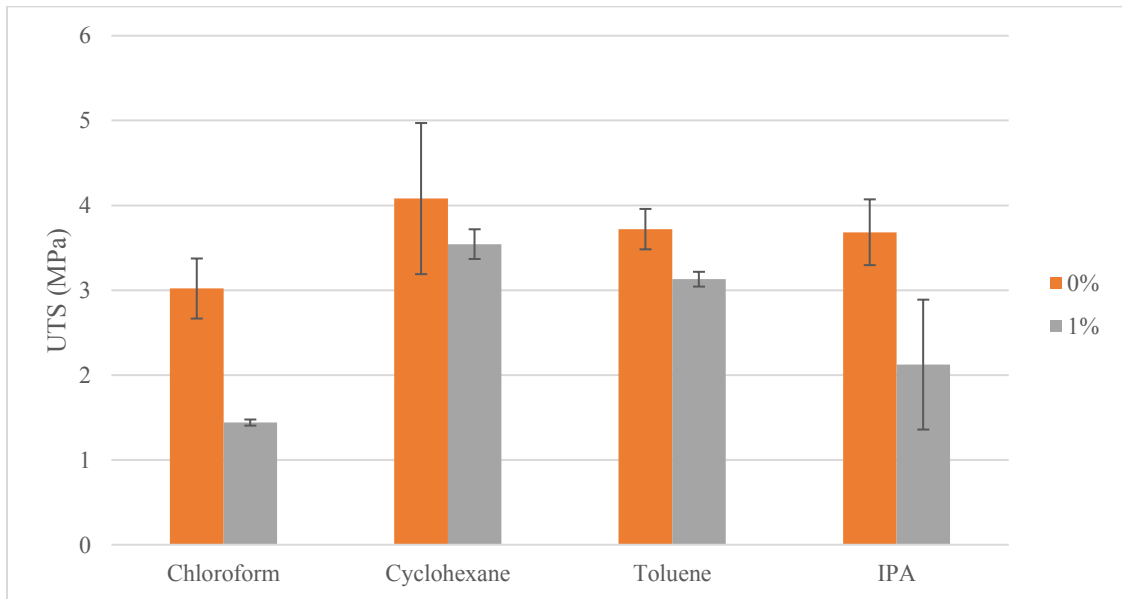


**Figure 3-44: UTS of different co-solution cured GNP/PDMS samples**

## 4 CONCLUSIONS

The effect of carbon-based nano-fillers of various morphologies and their effect on swelling of PDMS polymer matrices was explored by experimentation. Three types of carbon-based nano-filler – graphene nano-platelets (GNP), carbon black (CB), and graphene nano-scrolls (NS) – from volume fraction ranging from 0% to 4% were used as additives to the PDMS matrix. Experimental samples of 1 mm thick GNP/PDMS, CB/PDMS and NS/PDMS were manufactured via in-situ polymerization with solution mixing. A digital optic swelling measurement system was used to record both transient and steady-state dimensions for the nanocomposites immersed in organic solutions of toluene, chloroform, and acetone. The full experiments of this study included two sets of swelling experiments, characterization of polymer crosslinking density, characterization of the electrical resistivity, assessment of filler agglomeration via microscopy and X-ray diffraction analysis, and mechanical strength testing.

The first set of swelling experiments involved all three nanocomposites with volume fractions ranging from 0% to 4% swelled with swelling agents of toluene, chloroform, and acetone. The objectives for the first set of experiments was to determine the equilibrium swelling time, to elucidate the effect of the nano-filler morphology on the swelling of the nanocomposite, and to validate the Kraus relation that was assumed to describe the swelling behavior. The first set of swelling data showed an equilibrium time of approximately 4 hours for all three nanocomposites across all volume percentages. Hence, **the first conclusion was that the transient swelling process was not significantly affected by the addition of carbon-based nano-fillers.**

The steady-state swelling results for the three swelling agents were different where the swelling ratio with acetone was consistently recorded at 1.09 regardless of filler addition, volume

percentages of the filled nanocomposite, and different types of nano-fillers. Equilibrium data for all other swelling agents were plotted along with the linear Kraus equation that relates the swelling of nanocomposite to volume fraction. However, none of the experimental data obeyed the Kraus relationship. The equilibrium swelling ratio between CB/PDMS and NS/PDMS were similar within experimental error at all volume percentages, but both were approximately 25% higher than that of GNP/PDMS at 4% volume fraction in chloroform. The swelling ratio of NS/PDMS was 2.4% higher than that of CB/PDMS at 4% volume fraction. However, this small difference did not explain the effect of different nano-filler morphology on swelling. Therefore, the difference in swelling between GNP/PDMS, CB/PDMS and NS/PMDS remained undetermined and needed to be further explored. The first set of swelling experiments indicated a common factor between CB/PDMS and NS/PDMS which was the co-solution used during in-situ polymerization, which was different from GNP/PDMS. Hence, the assumption of the manufacturing process effecting swelling ratio of the nanocomposite arose and was explored in a second set of the swelling experiments.

The second set of swelling experiments tested different manufacturing parameters for 0% and 1% GNP/PDMS (or NS/PDMS). Pure PDMS (0%) and 1% volume fraction GNP/PDMS were created by in-situ polymerization with four different co-solutions: chloroform, toluene, isopropanol and cyclohexane. In addition, alternative manufacturing parameters of 'No-Sonication' and curing at room temperature were also employed for creating 1% GNP/PDMS. Equilibrium swelling ratios were determined for all samples with the previous three swelling agents. Similar to the first set of swelling experiments, none of the alternative manufacturing methods affected the swelling of PDMS in acetone, which was approximately constant at 1.09. Hence, **the second conclusion was that the effect of carbon nano-fillers on swelling is different depending on the swelling**

**solution.** Pure PDMS with alternative co-solutions exhibited a 4% increase in swelling ratio with samples cured with chloroform as compared to the other three co-solutions. However, none of all three nanocomposites tested in the first set of swelling experiments were cured with chloroform, instead with either isopropanol or cyclohexane. From the results with pure PDMS, it was determined that the co-solution has an insignificant effect on the polymer matrix. The swelling results for 1% GNP/PDMS with alternative co-solutions showed the highest to lowest swelling ratio for isopropanol, chloroform, toluene and finally cyclohexane. Coupled with the result of the highest swelling ratio out of all PDMS modified with 1% filler volume fraction being the no sonication sample, the assumption was made that the co-solution hindered the exfoliation of the nano-fillers. In addition, a lower degree of exfoliation was assumed to be the major factor with the 25% increase in swelling ratio between GNP/PDMS and NS/PDMS or CB/PDMS during the first set of swelling experiments.

Prior to exploring the effect of nano-filler exfoliation on swelling of PDMS, the polymer cross-linking density of all manufactured samples were tested to examine the influence of the polymer matrix on swelling. GNP/PDMS showed no change in cross-linking density with increasing filler volume fraction. In contrast, CB/PDMS and NS/PDMS exhibited a decreasing cross-linking density as filler volume increased. The relation between the cross-linking density and its corresponding swelling ratio indicated a major inflection point for the lowest level of filler addition (1% volume fraction). Therefore, a decrease in cross-linking density was a minor cause for swelling of CB/PDMS and NS/PDMS but not the primary factor. Further corroboration that nano-filler addition chiefly affects swelling and not a lack of cross-linking of the PDMS matrix was shown by the cross-linking density of all 0% and 1% GNP/PDMS made with alternative co-solutions and alternative manufacture parameters resulted in the same cross-linking density as pure

PDMS. Specifically, the 1% GNP/PDMS with no sonication had the same cross-linking density as the 1% GNP/PDMS with cyclohexane co-solution at 95%, but a difference in swelling ratio of 16.3%. With the results of cross-linking density, the presumption that the degree of nano-filler exfoliation chiefly affects swelling was more plausible.

Three methods were used to characterize the state of carbon nano-filler exfoliation within the nanocomposites: electrical resistivity measurements, digital imaging via electron and helium ion microscopy, and X-ray diffraction analysis. Even though electrical resistivity does not directly relate to filler exfoliation, a low degree of exfoliation will cause insulative behavior even after a theoretical percolation state is reached. This was the case with both CB/PDMS and NS/PDMS samples within this study, where these samples were fully insulative at the highest volume fraction. In contrast, GNP/PDMS reached became semi-conductive with filler addition. The difference in the electrical resistivity results further indicates that a high degree of agglomeration was present in CB/PDMS and NS/PDMS samples. SEM, TEM and HIB microscopy were performed, but they were not indicative of the degree of exfoliation due to the small field of view. However, HIB microscopy showed a clear image of graphene NS that was not found in previous technical literature. X-ray diffraction characterization of NS/PDMS and GNP/PDMS provided the most indicative results. The characteristic peak of pure GNP was still apparent in the NS/PDMS at around  $30.7^\circ$ , but was shifted  $10^\circ$  lower in GNP/PDMS. The peak in the XRD results of NS/PDMS indicated large aggregates of nano-fillers within the nanocomposite. In contrast, the peak at a lower diffraction angle for GNP/PDMS was the result of intercalation between the nano-fillers and the polymer chains. Even though nano-fillers in GNP/PDMS were still not fully exfoliated, the XRD results indicated reduced nano-filler aggregation. Hence, GNP/PDMS was assumed to have a higher degree of exfoliation than NS/PDMS. The exfoliation characterization confirmed the

previous assumption, and it was hence **concluded that a low degree of carbon nano-fillers exfoliation promotes increased swelling in nanocomposites**. It is presumed that the increase in swelling in the presence of filler agglomerates is due to the expansion of the agglomerated clusters inside the polymer network.

Finally, mechanical properties (elastic modulus and UTS) of all nanocomposites were investigated and contrasted to the swelling results. For CB/PDMS and NS/PDMS the modulus of elasticity decreased compared to PDMS with increasing nano-filler content. This result contradicts concepts such as the rule of mixture theory for composite materials. It was assumed that a lack of filler exfoliation created micro-void like features inside the nanocomposite, changing the material morphology and thus decreasing the mechanical properties. For GNP/PDMS, which is deemed to be a nanocomposite with a lesser degree of filler agglomeration, the mechanical properties were hardly affected with increasing nano-filler content. Elastic modulus data were also plotted against their respective cross-linking density and swelling ratio, which revealed that cross-linking density did not have a significance on the swelling behavior.

To summarize, the effect of carbon-based nano-fillers on the swelling of polymer nanocomposite was studied using optical measurement technique coupled with material characterizations for the polymer cross-linking density and the degree of filler exfoliation. The performed experimentation was successful in quantifying the swelling of nanocomposite. In addition, the experimental results indicated that a lack of nano-filler exfoliation is the primary factor for increased swelling of nanocomposites compared to the base polymer. It is presumed that in agglomerated nano-filler composites, increasing filler content causes the swelling ratio to rise.

## 5 EXTENDED WORK

The major conclusion derived from this thesis was that a low degree of nano-filler exfoliation significantly increases the swelling of nanocomposites. Due to the lack of nano-filler exfoliation, some original objectives of this study, i.e. the validation of the Kraus equation and identifying the Hildebrand parameter, were not achieved. The following section details possible extensions to this studies that may permit achieving the remaining objectives.

Firstly, to eliminate swelling effects from filler agglomeration, future studies should attempt extending the sonication time to 48 hours at 100% equipment power with an alternative tip. Also, shear mixing with a three-roll mill may be attempted as an alternative or additional method of manufacturing. Increasing the sonication time and power and/or introducing three-roll milling may increase the probability of achieving homogenous filler dispersion.

Secondly, testing of nanocomposites with homogeneously dispersed fillers should be performed to achieve the original objective of validating the Kraus equation. The employed experimental technique can then be used to validate both the Kraus equation and the Modified Kraus equation with IAF. With respect to the latter, additional microscopy characterization will need to be performed in order to determine the length of the nano-fillers. Once these models are validated, material constants can be determined which can be used to predict the swelling change for a given nanocomposites filler volume content. However, should the validation of the models be unsuccessful, a new model should be developed.

Thirdly, an attempt should be made to correlate the Hildebrand and/or Hansen parameters with the filler volume percentage. The Hildebrand and/or Hansen parameters of a certain polymer can be determined empirically by immersing the polymer in multiple organic solutions. The Hansen

parameter of the solution that swells the polymer the most would be closest in value of the polymer. The current study only employed three organic solutions as the swelling agents. If the sample size of swelling agents would be increased substantially a correlation between the Hansen parameter and the nano-filler volume percentage could be determined. If this relationship can be found between carbon nano-filler percentage and the quantified value of intermolecular force, swelling of nanocomposite can effectively be predicted in various combinations of carbon-based nanocomposites.

Fourthly, carbon-based nanocomposites could be employed in a micro-fluidic scenario. Suitable nanocomposites could be used to either construct micro-valves or micro-pumps while utilizing organic solution for actuation. Alternatively, due to the possible conductive nature of carbon-based nanocomposites, sensors or actuators can be constructed with the additional ability to resist swelling. Hence, sensors and actuators with limited to no variability can be created for micro-fluidic systems employing a set of organic solutions.

Lastly, all of the mentioned and future suggested studies are based on carbon-based PDMS nanocomposites. The same experimental method can be repeated for other types of nanocomposites to extend the knowledge on polymer swelling behavior.

## REFERENCES

- [1] Hussain, Farzana, Review article: polymer-matrix nanocomposites, processing, manufacturing, and application: an overview." *Journal of composite materials* 40.17 (2006): 1511-1575.
- [2] Liang, Jiajie, et al. "Electromagnetic interference shielding of graphene/epoxy composites." *Carbon* 47.3 (2009): 922-925.
- [3] Chung, D. D. L. "Electrical applications of carbon materials." *Journal of Materials Science* 39.8 (2004): 2645-2661.
- [4] Novoselov, Konstantin S., et al. "A roadmap for graphene." *Nature* 490.7419 (2012): 192-200.
- [5] Filipcsei G, Csetneki I, Szilágyi A, Zrínyi M. Magnetic field-responsive smart polymer composites. In *Oligomers-Polymer Composites-Molecular Imprinting 2007* (pp. 137-189). Springer Berlin Heidelberg.
- [6] Burke, John. "Solubility parameters: theory and application." (1984).
- [7] Barton, Allan FM. "Solubility parameters." *Chemical Reviews* 75.6 (1975): 731-753.
- [8] How to Recognize and Avoid the Common Causes of O-ring Failure  
<http://www.hydraulicspneumatics.com/200/TechZone/Seals/Article/False/6504/TechZone-Seals>
- [9] EPM, Inc. The Seal Man's O-Ring Handbook,  
[https://www.physics.harvard.edu/uploads/files/machinshop/epm\\_oring\\_handbook.pdf](https://www.physics.harvard.edu/uploads/files/machinshop/epm_oring_handbook.pdf)
- [10] Salimi-Moosavi, Hossein, Thompson Tang, and D. Jed Harrison. "Electroosmotic pumping of organic solvents and reagents in microfabricated reactor chips." *Journal of the American Chemical Society* 119.37 (1997): 8716-8717.

- [11] Kakuta, Masaya, Fiona G. Bessoth, and Andreas Manz. "Microfabricated devices for fluid mixing and their application for chemical synthesis." *The Chemical Record* 1.5 (2001): 395-405. Gerlach, Gerald, et al. "Chemical and pH sensors based on the swelling behavior of hydrogels." *Sensors and Actuators B: Chemical* 111 (2005): 555-561.
- [12] Richter, Andreas, et al. "Review on hydrogel-based pH sensors and microsensors." *Sensors* 8.1 (2008): 561-581.
- [13] Chawla, Krishan K. *Composite materials: science and engineering*. Springer Science & Business Media, 2012.
- [14] Becker, Holger, and Laurie E. Locascio. "Polymer microfluidic devices." *Talanta* 56.2 (2002): 267-287.
- [15] Yao, Tze-Jung, et al. "Micromachined rubber O-ring micro-fluidic couplers." *Micro Electro Mechanical Systems, 2000. MEMS 2000. The Thirteenth Annual International Conference on*. IEEE, 2000.
- [16] Alexandre, M. and Dubois, P. (2000). Polymer-layered Silicate Nanocomposites: Preparation, Properties and Uses of a New Class of Materials, *Mater. Sci. Eng. Rep.*, 28: 1–63. (Reproduced in part with permission from Elsevier \_ 2006.)
- [17] Schmidt, D., Shah, D. and Giannelis, E.P. (2002). New Advances in Polymer/Layered Silicate Nanocomposites, *Current Opinion in Solid State and Materials Science*, 6(3): 205–212.
- [18] Viculis, Lisa M., Julia J. Mack, and Richard B. Kaner. "A chemical route to carbon nanoscrolls." *Science* 299.5611 (2003): 1361-1361.
- [19] Xie, Xu, et al. "Controlled fabrication of high-quality carbon nanoscrolls from monolayer graphene." *Nano letters* 9.7 (2009): 2565-2570.

- [20] Xia, Dan, et al. "Fabrication of carbon nanoscrolls from monolayer graphene." *Small* 6.18 (2010).
- [21] Bellido, Edson P., and Jorge M. Seminario. "Molecular dynamics simulations of folding of supported graphene." *The Journal of Physical Chemistry C* 114.51 (2010): 22472-22477.
- [22] , Changgu, et al. "Measurement of the elastic properties and intrinsic strength of monolayer graphene." *science* 321.5887 (2008): 385-388.
- [23] Filippidou, M. K., et al. "A flexible strain sensor made of graphene nanoplatelets/polydimethylsiloxane nanocomposite." *Microelectronic Engineering* 142 (2015): 7-11.
- [24] Loomis, James, Ben King, and Balaji Panchapakesan. "Layer dependent mechanical responses of graphene composites to near-infrared light." *Applied Physics Letters* 100.7 (2012): 073108.
- [25] Li, Jing, Pui-Shan Wong, and Jang-Kyo Kim. "Hybrid nanocomposites containing carbon nanotubes and graphite nanoplatelets." *Materials Science and Engineering: A* 483 (2008): 660-663.
- [26] Zaman, Izzuddin, et al. "From carbon nanotubes and silicate layers to graphene platelets for polymer nanocomposites." *Nanoscale* 4.15 (2012): 4578-4586.
- [27] Oskouyi, Amirhossein Biabangard, and Pierre Mertiny. "Monte Carlo model for the study of percolation thresholds in composites filled with circular conductive nano-disks." *Procedia Engineering* 10 (2011): 403-408.
- [28] Du, Xu, et al. "Approaching ballistic transport in suspended graphene." *Nature nanotechnology* 3.8 (2008): 491-495.

- [29] Bunch, J. Scott, et al. "Impermeable atomic membranes from graphene sheets." *Nano letters* 8.8 (2008): 2458-2462.
- [30] Shen, Jianfeng, et al. "Mechanical, thermal and swelling properties of poly (acrylic acid)–graphene oxide composite hydrogels." *Soft Matter* 8.6 (2012): 1831-1836.
- [31] Hou, Chengyi, et al. "Graphene–polymer hydrogels with stimulus-sensitive volume changes." *Carbon* 50.5 (2012): 1959-1965.
- [32] Roy, Nabarun, Rajatendu Sengupta, and Anil K. Bhowmick. "Modifications of carbon for polymer composites and nanocomposites." *Progress in polymer science* 37.6 (2012): 781-819.
- [33] Huang, Jan-Chan. "Carbon black filled conducting polymers and polymer blends." *Advances in Polymer Technology* 21.4 (2002): 299-313.
- [34] Sumita, Masao, et al. "Dispersion of fillers and the electrical conductivity of polymer blends filled with carbon black." *Polymer Bulletin* 25.2 (1991): 265-271.
- [35] Hindermann-Bischoff, Manuela, and Françoise Ehrburger-Dolle. "Electrical conductivity of carbon black–polyethylene composites: Experimental evidence of the change of cluster connectivity in the PTC effect." *Carbon* 39.3 (2001): 375-382.
- [36] Chung, K. T., A. Sabo, and A. P. Pica. "Electrical permittivity and conductivity of carbon black-polyvinyl chloride composites." *Journal of Applied Physics* 53.10 (1982): 6867-6879.
- [37] Li, Fengkui, et al. "Polyurethane/conducting carbon black composites: structure, electric conductivity, strain recovery behavior, and their relationships." *Journal of Applied Polymer Science* 75.1 (2000): 68-77.

- [38] Kraus, Gerard. "Swelling of filler-reinforced vulcanizates." *Journal of Applied Polymer Science* 7.3 (1963): 861-871.
- [39] Rattanasom, N., T. Saowapark, and C. Deeprasertkul. "Reinforcement of natural rubber with silica/carbon black hybrid filler." *Polymer Testing* 26.3 (2007): 369-377.
- [40] Schadler, L.S., Giannaris, S.C. and Ajayan, P.M. (1998). Load Transfer in Carbon Nanotube Epoxy Composites, *Applied Physics Letters*, 73(26): 3842–3844.
- [41] Xiao, K.Q. and Zhang, L.C. (2004). The Stress Transfer Efficiency of a Single-walled Carbon Nanotube in Epoxy Matrix, *Journal of Materials Science*, 39(14): 4481–4486.
- [42] Lau, K.T., Lu, M., Lam, C.K., Cheung, H.Y., Sheng, F.L. and Li, H.L. (2005). Thermal and Mechanical Properties of Single-walled Carbon Nanotube Bundle-reinforced Epoxy Nanocomposites: the Role of Solvent for Nanotube Dispersion, *Composites Science and Technology*, 65(5): 719–725.
- [43] Valentini, L., Puglia, D., Frulloni, E., Armentano, I., Kenny, J.M. and Santucci, S. (2004). Dielectric Behavior of Epoxy Matrix/Single-walled Carbon Nanotube Composites, *Composites Science and Technology*, 64(1): 23–33.
- [44] Sandler, J., Shaffer, M.S.P., Prasse, T., Bauhofer, W., Schulte, K. and Windle, A.H. (1999). Development of a Dispersion Process for Carbon Nanotubes in an Epoxy Matrix and the Resulting Electrical Properties, *Polymer*,
- [45] Monteiro-Riviere, N.A., Nemanich, R.J., Inman, A.O., Wang, Y.Y. and Riviere, J.E. (2005). Multi-walled Carbon Nanotube Interactions with Human Epidermal Keratinocytes, *Toxicology Letters*, 155: 377–384.
- [46] Nancy, A., Monteiro-Riviere, and Alfred, O. (2006). Inman Challenges for Assessing Carbon Nanomaterial Toxicity to the Skin, *Carbon*, 44: 1070–1078.

- [47] Shvedova, A., Castranova, V., Kisin, E., Schwegler-Berry, D., Murray, A.R., Gandelsman, V.Z., Maynard, A. and Baron, P. (2003). Exposure to Carbon Nanotube Material: Assessment of Nanotube Cytotoxicity Using Human Keratinocyte Cells, *Journal of Toxicology and Environmental Health, Part A*, 66: 1909–1926.
- [48] Mazumder, S.K. (ed.). (2002). *Composites Manufacturing, Materials, Product and Process Engineering*, CRC Taylor & Francis, ISBN 0-8493-0585-3.
- [49] Lao, S., Ho, W., Ngyuen, K., Koo, J.H., et al. (2005). Micro Structural Analysis of Nylon 11 Nanocomposites, SAMPE, Seattle, WA.
- [50] Wu, C.L., Zhang, M.Q., Rong, M.Z. and Friedrich, K. (2002). Tensile Performance Improvement of Low Nanoparticles Filled-polypropylene Composites, *Composite Science and Technology*, 62: 1327–1340.
- [51] Zhang, Z. and Yang, J.L. (2004). Creep Resistant Polymeric Nanocomposites, *Polymer*, 45: 3481–3485.
- [52] Koo, J.H., Pilato, L.A. and Wissler, G.E. (2005). Polymer Nanostructured Materials for Propulsion System, In: *Conference Proceedings for AIAA-2005-3606*, 41st AIAA/ASME/SAE/ASEE Joint Propulsion Conference & Exhibit, Tucson, AZ, 10–13 July 2005.
- [53] Koo, J.H., Stretz, J., Weispfenning, Z., Luo, P. and Wootan, W. (2004). Nanocomposite Rocket Ablative Materials: Subscale Ablation Test, In: *SAMPE Symposium*, Long Beach, California, May, 2004.
- [54] Koo, J.H., Pilato, L.A., Wissler, G., Lee, A., Abusafieh, A. and Weispfenning, J. (2005). Epoxy Nanocomposites for Carbon Reinforced Polymer Matrix Composites, SAMPE, CA.

- [55] Chen, Y.C., Zhou, S.X. and Wu, L.M. (2005). *European Polymer Journal* (submitted 2005).
- [56] Chen, Y.C., Zhou, S.X., Yang, H.H. and Wu, L.M. (2005). Structure and Properties of Polyurethane/Nanosilica Composites, *Journal of Applied Polymer Science*, 95(5): 1032–1039.
- [57] Liu, Pinggui, et al. "Preparation and characterization of poly (vinyl acetate)-intercalated graphite oxide nanocomposite." *Journal of Materials Chemistry* 10.4 (2000): 933-935.
- [58] Jang, Jin Young, et al. "Graphite oxide/poly (methyl methacrylate) nanocomposites prepared by a novel method utilizing macroazoinitiator." *Composites Science and Technology* 69.2 (2009): 186-191.
- [59] Pötschke, Petra, Arup R. Bhattacharyya, and Andreas Janke. "Melt mixing of polycarbonate with multiwalled carbon nanotubes: microscopic studies on the state of dispersion." *European Polymer Journal* 40.1 (2004): 137-148.
- [60] Lin, Bin, Uttandaraman Sundararaj, and Petra Pötschke. "Melt Mixing of Polycarbonate with Multi-Walled Carbon Nanotubes in Miniature Mixers." *Macromolecular Materials and Engineering* 291.3 (2006): 227-238.
- [61] Pötschke, Petra, et al. "Melt mixing as method to disperse carbon nanotubes into thermoplastic polymers." *Fullerenes, nanotubes, and carbon nanostructures* 13.S1 (2005): 211-224.
- [62] Kim, Hyunwoo, Yutaka Miura, and Christopher W. Macosko. "Graphene/polyurethane nanocomposites for improved gas barrier and electrical conductivity." *Chemistry of Materials* 22.11 (2010): 3441-3450.

- [63] Liu, Pinggui, et al. "Preparation and characterization of poly (vinyl acetate)-intercalated graphite oxide nanocomposite." *Journal of Materials Chemistry* 10.4 (2000): 933-935.
- [64] Jang, Jin Young, et al. "Graphite oxide/poly (methyl methacrylate) nanocomposites prepared by a novel method utilizing macroazoinitiator." *Composites Science and Technology* 69.2 (2009): 186-191.
- [65] Wang, Shiren, et al. "Thermal expansion of graphene composites." *Macromolecules* 42.14 (2009): 5251-5255.
- [66] Lee, Yu Rok, et al. "Properties of waterborne polyurethane/functionalized graphene sheet nanocomposites prepared by an in-situ method." *Macromolecular Chemistry and Physics* 210.15 (2009): 1247-1254.
- [67] Lee, C., L. Jug, and E. Meng. "High Strain And Biocompatible Screen Printed Nanocomposite Based Conductive PDMS Strain Sensors." *Hilton Head 2012 (Hilton Head Island, SC)* (2012): 161.
- [68] Bashar, Mohammad, Pierre Mertiny, and Uttandaraman Sundararaj. "Effect of nanocomposite structures on fracture behavior of epoxy-clay nanocomposites prepared by different dispersion methods." *Journal of Nanomaterials* 2014 (2014): 70.
- [69] Bourlinos, Athanasios B., et al. "Liquid-phase exfoliation of graphite towards solubilized graphenes." *small* 5.16 (2009): 1841-1845.
- [70] Hernandez, Yenny, et al. "High-yield production of graphene by liquid-phase exfoliation of graphite." *Nature nanotechnology* 3.9 (2008): 563-568.
- [71] Kim, Hyunwoo, Ahmed A. Abdala, and Christopher W. Macosko. "Graphene/polymer nanocomposites." *Macromolecules* 43.16 (2010): 6515-6530.

- [72] Girifalco, L. A. & Good, R. J. A theory for the estimation of surface and interfacial energies. 1. Derivation and application to interfacial tension. *J. Phys. Chem.* 61, 904–909 (1957).
- [73] Hodak, M. & Girifalco, L. A. Fullerenes inside carbon nanotubes and multi-walled carbon nanotubes: optimum and maximum sizes. *Chem. Phys. Lett.* 350, 405–411 (2001).
- [74] Papirer, Eugene, et al. "Comparison of the surface properties of graphite, carbon black and fullerene samples, measured by inverse gas chromatography." *Carbon* 37.8 (1999): 1265-1274.
- [75] Ericson, Lars, M. (2000). Strength Characterization of Suspended Single-Wall Carbon Nanotube Ropes, Masters Thesis, Rice University, Oct 2000.
- [76] Jana, S.C. and Jain, S. (2001). Dispersion of Nanofillers in High Performance Polymers using Reactive Solvents as Processing Aids, *Polymer*, 42: 6897–6905.
- [77] Mark, James E., ed. *Physical properties of polymers handbook*. Vol. 1076. New York: Springer, 2007.
- [78] Hildebrand, J. H., and R. L. Scott. "Solubility of non-electrolytes Reinhold Pub." *Corp, New York* (1950): 247.
- [79] Hildebrand, Joel Henry, and Robert Lane Scott. *Regular solutions*. Prentice-Hall, 1962.
- [80] Hansen, Charles M. "The three dimensional solubility parameter." *Danish Technical: Copenhagen* (1967): 14.
- [81] Hansen, Charles M. "The universality of the solubility parameter." *Industrial & engineering chemistry product research and development* 8.1 (1969): 2-11.
- [82] Anfimova, E. A., A. S. Lykin, and B. N. Anfimov. "Equilibrium swelling of filled vulcanizates of natural rubber." *Polymer Science USSR* 24.2 (1982): 455-461.

- [83] Rubinstein, Michael, and Ralph H. Colby. *Polymer physics*. Vol. 23. New York: Oxford University Press, 2003.
- [84] Bhattacharya, Mithun, and Anil K. Bhowmick. "Polymer–filler interaction in nanocomposites: New interface area function to investigate swelling behavior and Young's modulus." *Polymer* 49.22 (2008): 4808-4818.
- [85] Bandyopadhyay, Abhijit, Mousumi De Sarkar, and Anil K. Bhowmick. "Polymer–filler interactions in sol–gel derived polymer/silica hybrid nanocomposites." *Journal of Polymer Science Part B: Polymer Physics* 43.17 (2005): 2399-2412.
- [86] Burnside, S. D., & Giannelis, E. P. (2000). Nanostructure and properties of polysiloxane-layered silicate nanocomposites. *Journal of Polymer Science Part B: Polymer Physics*, 38(12), 1595-1604.
- [87] Burnside, S. D., & Giannelis, E. P. (1995). Synthesis and properties of new poly (dimethylsiloxane) nanocomposites. *Chemistry of materials*, 7(9), 1597-1600.
- [88] Marquez, A., Uribe, J., & Cruz, R. (1997). Conductivity variation induced by solvent swelling of an elastomer–carbon black–graphite composite. *Journal of applied polymer science*, 66(12), 2221-2232.
- [89] Mostafa, A., Abouel-Kasem, A., Bayoumi, M. R., & El-Sebaie, M. G. (2009). Effect of carbon black loading on the swelling and compression set behavior of SBR and NBR rubber compounds. *Materials & Design*, 30(5), 1561-1568.
- [90] Araby, S., Zhang, L., Kuan, H. C., Dai, J. B., Majewski, P., & Ma, J. (2013). A novel approach to electrically and thermally conductive elastomers using graphene. *Polymer*, 54(14), 3663-3670.

- [91] Araby, S., Meng, Q., Zhang, L., Kang, H., Majewski, P., Tang, Y., & Ma, J. (2014). Electrically and thermally conductive elastomer/graphene nanocomposites by solution mixing. *Polymer*, 55(1), 201-210.
- [92] Zhang, L., Wang, Z., Xu, C., Li, Y., Gao, J., Wang, W., & Liu, Y. (2011). High strength graphene oxide/polyvinyl alcohol composite hydrogels. *Journal of Materials Chemistry*, 21(28), 10399-10406.
- [93] Shen, J., Yan, B., Li, T., Long, Y., Li, N., & Ye, M. (2012). Mechanical, thermal and swelling properties of poly (acrylic acid)–graphene oxide composite hydrogels. *Soft Matter*, 8(6), 1831-1836.
- [94] Huang, Y., Zeng, M., Ren, J., Wang, J., Fan, L., & Xu, Q. (2012). Preparation and swelling properties of graphene oxide/poly (acrylic acid-co-acrylamide) super-absorbent hydrogel nanocomposites. *Colloids and Surfaces A: Physicochemical and Engineering Aspects*, 401, 97-106.
- [95] Tai, Z., Yang, J., Qi, Y., Yan, X., & Xue, Q. (2013). Synthesis of a graphene oxide–polyacrylic acid nanocomposite hydrogel and its swelling and electroresponsive properties. *RSC Advances*, 3(31), 12751-12757.
- [96] Liu, R., Liang, S., Tang, X. Z., Yan, D., Li, X., & Yu, Z. Z. (2012). Tough and highly stretchable graphene oxide/polyacrylamide nanocomposite hydrogels. *Journal of Materials Chemistry*, 22(28), 14160-14167.
- [97] Favre, E. "Swelling of crosslinked polydimethylsiloxane networks by pure solvents: influence of temperature." *European Polymer Journal* 32.10 (1996): 1183-1188.

- [98] Hedden, Ronald C., Himanshu Saxena, and Claude Cohen. "Mechanical properties and swelling behavior of end-linked poly (dimethylsiloxane) networks." *Macromolecules* 33.23 (2000): 8676-8684.
- [99] Bandyopadhyay, Abhijit, Mousumi De Sarkar, and Anil K. Bhowmick. "Polymer–filler interactions in sol–gel derived polymer/silica hybrid nanocomposites." *Journal of Polymer Science Part B: Polymer Physics* 43.17 (2005): 2399-2412.
- [100] Gevers, Lieven EM, Ivo FJ Vankelecom, and Pierre A. Jacobs. "Solvent-resistant nanofiltration with filled polydimethylsiloxane (PDMS) membranes." *Journal of membrane science* 278.1 (2006): 199-204.
- [101] S.D. Burnside and E.P. Giannelis, "Nanostructure and properties of polysiloxane-layered silicate nanocomposites", *Journal of Polymer Science Part B* 38(12), pp. 1595–1604, 2000.
- [102] Lee, Jessamine Ng, Cheolmin Park, and George M. Whitesides. "Solvent compatibility of poly (dimethylsiloxane)-based microfluidic devices." *Analytical Chemistry* 75.23 (2003): 6544-6554.
- [103] Alexandre, M. and Dubois, P. (2000). Polymer-layered Silicate Nanocomposites: Preparation, Properties and Uses of a New Class of Materials, *Mater. Sci. Eng. Rep.*, 28: 1–63.
- [104] Ibrahim, I. A. M., et al. "Elastic behavior of silica/poly (dimethylsiloxane) nanocomposites: nano-size effects." *IOP Conference Series: Materials Science and Engineering*. Vol. 40. No. 1. IOP Publishing, 2012.
- [105] Camenzind, Adrian, et al. "Structure & strength of silica-PDMS nanocomposites." *Polymer* 51.8 (2010): 1796-1804.

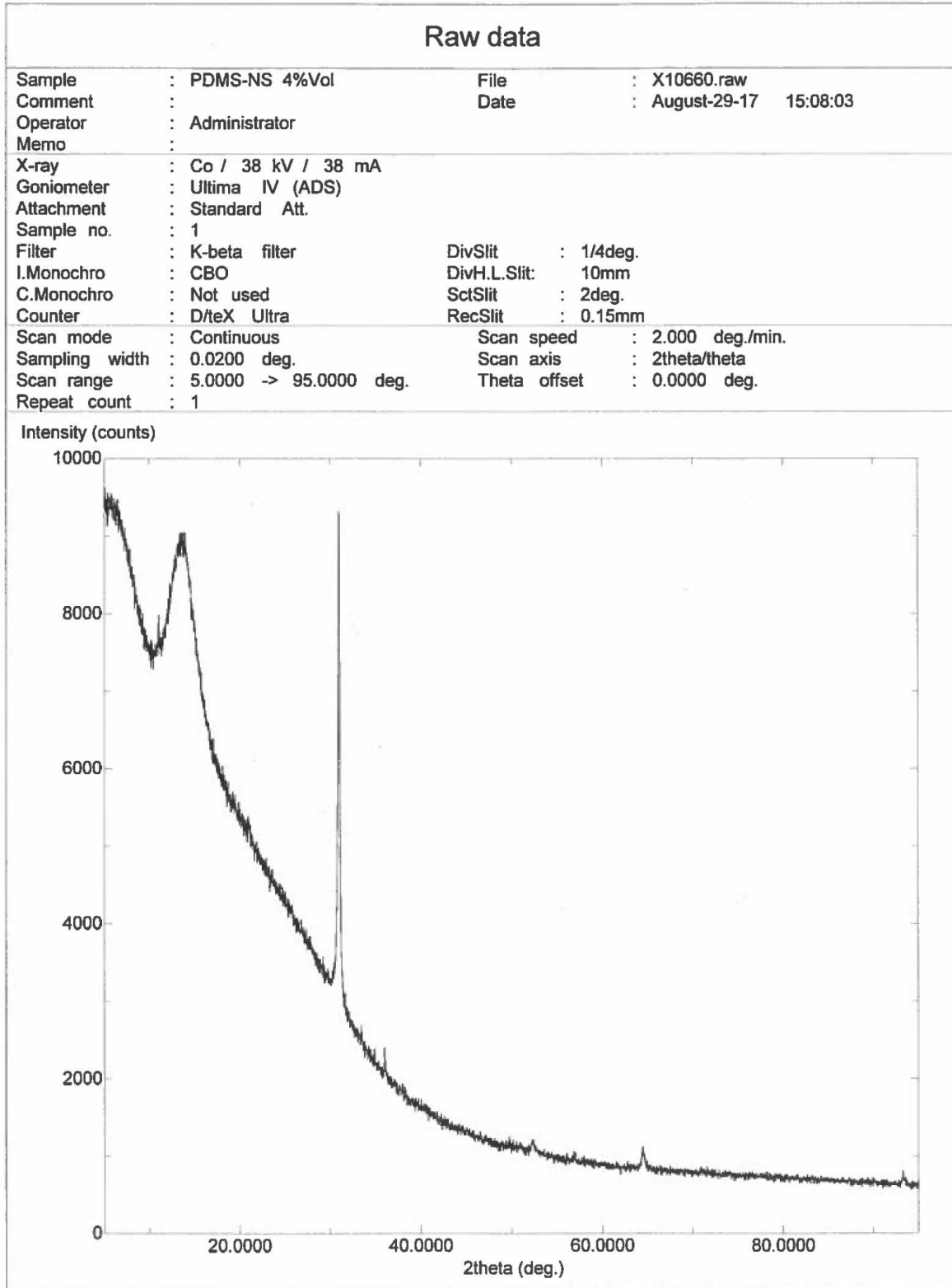
- [106] Reichert, P., Kressler, J., Thomann, R., Mulhaupt R. and Stoppelmann, G. (1998).  
Nanocomposites Based on a Synthetic Layer Silicate and Polyamide-12, *Acta Polymer*,  
49(2–3): 116–123.
- [107] Yano, K. and Usuki, A. (1993). Synthesis and Properties of Polyimide-Clay Hybrid, *J. Polym. Sci., Part A: Polym. Chem.*, 31: 2493–2498.
- [108] Bhattacharya, Sati N., Rahul K. Gupta, and Musa R. Kamal. "Polymeric nanocomposites." *Hanser, Munich* (2008).
- [109] Szabo, T.; Berkesi, O.; Forgo, P.; Josepovits, K.; Sanakis, Y.; Petridis, D.; Dekany, I. *Chem. Mater.* 2006, 18, 2740–2749.
- [110] Schniepp, Hannes C., et al. "Functionalized single graphene sheets derived from splitting graphite oxide." *The Journal of Physical Chemistry B* 110.17 (2006): 8535-8539.
- [111] McAllister, Michael J., et al. "Single sheet functionalized graphene by oxidation and thermal expansion of graphite." *Chemistry of materials* 19.18 (2007): 4396-4404.
- [112] Johnson, David W., Ben P. Dobson, and Karl S. Coleman. "A manufacturing perspective on graphene dispersions." *Current Opinion in Colloid & Interface Science* 20.5 (2015): 367-382.
- [113] Ibrahim, I. A. M., et al. "Elastic behavior of silica/poly (dimethylsiloxane) nanocomposites: nano-size effects." *IOP Conference Series: Materials Science and Engineering*. Vol. 40. No. 1. IOP Publishing, 2012.
- [114] Camenzind, Adrian, et al. "Structure & strength of silica-PDMS nanocomposites." *Polymer* 51.8 (2010): 1796-1804.

- [115] Raasch, Jonathan, et al. "Characterization of polyurethane shape memory polymer processed by material extrusion additive manufacturing." *Additive Manufacturing* 8 (2015): 132-141.
- [116] Ivey, Marcus A. *Towards the Development of Pseudoductile FRP Rebar*. Diss. University of Alberta, 2015.
- [117] Chandrasekaran, Swetha, Christian Seidel, and Karl Schulte. "Preparation and characterization of graphite nano-platelet (GNP)/epoxy nano-composite: mechanical, electrical and thermal properties." *European Polymer Journal* 49.12 (2013): 3878-3888.
- [118] Li, Jing, and Jang-Kyo Kim. "Percolation threshold of conducting polymer composites containing 3D randomly distributed graphite nanoplatelets." *Composites science and technology* 67.10 (2007): 2114-2120.
- [119] Kim, Kwanpyo, et al. "Multiply folded graphene." *Physical Review B* 83.24 (2011): 245433.
- [120] Xie, Xu, et al. "Controlled fabrication of high-quality carbon nanoscrolls from monolayer graphene." *Nano letters* 9.7 (2009): 2565-2570.
- [121] Maitra, Urmimala, et al. "Strategies for the synthesis of graphene, graphene nanoribbons, nanoscrolls and related materials." *CHIMIA International Journal for Chemistry* 66.12 (2012): 941-948.
- [122] Wang, Guoxiu, et al. "Facile synthesis and characterization of graphene nanosheets." *The Journal of Physical Chemistry C* 112.22 (2008): 8192-8195.
- [123] Liang, Jiajie, et al. "Molecular-level dispersion of graphene into poly (vinyl alcohol) and effective reinforcement of their nanocomposites." *Advanced Functional Materials* 19.14 (2009): 2297-2302.

- [124] McAllister, Michael J., et al. "Single sheet functionalized graphene by oxidation and thermal expansion of graphite." *Chemistry of materials* 19.18 (2007): 4396-4404.
- [125] Johnston, I. D., et al. "Mechanical characterization of bulk Sylgard 184 for microfluidics and microengineering." *Journal of Micromechanics and Microengineering* 24.3 (2014): 035017.
- [126] Schneider, Florian, et al. "Process and material properties of polydimethylsiloxane (PDMS) for Optical MEMS." *Sensors and Actuators A: Physical* 151.2 (2009): 95-99.
- [127] Loomis, James, et al. "Graphene-nanoplatelet-based photomechanical actuators." *Nanotechnology* 23.4 (2012): 045501.
- [128] Kim, Hyunwoo, and Christopher W. Macosko. "Processing-property relationships of polycarbonate/graphene composites." *Polymer* 50.15 (2009): 3797-3809.

## **APPENDICES**

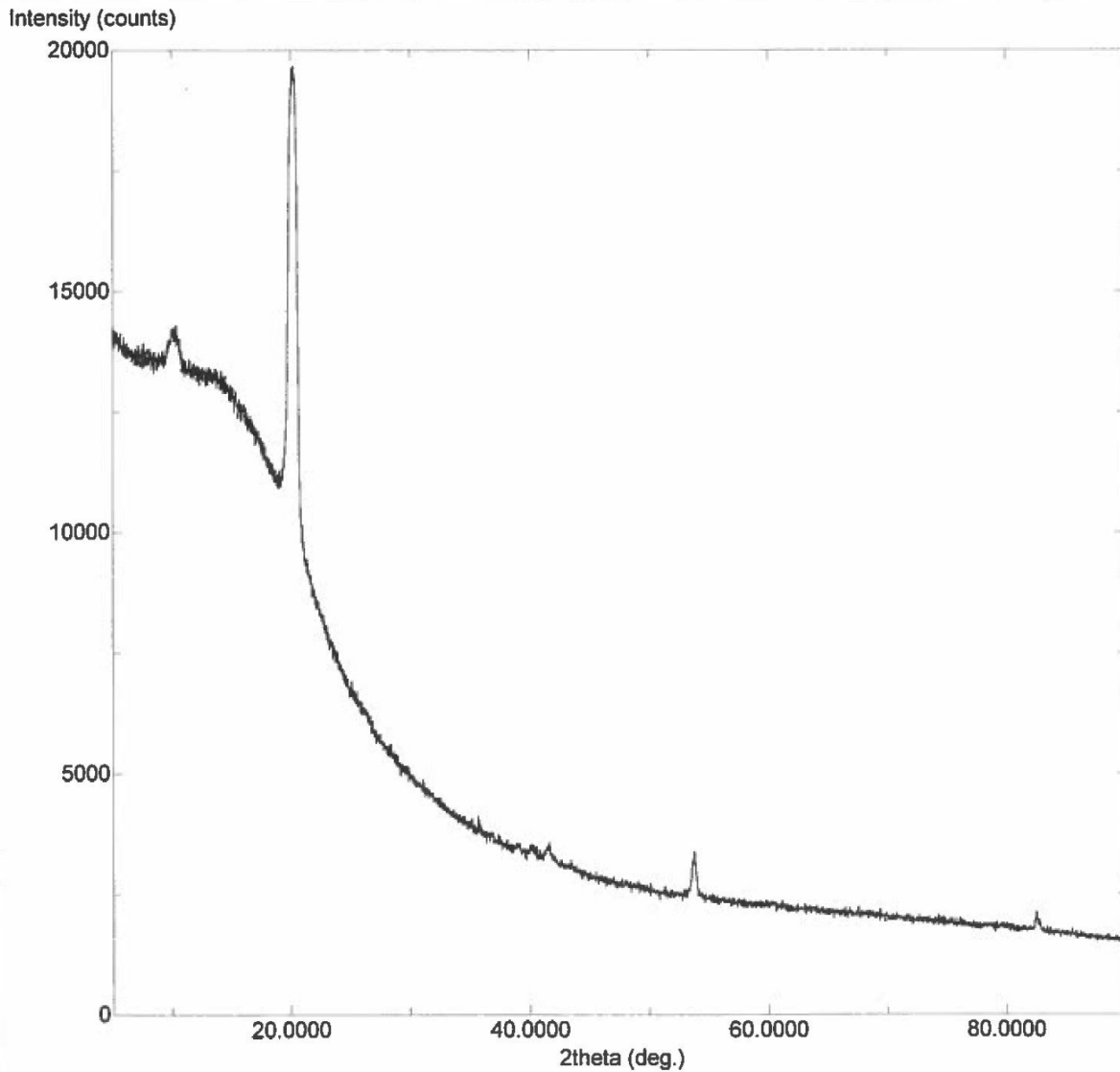
# APPENDIX A – SAMPLE XRD CHARACTERIZATION SHEETS



August-29-2017 15:54:45 Page-1

# Raw data

Sample	: GNP-PDMS 4%	File	: X10590.raw
Comment	:	Date	: August-17-17 09:04:36
Operator	: Administrator		
Memo	:		
X-ray	: Co / 38 kV / 38 mA		
Goniometer	: Ultima IV		
Attachment	: Standard Att.		
Sample no.	: 1		
Filter	: K-beta filter	DivSlit	: 2/3deg. Monochro RS: 0.8mm
I.Monochro	: CBO	DivH.L.Slit:	: 10.00mm
C.Monochro	: Fixed Monochro.(U4)	SctSlit	: Open
Counter	: D/teX Ultra	RecSlit	: Open
Scan mode	: Continuous	Scan speed	: 2.000 deg./min.
Sampling width	: 0.0200 deg.	Scan axis	: 2theta/theta
Scan range	: 5.0000 -> 90.0000 deg.	Theta offset	: 0.0000 deg.
Repeat count	: 1		



August-17-2017 09:48:48 Page-1

## APPENDIX B – ADDITIONAL MODULUS CORRELATION GRAPHS

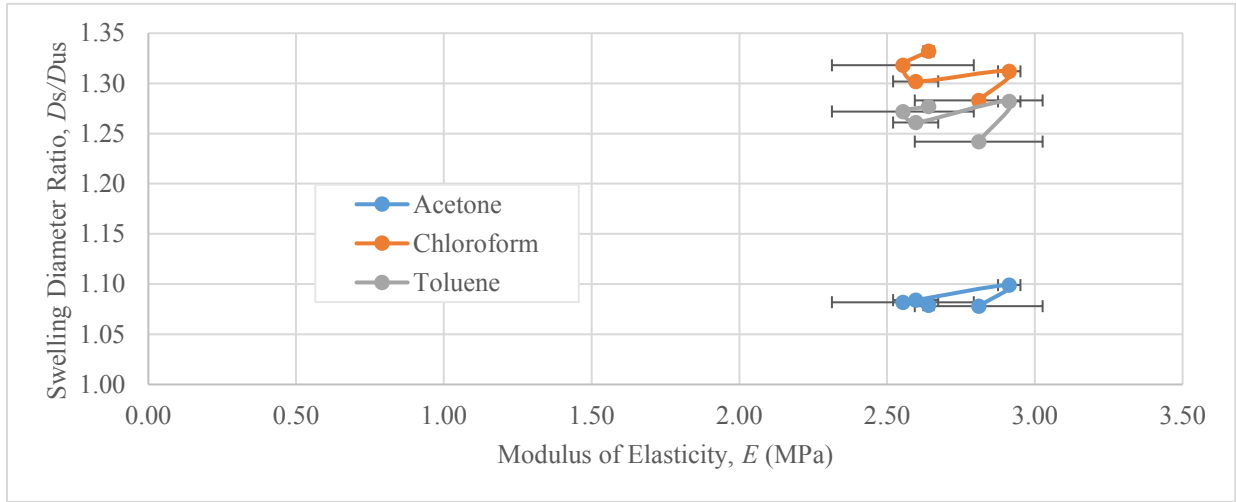


**Figure B-1: Swelling ratios in chloroform, toluene, and acetone of GNP/PDMS to corresponding modulus of elasticity**

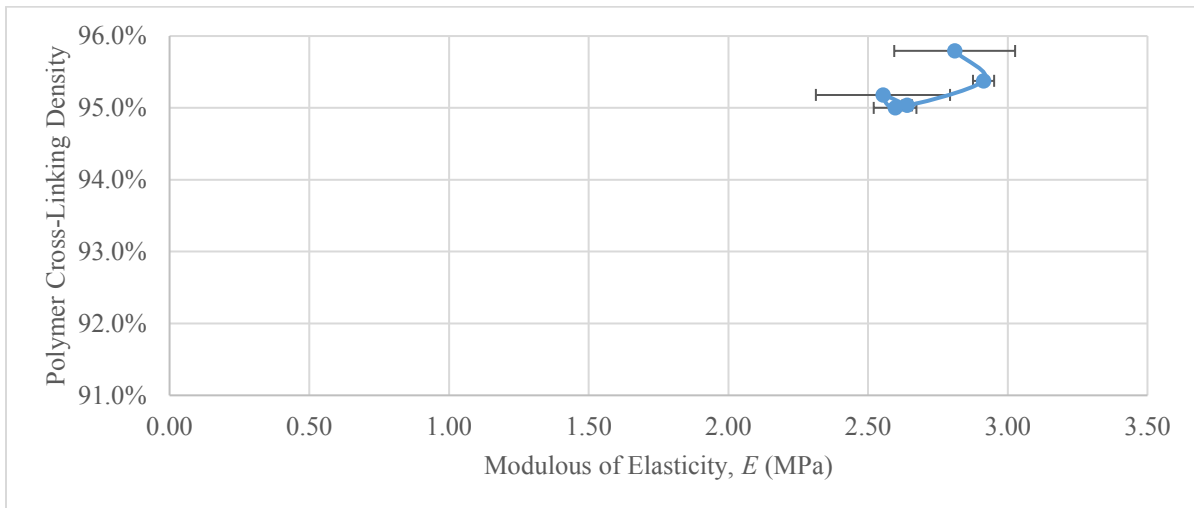


**Figure B-2: Crosslinking-densities of GNP/PDMS to corresponding modulus of elasticity**

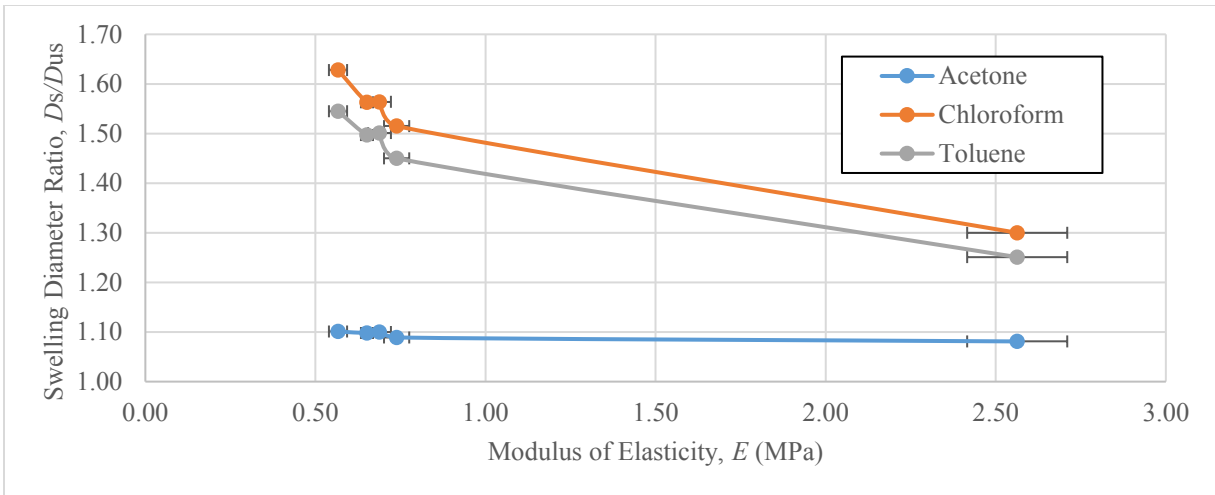


**Figure B-3: Swelling ratios in chloroform, toluene, and acetone of CB/PDMS to corresponding modulus of elasticity**

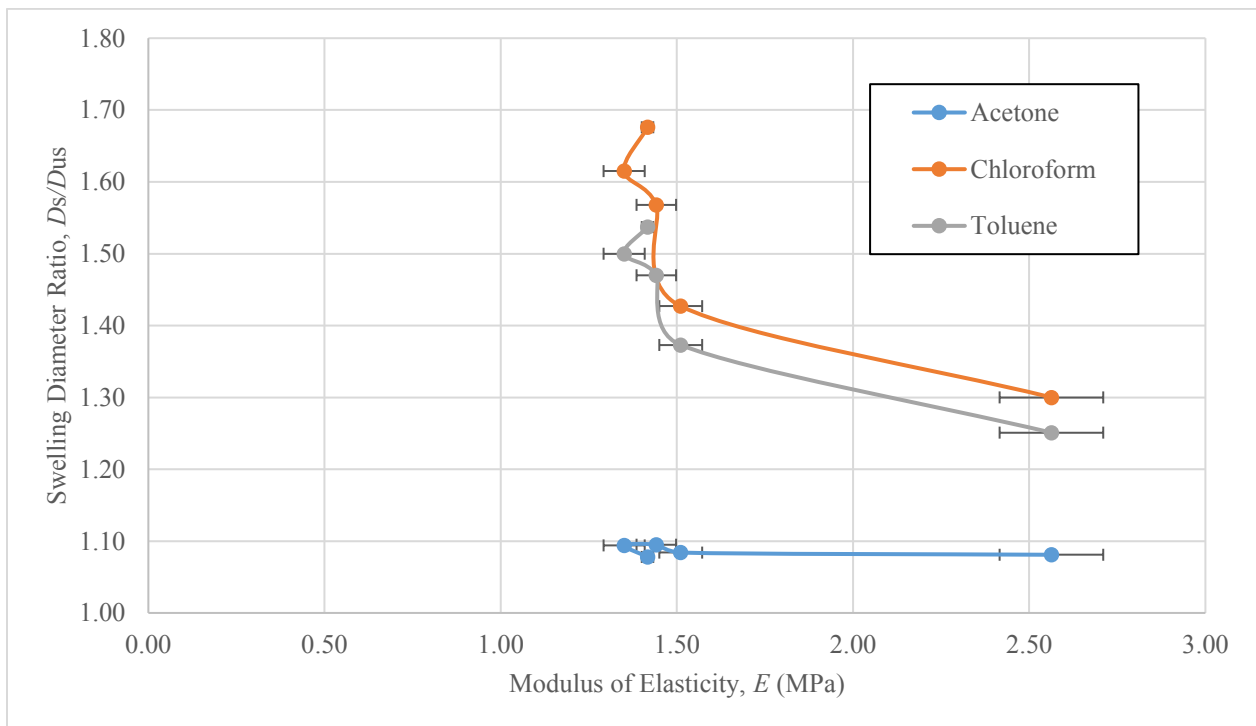


**Figure B-4: Swelling ratios in chloroform, toluene, and acetone of NS/PDMS to corresponding modulus of elasticity**